ADE301 278

(12)

A136393

DNA-TR-82-20

BASIC MECHANISMS OF RADIATION EFFECTS ON ELECTRONIC MATERIALS, DEVICES, AND INTEGRATED CIRCUITS

Joseph R. Srour
Northrop Corporation
One Research Park
Palos Verdes Peninsula, California 90274

1 August 1982

Technical Report

CONTRACT No. DNA 001-82-C-0055

APPROVED FOR PUBLIC RELEASE; DISTRIBUTION UNLIMITED.

DTIC
DEC 27 1983
A

THIS WORK WAS SPONSORED BY THE DEFENSE NUCLEAR AGENCY UNDER RDT&E RMSS CODE B323082466 X99QAXVA00038 H2590D.

DTIC FILE COPY

Prepared for
Director
DEFENSE NUCLEAR AGENCY
Washington, DC 20305

83 11 30 018

Destroy this report when it is no longer
needed. Do not return to sender.

PLEASE NOTIFY THE DEFENSE NUCLEAR AGENCY,
ATTN: STTI, WASHINGTON, D.C. 20305, IF
YOUR ADDRESS IS INCORRECT, IF YOU WISH TO
BE DELETED FROM THE DISTRIBUTION LIST, OR
IF THE ADDRESSEE IS NO LONGER EMPLOYED BY
YOUR ORGANIZATION.

UNCLASSIFIED

SECURITY CLASSIFICATION OF THIS PAGE (When Data Entered)

REPORT DOCUMENTATION PAGE		READ INSTRUCTIONS BEFORE COMPLETING FORM
1. REPORT NUMBER DNA-TR-82-20	2. GOVT ACCESSION NO. AD-A136 393	3. RECIPIENT'S CATALOG NUMBER
4. TITLE (and Subtitle) BASIC MECHANISMS OF RADIATION EFFECTS ON ELECTRONIC MATERIALS, DEVICES, AND INTEGRATED CIRCUITS		5. TYPE OF REPORT & PERIOD COVERED Technical Report 6. PERFORMING ORG. REPORT NUMBER NRTC 82-21R
7. AUTHOR(s) Joseph R. Srour		8. CONTRACT OR GRANT NUMBER(s) DNA 001-82-C-0055
9. PERFORMING ORGANIZATION NAME AND ADDRESS Northrop Corporation One Research Park Palos Verdes Peninsula, California 90274		10. PROGRAM ELEMENT, PROJECT, TASK AREA & WORK UNIT NUMBERS Task X99QAXVA-00038
11. CONTROLLING OFFICE NAME AND ADDRESS Director Defense Nuclear Agency Washington, D.C. 20305		12. REPORT DATE 1 August 1982 13. NUMBER OF PAGES 100
14. MONITORING AGENCY NAME & ADDRESS(if different from Controlling Office)		15. SECURITY CLASS. (of this report) UNCLASSIFIED 15a. DECLASSIFICATION/DOWNGRADING SCHEDULE N/A since UNCLASSIFIED

16. DISTRIBUTION STATEMENT (of this Report)

Approved for public release; distribution unlimited.

17. DISTRIBUTION STATEMENT (of the abstract entered in Block 20, if different from Report)

18. SUPPLEMENTARY NOTES

This work was sponsored by the Defense Nuclear Agency under RDT&E RMSS Code B323082466 X99QAXVA00038 H2590D.

19. KEY WORDS (Continue on reverse side if necessary and identify by block number)

Radiation Effects
Basic Mechanisms
Silicon
Silicon Devices
Silicon Dioxide
MOS Devices
Single Event Phenomena
Defects
Integrated Circuits
Damage Coefficients

20. ABSTRACT (Continue on reverse side if necessary and identify by block number)

This report describes in a tutorial manner the basic mechanisms of radiation effects on electronic materials, devices, and integrated circuits. Radiation effects in bulk silicon and in silicon devices are treated. Ionizing radiation effects in silicon dioxide films and silicon MOS devices are discussed. Single event phenomena are considered. Key literature references and a bibliography are provided.

DD FORM 1 JAN 73 1473 EDITION OF 1 NOV 65 IS OBSOLETE

UNCLASSIFIED

SECURITY CLASSIFICATION OF THIS PAGE (When Data Entered)

Preface

The author wishes to acknowledge discussions with his colleagues, Drs. Ali Bahraman, Arne H. Kalma, Siegfried Othmer, and Zef Shanfield, that were helpful in the preparation of this report.

Distribution/
Availability Codes
Dist | Avail and/or Special
A-1

TABLE OF CONTENTS

Section			Page
1.0	INTRODUCTION		9
2.0	BACKGROUND INFORMATION		12
	2.1	Radiation Environments	12
	2.2	Interaction of Particles with Targets	12
	2.3	Dominant Basic Mechanisms	18
	2.4	Terminology	20
3.0	RADIATION EFFECTS IN BULK SILICON AND IN BIPOLAR DEVICES		23
	3.1	Introduction	23
	3.2	Radiation-Induced Defects in Silicon and Their Properties	23
	3.3	Neutron Effects	36
	3.4	Damage Coefficients and Damage Correlations	48
	3.5	Radiation Effects on Bipolar Transistors	52
4.0	IONIZING RADIATION EFFECTS IN SiO_2 FILMS AND SILICON MOS DEVICES		59
	4.1	Introduction	59
	4.2	Positive Charge Buildup, Interface State Production, and Electron Trap Creation	59
	4.3	Threshold Voltage Shifts and Channel Mobility Degradation	69
	4.4	Silicon-on-Sapphire Devices	72
5.0	SINGLE EVENT PHENOMENA		75
6.0	ADDITIONAL TOPICS		80
	6.1	Device Failure Mechanisms	80
	6.2	Gallium Arsenide Devices	80
	6.3	Optical Properties	80
	6.4	Hardness Assurance Example	83
7.0	REFERENCES AND BIBLIOGRAPHY		85
	7.1	References	85
	7.2	Bibliography	87

LIST OF ILLUSTRATIONS

Figure		Page
1	Three areas where basic mechanisms understanding plays an important role	10
2	Schematic illustration of an integrated circuit in a radiation environment	10
3	Various radiation environments and sources of radiation	13
4	Irradiating particles associated with the environments and sources listed in Figure 3.	13
5	Three primary particle categories	14
6	Properties of particles and targets that affect their interactions.	14
7	Type of interactions that can occur between primary particles and target atoms.	16
8	Illustration of the relative importance of the three photon interactions as a function of Z and photon energy.	17
9	Dominant basic effects of radiation on electronic materials	19
10	Stopping power versus particle energy for electrons and protons incident on silicon	19
11	Important effects produced by displacement and ionization.	21
12	Important examples of the commonly used radiation effects terminology	21
13	Various defects that can occur in irradiated silicon.	24
14	Schematic illustration of three types of simple defects in a lattice structure.	25
15	Basic phenomena which cause devices to degrade in a radiation environment	26
16	Illustration of five effects that can occur due to the presence of defect centers in the silicon bandgap	27

LIST OF ILLUSTRATIONS (Continued)

Figure		Page
17	Illustration of the energy levels and charge states associated with the vacancy in silicon	29
18	Relative amount of damage present in electron-irradiated silicon versus time following the radiation burst	30
19	Characteristic recovery time versus reciprocal temperature derived from data of the type shown in Figure 18	31
20	Several ways to alter the charge state of defects	32
21	Several mechanisms thought to be responsible for ionization-enhanced annealing	33
22	Illustration of the injection-level dependence of minority-carrier lifetime in irradiated silicon	35
23	Illustration of the two-level model for describing the observed injection-level dependence of carrier lifetime	36
24	Illustration of the Gossick model for defect clusters in neutron-irradiated n-type silicon	37
25	Effects of neutron bombardment on the electrical properties of bulk silicon	38
26	Illustration of the relative sensitivity of lifetime, carrier concentration, and mobility to neutron bombardment	38
27	Neutron energy dependence of displacement damage in silicon	39
28	Illustration of the short-term and long-term recovery processes that occur in neutron-irradiated silicon	40
29	Annealing factor versus time for 11 ohm-cm p-type bulk silicon samples irradiated with bursts of 14-MeV and reactor neutrons	42
30	Annealing factor versus time for pnp transistors irradiated with bursts of 14-MeV and reactor neutrons	42
31	Annealing factor at 20 msec after a fission neutron burst versus electron density for n- and p-base solar cells	43

LIST OF ILLUSTRATIONS (Continued)

Figure		Page
32	Annealing factor versus time for p-base solar cells irradiated with bursts of 14-MeV and reactor neutrons.	44
33	Annealing factor versus time for npn transistors irradiated with a burst of 14-MeV neutrons	44
34	Short-term annealing nomograph for fission-neutron-irradiated silicon devices	45
35	Dependencies for stable damage in neutron-irradiated silicon.	46
36	Illustration of the resistivity dependence of the low-injection-level value of K_r for neutron-irradiated n-type bulk silicon.	47
37	Illustration of the resistivity dependence of the low-injection-level value of K_r for neutron-irradiated p-type bulk silicon.	47
38	Illustration of the injection-level dependence of recombination lifetime damage coefficient for 14-MeV neutron-irradiated bulk p-type silicon	48
39	Parameters that damage coefficients depend on in silicon.	49
40	Damage coefficients and carrier removal rate for neutron-irradiated silicon	50
41	Comparison of the effectiveness of various particles in degrading carrier lifetime in silicon	51
42	Example damage correlations for electron-, proton-, and neutron-irradiated silicon	52
43	Electron-hole pair generation energies for silicon and silicon dioxide.	53
44	Schematic illustration of a bipolar transistor	54
45	Schematic diagram of an I^2L cell in a bipolar integrated circuit	55
46	Example of neutron-induced current gain degradation in a bipolar transistor	56

LIST OF ILLUSTRATIONS (Continued)

Figure		Page
47	Additional radiation-induced effects in bipolar transistors and integrated circuits	56
48	Effects of ionizing radiation in silicon MOS devices	60
49	Schematic illustration of an MOS transistor	60
50	Energy band diagram for the metal-SiO_2-silicon system: a) zero bias; b) positive bias plus ionizing radiation	62
51	Illustration of recombination, transport, and trapping of carriers in SiO_2 films	63
52	Capacitance-voltage curves corresponding to the conditions illustrated in Figure 51	64
53	Yield versus field curves for various particles incident on SiO_2 films	65
54	Flatband voltage shift versus voltage applied during irradiation for MOS capacitors irradiated at both 77°K and room temperature	66
55	Information concerning radiation-induced interface states at the SiO_2-Si interface	67
56	Information concerning radiation-induced electron traps in SiO_2 films	68
57	Illustration of the effect of positive charge buildup and interface state production on the threshold voltage in irradiated n- and channel MOS transistors	70
58	Illustration of transient changes in threshold voltage following an ionizing burst	71
59	Illustration of channel mobility degradation in irradiated MOS transistors	71
60	Schematic illustration of an n-channel silicon-on-sapphire MOS transistor	73
61	Illustration of radiation-induced changes in back-channel leakage current for silicon-on-sapphire MOS transistors	73
62	Types of single event phenomena	76

LIST OF ILLUSTRATIONS (Continued)

Figure		Page
63	Illustration of the ionized track produced by a 5-MeV alpha particle incident on a dynamic RAM cell.	76
64	Calculated threshold voltage shift as a function of gate oxide thickness for a single 2-MeV alpha particle incident on MOS transistors of various sizes	78
65	Calculated dimensions for an average disordered region produced in silicon by an incident 14-MeV neutron.	78
66	Illustration of a neutron-produced disordered region in an I^2L cell	79
67	Failure mechanisms for semiconductor devices	81
68	Radiation effects on GaAs materials and devices.	82
69	Optical properties of materials that are altered by radiation.	82
70	Comparison of the charge buildup process in an MOS structure produced by ionizing radiation and by the F4I technique.	84
71	Comparison of C-V curves obtained after Co^{60} irradiation and after the F4I test	84

1.0 INTRODUCTION

Alteration of the electrical properties of solid-state devices and integrated circuits by impinging radiation is a well-known phenomenon. Since such changes may cause an electronic subsystem to fail, there is considerable emphasis at present on devising methods to avoid radiation-induced degradation. Development of radiation-hardened devices and circuits is an appealing approach to solving this problem for many applications since it would minimize the need for shielding or other system hardening techniques. A key step in developing hardened electronics is gaining a detailed understanding of the basic effects produced in electronic materials, devices, and integrated circuits by radiation. As indicated in Figure 1, once the basic mechanisms are understood, several steps can then be undertaken systematically. First, reliable predictions of the radiation response of devices and circuits in environments of interest can be made. Second, basic insight can lead to the development of novel device hardening approaches. Third, procedures for assuring that circuits will withstand specific radiation exposure levels can be developed.

In this report, the basic mechanisms of radiation effects on electronic materials, devices, and integrated circuits are treated. Emphasis is placed on effects occurring in the most commonly employed device materials: silicon and silicon dioxide. The focus is on radiation-induced changes in the electrical properties of these materials and the effects of such changes on device properties. To gain detailed insight regarding the effects that occur when an integrated circuit is placed in a radiation environment (Figure 2), knowledge in several areas is important: atomic, nuclear, solid-state, and semiconductor device physics. It is also important that integrated circuit processing procedures be understood, particularly when developing radiation hardening techniques. An understanding of the physical phenomena that give rise to a specific radiation environment is not vital. Some familiarity with the technical areas listed in Figure 2 is assumed here, but much of the material is presented in overview fashion so

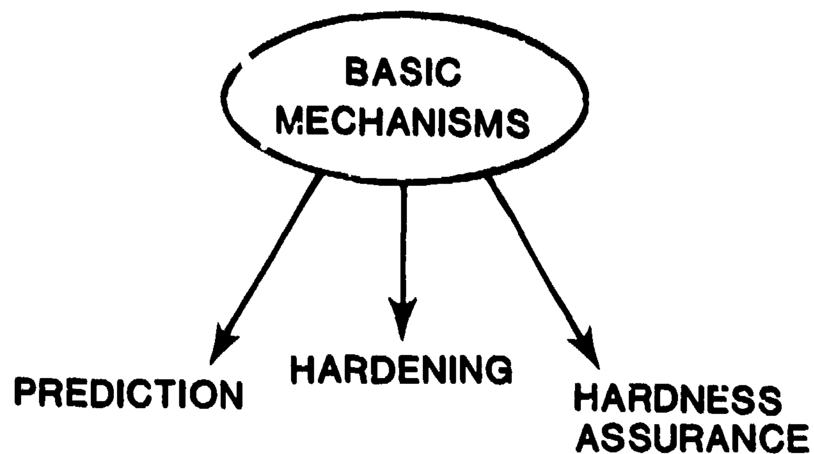

Figure 1. Three areas where basic mechanisms understanding plays an important role.

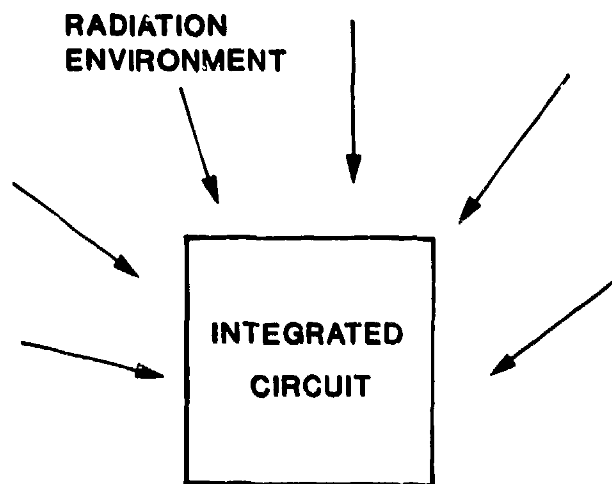

- ATOMIC AND NUCLEAR PHYSICS
- SOLID-STATE AND SEMICONDUCTOR DEVICE PHYSICS
- INTEGRATED CIRCUIT PROCESSING

Figure 2. Schematic illustration of an integrated circuit in a radiation environment. Listed are areas of expertise that are important for understanding and predicting radiation effects and developing device hardening and hardness assurance procedures.

that readers with differing technical backgrounds should be able to digest the key points. The device physics aspects of radiation effects are emphasized.

Background information is presented in Section 2.0. Radiation sources and environments and the types of irradiating particles encountered are discussed, and a qualitative review of the relevant aspects of atomic and nuclear physics is given. The dominant basic mechanisms that occur in irradiated materials are discussed, and useful radiation effects terminology is presented. Displacement damage and ionization effects in bulk silicon and bipolar devices are treated in Section 3.0. In Section 4.0, ionizing radiation effects in SiO_2 films and silicon MOS devices are described. Section 5.0 considers single event phenomena. Section 6.0 treats several additional topics, including a summary of device failure mechanisms, radiation effects on GaAs devices, radiation-induced changes in optical properties, and a hardness assurance example that arose from an understanding of basic mechanisms. In Section 7.0, a bibliography is given along with specific literature references.

2.0 BACKGROUND INFORMATION

2.1 RADIATION ENVIRONMENTS

Figure 3 lists various radiation environments and radiation sources. The space radiation environment is naturally occurring and is of concern for earth-orbiting satellites and for missions to other planets. Another natural radiation environment is due to materials containing trace radioactive elements (such as uranium and thorium) which, when incorporated in packaged integrated circuits, can cause occasional transient upsets (e.g., alpha-particle-induced soft errors). Two man-made sources of radiation are nuclear explosions and nuclear reactors. Additional sources of radiation also arise during integrated circuit processing. For example, ion implantation machines are routinely employed in processing. Additionally, X-ray and electron-beam lithography equipment is being utilized at some facilities for VLSI circuit fabrication. Radiation damage occurs in all three cases.

The environments and sources of radiation mentioned above give rise to various particles (Figure 4) that may impinge on materials, devices, and circuits and cause undesirable effects. For example, nuclear reactors produce neutrons and gamma rays. The rate at which particles bombard a given device varies substantially. For example, a burst of electrons 100 nsec wide can be delivered by linear accelerators; on the other hand, the radiation environment in a power reactor is essentially steady state. Another variable is the particle energy. For a given type of particle, the particle energy may vary by orders of magnitude depending on the radiation source or environment and the application.

2.2 INTERACTION OF PARTICLES WITH TARGETS

The various types of particles listed in Figure 4 can be separated into three primary categories: photons, charged particles, and neutrons (Figure 5). When a target is bombarded by radiation, the nature of the interaction between the impinging particle and the target depends on several properties (Figure 6). The relevant particle properties are mass, charge, and kinetic energy. Target properties of importance are mass, charge, and density.

RADIATION SOURCES AND ENVIRONMENTS

- SPACE
- MATERIALS
- NUCLEAR EXPLOSION
- NUCLEAR REACTOR
- INTEGRATED CIRCUIT PROCESSING

Figure 3. Various radiation environments and sources of radiation.

IRRADIATING PARTICLES

- NEUTRONS
- GAMMA RAYS
- X-RAYS
- ELECTRONS
- PROTONS
- ALPHA PARTICLES
- IONS
- COSMIC RAYS
  - PROTONS
  - ELECTRONS
  - ALPHA PARTICLES
  - HEAVIER IONS

Figure 4. Irradiating particles associated with the environments and sources listed in Figure 3.

PARTICLE CATEGORIES

- PHOTONS
  - X-RAYS
  - GAMMA RAYS
- CHARGED PARTICLES
  - ELECTRONS
  - PROTONS
  - ALPHA PARTICLES
  - IONS
- NEUTRONS

Figure 5. Three primary particle categories.

PARTICLE INTERACTION WITH TARGETS

NATURE OF INTERACTION DEPENDS ON:

- PARTICLE PROPERTIES
  - MASS
  - CHARGE
  - KINETIC ENERGY
- TARGET PROPERTIES
  - MASS
  - CHARGE
  - DENSITY

Figure 6. Properties of particles and targets that affect their interactions.

There are various types of interactions that can occur between the primary particles and target atoms, as listed in Figure 7. Photons have zero rest mass and are electrically neutral. They interact with target atoms through the photoelectric effect, Compton scattering, and pair production. In all three cases, the interaction produces energetic free electrons. The energy range in which photoelectric collisions dominate depends on the atomic number Z of the material, as discussed below. The probability of a photoelectric interaction decreases with increasing photon energy and increases with Z. If the incident photon is energetic enough to emit an electron from the K shell, then most (~80%) of the collisions are with K-shell electrons. In the photoelectric process the incident photon energy is completely absorbed by the emitted electron (photoelectron). If a K-shell electron was involved, then an L-shell electron will drop into the remaining empty state. Either a characteristic X-ray or a low-energy Auger electron is emitted from the L shell, depending on the value of Z.

In contrast to the photoelectric effect, Compton scattering does not involve complete absorption of the incident photon. In Compton scattering, the photon energy is much greater than the binding energy of atomic electrons (such as those in the K shell). The incident photon gives up a portion of its energy to scatter an atomic electron, thereby creating an energetic Compton electron, and the lower-energy scattered photon continues to travel in the target material. As the photon energy increases, Compton scattering dominates over the photoelectric effect.

The third type of photon interaction, pair production, has a threshold energy of 1.02 MeV. At this energy, a photon striking a high-Z target will be completely absorbed and cause a positron-electron pair to form. (A positron has the same rest mass and charge as an electron, except that the charge is positive.)

Figure 8 illustrates the relative importance of the three photon interactions as a function of Z and photon energy. The solid lines correspond to equal interaction cross sections for the neighboring effects. For silicon

TYPES OF INTERACTIONS

- PHOTONS
  - PHOTOELECTRIC EFFECT
  - COMPTON SCATTERING
  - PAIR PRODUCTION
- CHARGED PARTICLES
  - RUTHERFORD SCATTERING
  - NUCLEAR INTERACTIONS (HEAVY PARTICLES)
- NEUTRONS
  - NUCLEAR INTERACTIONS
    - ELASTIC SCATTERING
    - INELASTIC SCATTERING
    - TRANSMUTATION REACTIONS

Figure 7. Type of interactions that can occur between primary particles and target atoms.

($Z = 14$), the photoelectric effect dominates at energies <50 keV and pair production dominates at energies >20 MeV. In the intervening energy range, Compton scattering dominates. Thus, over a broad photon energy range, energetic Compton electrons are produced which undergo subsequent charged-particle interactions. Such interactions are now described.

Charged particles incident on a target interact primarily by Rutherford scattering (Coulomb scattering). This interaction can cause both excitation and liberation (ionization) of atomic electrons. Additionally, through Rutherford scattering sufficient energy can be transferred to atoms to displace them from their normal lattice positions. Heavy charged particles can also undergo nuclear interactions of the type described below for neutrons. For example,

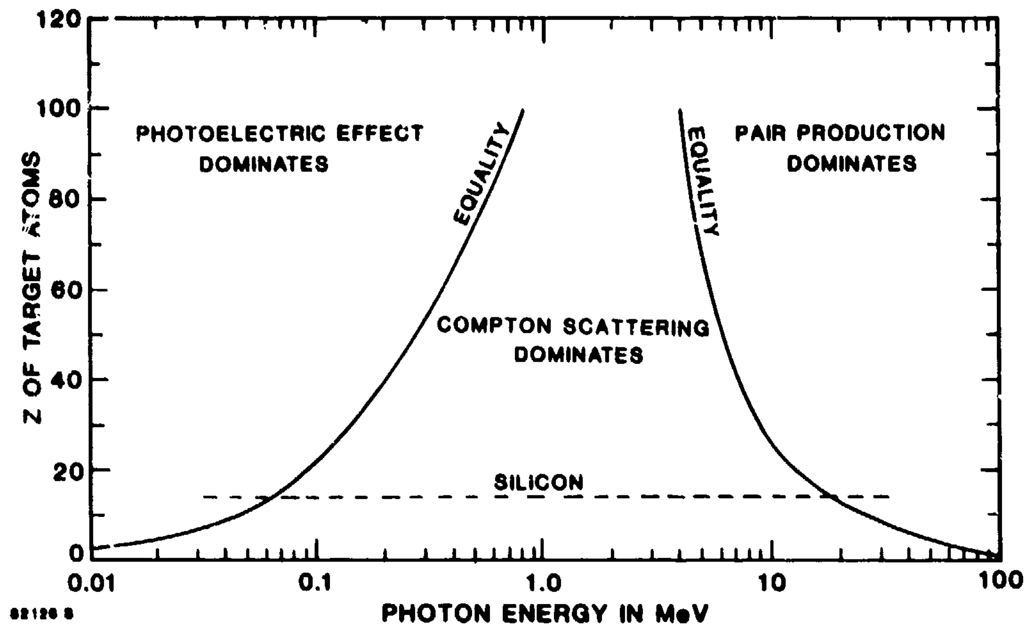

Figure 8. Illustration of the relative importance of the three photon interactions as a function of Z and photon energy. The solid lines correspond to equal interaction cross sections for the neighboring effects. The dashed line illustrates the situation for photon interactions with silicon.

a proton can be absorbed in a target nucleus, and the nucleus then emits an alpha particle.

Neutrons incident on a target undergo the following nuclear interactions: elastic scattering, inelastic scattering, and transmutation. In an elastic collision, the neutron gives up a portion of its energy to an atom of the target material, and can dislodge the atom from its lattice position. This process will occur as long as the imparted energy is greater than that required for displacement (~25 eV for most materials). The displaced atom is referred to as the primary recoil (or primary knock-on); it subsequently will lose energy to ionization and can also displace other lattice atoms. Inelastic neutron scattering involves capture of the incident neutron by the nucleus of the target atom and subsequent emission of the neutron at a lower energy. Kinetic energy is lost in this process and the target nucleus

is left in an excited state. The excited nucleus returns to its original state by emission of a gamma ray. The kinetic energy of the emitted neutron is reduced, compared to the incident neutron, by the energy of the gamma ray. Inelastic neutron scattering can also cause displacement of the target atom to occur. The transmutation reaction involves capture of the incident neutron by the target nucleus and subsequent emission of another particle, such as a proton or an alpha particle. The remaining atom is thereby transmuted, i.e., converted from one element into another. The dominant processes in the case of silicon irradiated with fast neutrons (i.e., neutrons with an energy $\gtrsim 1$ MeV) are the production of displaced atoms and ionization.

2.3 DOMINANT BASIC MECHANISMS

Upon considering the various types of particles, particle energy ranges, and the variety of interactions that can occur, one might view the situation as being exceedingly complex in terms of the effects produced in irradiated materials and devices. In practice, however, for the environments of most interest for radiation effects on electronics two basic mechanisms dominate (Figure 9): displacement of atoms from their lattice sites (displacement damage) and generation of electron-hole pairs (ionization). In general, particles passing through electronic materials deposit a portion of their energy into ionization and the remainder into displacement. Some particles, such as fast neutrons, primarily produce displacement damage, whereas other particles, such as low energy electrons (e.g., 10 keV), give up all their energy into ionization.

For energetic electrons and protons, the amount of energy deposited into ionization can be obtained from the stopping power tabulations of Berger and Seltzer[1] and Janni,[2] respectively. Figure 10 shows stopping power versus particle energy for electrons and protons incident on silicon. The absorbed ionizing dose is proportional to the integral of the product of the particle fluence and the stopping power over the specimen thickness. (Absorbed dose and fluence are defined in the next subsection.) Electrons and protons also produce displacement damage. For electrons, an incident particle energy of ~ 150 keV is the minimum required to produce displacements

DOMINANT BASIC MECHANISMS

- DISPLACEMENT OF LATTICE ATOMS
- IONIZATION

Figure 9. Dominant basic effects of radiation on electronic materials.

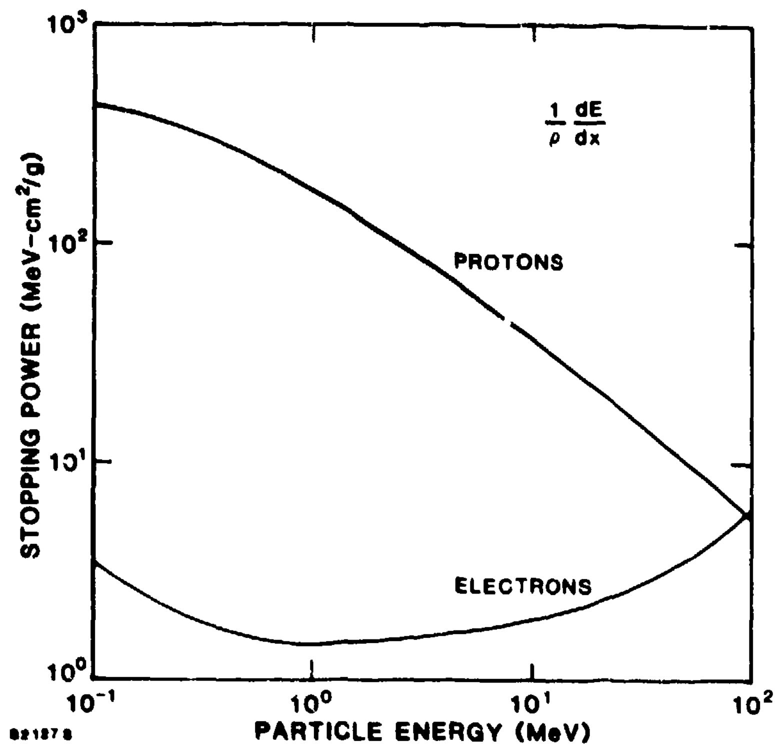

Figure 10. Stopping power versus particle energy for electrons and protons incident on silicon.[1,2]

in silicon. For protons, the threshold is ~100 eV. Estimates of the number of displacements produced by particles with energies above these thresholds can be made based on calculated displacement cross sections.[3]

For neutrons incident on silicon, the probabilities for the various previously described interactions to occur can be expressed in terms of the appropriate neutron cross sections.[4] Once a silicon knock-on is produced, it can then be treated as a silicon ion incident on a silicon target. Viewing the situation in this manner allows one to consider ionization and displacement processes in the same way for incident neutrons, alpha particles, and other ions. The partitioning of energy loss into ionization and displacement for these cases is commonly performed using the Lindhard model.[5,6] This model is a unified theory of atomic stopping that applies for any atomic numbers of the incident particle and the target.

Important examples of the effects of displacement damage and ionization in silicon and silicon devices are given in Figure 11. Displacement damage gives rise to various energy levels in the silicon bandgap, which is discussed in Section 3.0. Scattering centers are also produced which cause a reduction in carrier mobility. Ionization causes photocurrents to flow in devices containing pn junctions. Another ionizing radiation effect is permanent trapping of free charge (referred to as charge buildup) in the oxide layers contained in MOS devices. This effect and other MOS-related phenomena are discussed in Section 4.0.

In general, when materials and devices are irradiated, both transient and permanent effects on electrical properties occur. Both situations will be considered in this tutorial.

2.4 TERMINOLOGY

Important examples of the commonly used radiation effects terminology are presented in Figure 12. The rate of incidence of particles on a material is given in terms of the particle flux, expressed in particles/cm^2.sec. The time integral of the flux is referred to as the particle fluence, expressed in particles/cm^2.

IMPORTANT CONSEQUENCES OF DISPLACEMENT AND IONIZATION

- DISPLACEMENT DAMAGE EFFECTS
  - ENERGY LEVELS IN THE BANDGAP
  - SCATTERING CENTERS
- IONIZATION EFFECTS
  - PHOTOCURRENTS
  - CHARGE BUILDUP

Figure 11. Important effects produced by displacement and ionization.

TERMINOLOGY

- FLUX: particles / $cm^2 \cdot sec$
- FLUENCE: particles / cm^2
- NEUTRONS:
  - REACTOR NEUTRONS (fission)
  - 14-MeV NEUTRONS (fusion)
  - > 10 keV
  - 1-MeV equivalent
- IONIZING RADIATION
  - TOTAL ABSORBED DOSE
    - One rad(Si) = 100 ergs/gram(Si) (=0.01 J/kg)
    - One gray (Gy) = 100 rads (= 1 J/kg)
  - IONIZING DOSE RATE
    - rad(Si)/sec

Figure 12. Important examples of the commonly used radiation effects terminology.

For neutron bombardment, nuclear reactors typically provide a fission spectrum of neutrons with energies in the range from a few keV to ~20 MeV. (The number spectrum peaks near 1 MeV.) Irradiations are also performed with 14-MeV, or fusion, neutron sources. The question has arisen as to how one should express the neutron fluence for a given irradiation of silicon devices. .e problem is that neutron sources providing differing energy spectra are employed in various simulation experiments. Since the amount of displacement damage produced in silicon is neutron energy dependent, as discussed in Section 3.0, this makes it difficult to compare directly results obtained by workers using different radiation sources. Fluences for reactor irradiations are commonly expressed in terms of the number of neutrons with energies greater than 10 keV, which is based on a common method for performing neutron dosimetry. However, for the purpose of allowing meaningful comparisons to be made, neutron fluences are often expressed in 1-MeV equivalent terms.[†*] To do so, one must take into account both the energy dependence of neutron damage and the neutron energy content of the spectrum obtained from a given source. This information is then used to determine that fluence of 1-MeV neutrons which would produce the same amount of damage in silicon as the experimental fluence. (For water-moderated reactors, such as the TRIGA reactor at the Northrop Corporation, the >10-keV fluence is nearly equal to the 1-MeV equivalent fluence.)

The energy deposited in materials by ionizing radiation is expressed in terms of the rad (radiation absorbed dose). One rad is equal to an absorbed energy of 100 ergs per gram of material. The material in which the dose is deposited must be specified (such as rads(Si)) when using this unit. (The energy loss per unit mass differs from one material to another because of differing atomic properties.) Ionizing dose rate is commonly expressed in rads/sec. The SI unit of absorbed dose is the gray (Gy), which is equal to an absorbed energy of 1 joule per kg, or 100 rads.

[†] For more information, see A.I. Namenson, E.A. Wolicki, and G.C. Messenger, IEEE Trans. Nucl. Sci. 29, 1018 (1982).

[*] A more formal method for expressing the effect of neutrons in materials involves the concept of kerma. For a discussion of this, see "Neutron Fluence, Neutron Spectra, and Kerma," International Commission on Radiation Units and Measurements Report 13, Sept. 5, 1969.

3.0 RADIATION EFFECTS IN BULK SILICON AND IN BIPOLAR DEVICES

3.1 INTRODUCTION

The dominant basic effects of radiation on electronic materials -- ionization and displacement -- cause various phenomena to occur in silicon devices. Radiation-induced changes in the electrical properties of bulk silicon and silicon bipolar transistors are described in this section. Types of radiation-induced defects are discussed, and the changes that these defects give rise to are described. Other aspects of defect behavior, including charge state effects, defect motion, and ionization-enhanced annealing, are considered. The injection-level dependence of carrier lifetime is described, and damage coefficients appropriate for silicon irradiated by different particles are given. Neutron effects on silicon are treated, including the neutron energy dependence of damage introduction and short-term annealing phenomena. The effects of displacement damage and ionization on the properties of bipolar transistors are described, including gain degradation mechanisms, photocurrents, and surface effects.

3.2 RADIATION-INDUCED DEFECTS IN SILICON AND THEIR PROPERTIES

As described in Section 2.2, energetic photons, charged particles, and neutrons incident on silicon can cause displacement of the target atoms to occur. In the photon case, this process occurs through the production of energetic Compton electrons which then interact with target nuclei. As long as a minimum of $\sim$25 eV is transferred to the nucleus, displacement of the atom will result. The absence of an atom from its normal lattice site is referred to as a vacancy, and this is one example of a radiation-induced defect.

Figure 13 lists various defects that can occur in irradiated silicon. Simple defects are also referred to as point, or isolated, defects. Regions containing large numbers of relatively closely spaced defects can also occur, and such a grouping is termed a defect cluster. When a displaced atom moves into a non-lattice position, the resulting defect is referred to as an interstitial. The vacancy-interstitial combination is called a close pair, or a Frenkel pair. Two adjacent vacancies form a defect known as the divacancy;

RADIATION-INDUCED DEFECTS

- SIMPLE DEFECTS (ISOLATED, POINT)
  - VACANCIES
  - DIVACANCIES etc.
  - VACANCY-IMPURITY COMPLEXES
  - INTERSTITIALS
  - DI-INTERSTITIALS etc.
  - INTERSTITIAL-IMPURITY COMPLEXES
- DEFECT CLUSTERS

Figure 13. Various defects that can occur in irradiated silicon.

a di-interstitial can also occur. Larger local groupings of vacancies are also observed in irradiated silicon. Vacancies and interstitials can also form additional types of simple defects when they are adjacent to impurity atoms. Such defects are termed defect-impurity complexes. For example, the vacancy-phosphorus pair is a defect that is observed in silicon. Figure 14 shows a schematic illustration of three types of simple defects in a lattice structure.

If a displaced atom is given a relatively large amount of kinetic energy by an incident particle, the primary knock-on can displace many additional atoms and thereby cause the formation of a region of disorder, or defect cluster. This process occurs for incident neutrons with energy in the MeV range. On the other hand, MeV electrons and photons produce primarily isolated defects in silicon. Protons produce a mixture of isolated defects and small defect clusters.

A well-known concept in semiconductor physics is that impurity atoms in the silicon lattice have discrete energy levels associated with them which lie in the bandgap between the conduction band minimum and the valence band maximum. In general, any disturbance of lattice periodicity may give rise to energy levels in the bandgap. Radiation-induced defects have such

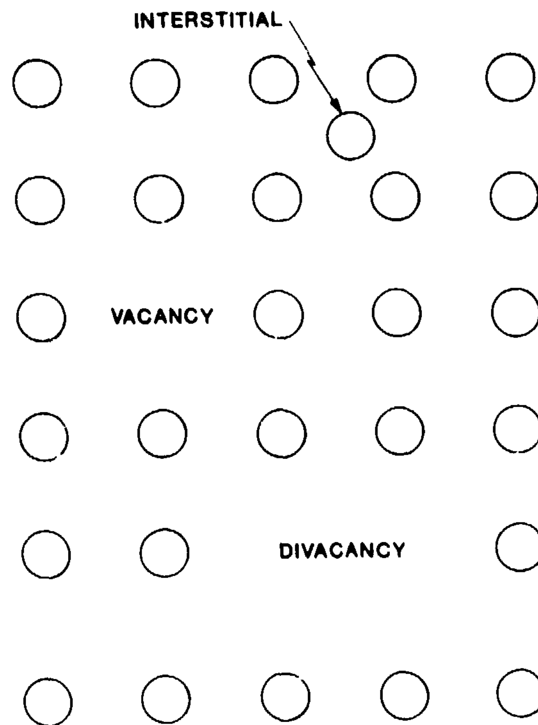

Figure 14. Schematic illustration of three ty es of simple defects in a lattice structure.

levels associated with them and it is these defect states, or centers, that have a major impact on the electrical behavior of semiconductor devices. Thus, the basic phenomena which cause devices to degrade in a radiation environment are (Figure 15): a) incident particles displace atoms; b) the resulting defects give rise to new energy levels; c) these levels alter device electrical properties. The fundamental effects of defect centers on electrical properties are now described.

Figure 16 illustrates five effects that can occur due to the presence of radiation-induced defect centers in the silicon bandgap. Process 1 is the thermal generation of electron-hole pairs through a level near midgap. This process can be viewed as the thermal excitation of a bound valence-band electron to the defect center and the subsequent excitation of that electron to the conduction band, thereby generating a free electron-hole pair. Alternatively, it can be viewed as hole emission from the center

BASIC PHENOMENA WHICH LEAD TO DEVICE DEGRADATION

- DISPLACEMENT OF ATOMS BY INCIDENT PARTICLES
- DEFECTS GIVE RISE TO ENERGY LEVELS IN THE BANDGAP
- DEFECT LEVELS ALTER DEVICE ELECTRICAL PROPERTIES

Figure 15. Basic phenomena which cause devices to degrade in a radiation environment.

followed by electron emission. Only centers with an energy level near midgap make a significant contribution to carrier generation; an exponential decrease in generation rate occurs as the energy level position is moved from midgap.[7] In addition, emission processes dominate over capture processes at a defect level only when the free carrier concentrations are significantly less than their thermal equilibrium values. Thus, thermal generation of electron-hole pairs through radiation-induced defect centers near midgap is important in device depletion regions. Introduction of such centers is the mechanism for leakage current increases in silicon devices. (Generation lifetime, τ_g, is a characteristic time associated with carrier generation in a depletion region, and that parameter is used below in the damage coefficient discussion.)

Process 2 is the recombination of electron-hole pairs. In this process, a free carrier of one sign is first captured at the defect center, followed by capture of a carrier of the opposite sign. Recombination removes electron-hole pairs as opposed to the generation process. In general, the recombination rate depends on the defect center (or recombination center) density, the free carrier concentrations, the electron and hole capture cross sections, and the energy level position. The mean time a minority carrier spends in its band before recombining is referred to as the recombination

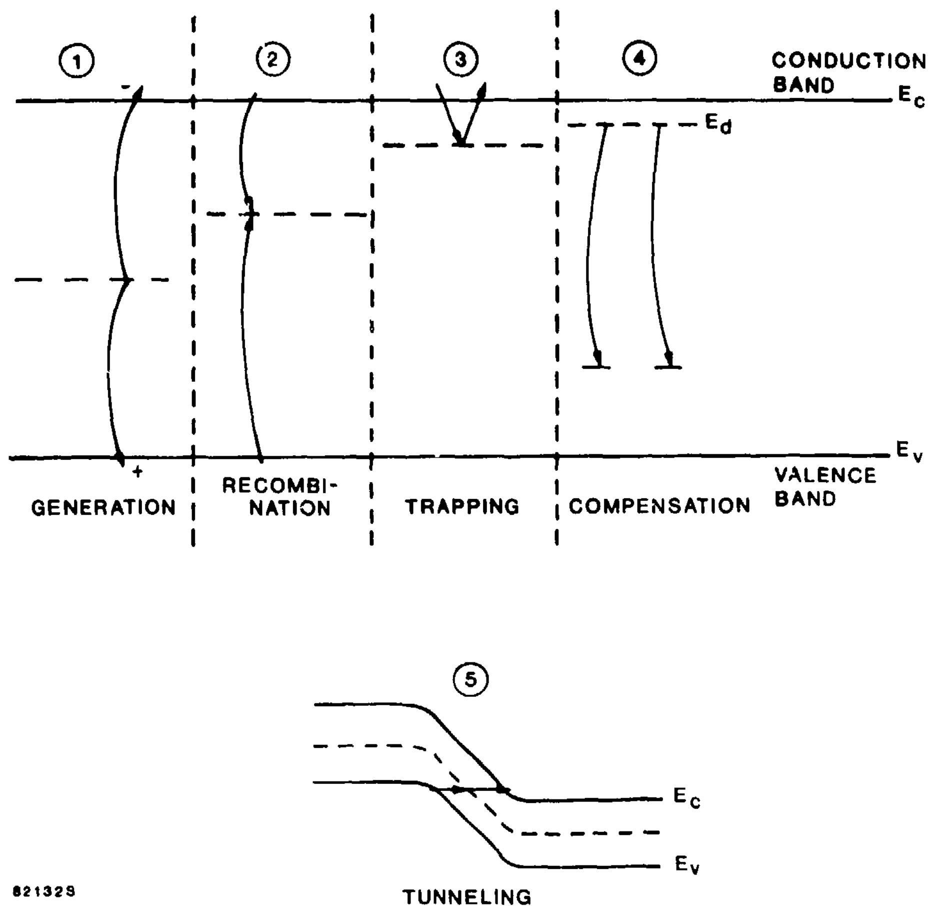

Figure 16. Illustration of five effects that can occur due to the presence of defect centers in the silicon bandgap.

lifetime, τ_r. Radiation-induced recombination centers cause τ_r to decrease; this is the dominant mechanism for gain degradation in bipolar transistors.

Process 3 is the temporary trapping of carriers at a typically shallow level. In this process, a carrier is captured at a defect center and is later emitted to its band, with no recombination event taking place. In general, trapping of both majority and minority carrier can occur (at separate levels). Radiation-induced traps are responsible for increasing the transfer inefficiency in charge-coupled devices.[8]

Process 4 is the compensation of donors or acceptors by radiation-induced centers. In the example shown in Figure 16, some of the free electrons available from the donor level are compensated by deep-lying radiation-induced acceptors. The result is a reduction in the equilibrium majority-carrier concentration. This "carrier removal" process will cause an alteration in any device or circuit property that depends on carrier concentration. For example, the resistance of the collector in bipolar transistors will increase due to carrier removal.

Process 5 is the tunneling of carriers through a potential barrier by means of defect levels. This defect-assisted (also called trap-assisted) tunneling process can cause device currents to increase in certain situations. For example, there may be a defect-assisted tunneling component of the reverse current in a pn junction diode.

In summary, radiation-induced levels in the bandgap can give rise to five processes: generation, recombination, trapping, compensation, and tunneling. In principle, any combination, or all, of these processes can occur through the same level. The role a particular level plays depends on variables such as carrier concentration, temperature, and the device region in which it resides (e.g., in a depletion region).

Radiation-induced defects also act as scattering centers and cause the carrier mobility to decrease. The mobility decreases with increasing ionized impurity concentration. In a similar manner, the introduction of charged radiation-induced defects also causes the mobility to decrease. This effect should be stronger at temperatures considerably less than 300°K because ionized impurity scattering dominates over lattice scattering in that regime.

A discussion of defect charge states and defect motion is now presented, using the vacancy in silicon as an example. The charge state of a defect refers to the occupancy of the associated defect levels in the bandgap by holes or electrons. For example, if a defect is occupied by one electron, the defect is in a single-negative charge state. Defect charge state is an important basic property in terms of the relative mobility of defects in the lattice and the relative changes in the electrical

properties of semiconductors. Figure 17 shows energy levels and charge states associated with the vacancy in silicon.* The charge state of any defect is determined by the position of the Fermi level with respect to the defect levels. For example, if the Fermi level is below the energy level at ~0.4 eV from the conduction band edge, but above the level near the valence band edge, the vacancy will be in a neutral charge state. The ease with which the vacancy can diffuse through the silicon lattice is charge-state dependent. In other words, the activation energy for vacancy motion depends on the charge state. For example, vacancies in a single-negative charge state are much more mobile in silicon at a given temperature than neutral vacancies.

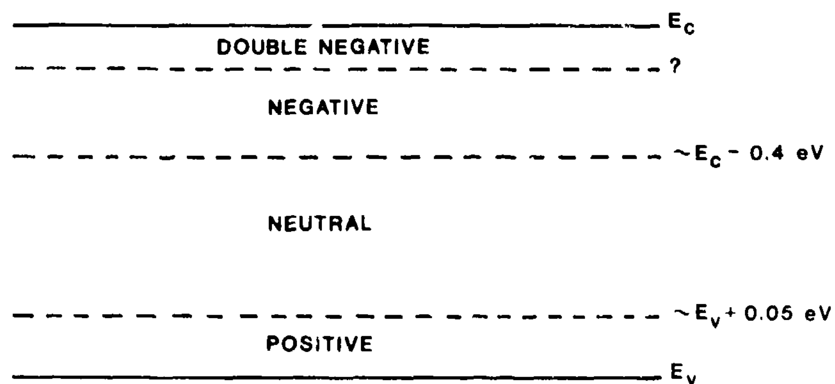

Figure 17. Illustration of the energy levels and charge states associated with the vacancy in silicon.

The vacancy is quite mobile in silicon at room temperature (i.e., ~300°K), and hence is referred to as an unstable defect. After vacancy introduction by irradiation, vacancies move through the lattice and form more stable defects, such as divacancies and vacancy-impurity complexes. If electrical properties are monitored during this defect rearrangement process (referred to as annealing), a decrease in the effectiveness of the damage with increasing time is typically observed. An example of this is

*Recent work (G.D. Watkins and J.R. Troxell, Phys. Rev. Lett. 44, 593 (1980)) indicates that the level structure associated with positive charge states of the vacancy is more complicated than that shown here. However, that work probably does not affect the discussion below of the charge-state dependence of vacancy motion.

shown in Figure 18, where the relative amount of damage present in p-type silicon following bombardment with a 40-nsec burst of electrons (average energy ~1.4 MeV) is plotted versus time following the burst.[9] To obtain these data, carrier lifetime (which depends on the amount of damage present) was measured as a function of time. Data are shown for four irradiation temperatures, and a pronounced recovery stage (i.e., a decrease in the amount of damage present) is observed in all cases. A characteristic recovery time can be extracted from the data, since they exhibit a simple exponential decrease in the amount of damage present (i.e., first-order kinetics is followed). Figure 19 shows recovery times obtained in this manner at various temperatures.[9] This plot yields an activation energy (0.32 eV) associated with defect motion. If the data are extrapolated to low temperatures, good agreement with the electron spin resonance (ESR) data of Watkins[10] is obtained (solid circles). He attributed his ESR observations to the motion of neutral vacancies. Thus, the transient process exhibited in Figure 18 is most likely due to reordering of radiation-induced isolated vacancies in a neutral charge state. Near room temperature, these findings indicate that stable defects are formed within a few seconds after the radiation burst.

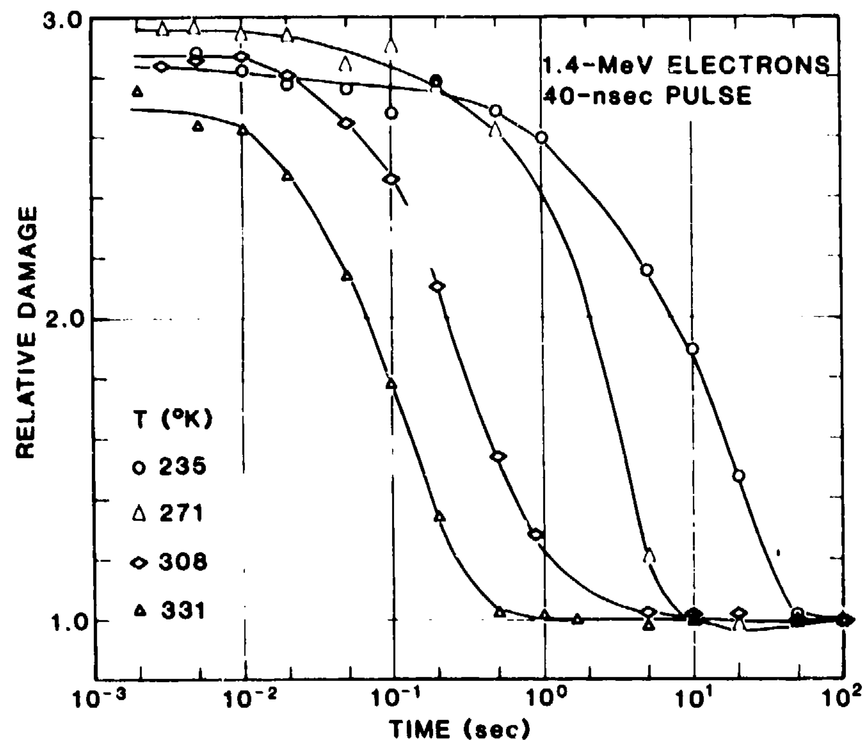

Figure 18. Relative amount of damage present in electron-irradiated silicon versus time following the radiation burst.[9] Data obtained at four temperatures are shown.

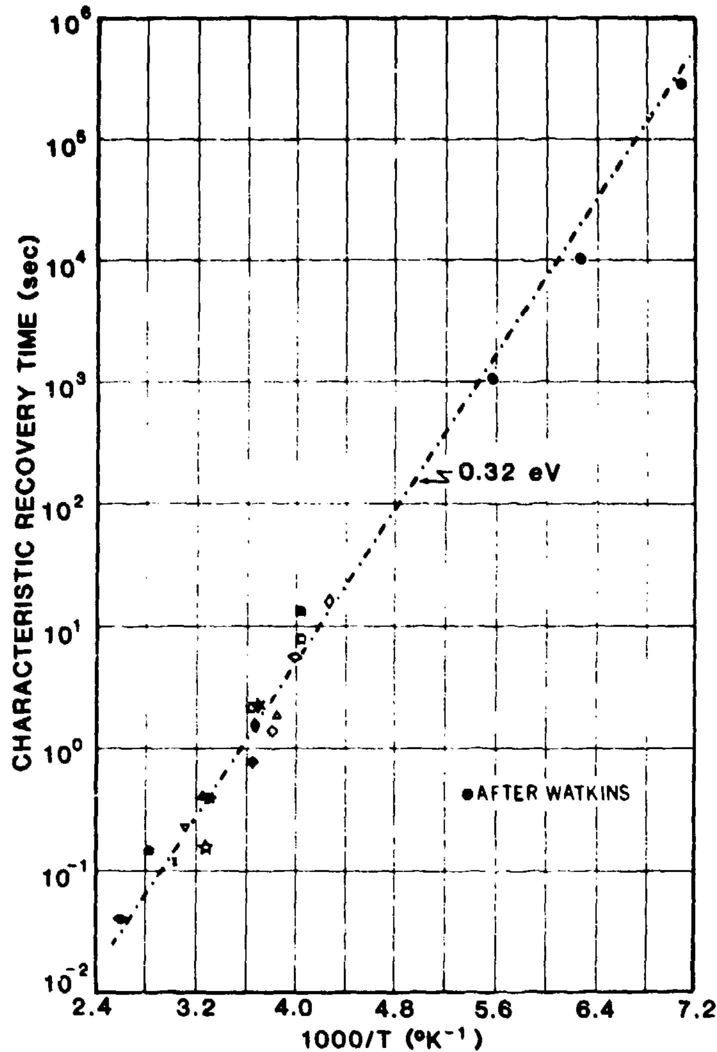

Figure 19. Characteristic recovery time versus reciprocal temperature derived from data of the type shown in Figure 18.[9] Data obtained by Watkins using ESR are also shown.[10]

There are several ways to alter the charge state of defects (Figure 20). By varying the resistivity or type (i.e., n- or p-type) of the irradiated material, the Fermi level position will vary. For example, if the experiment leading to the data of Figures 18 and 19 were performed for n-type silicon, vacancies would be introduced in a negative charge state and would then rearrange much faster than in p-type material. Another way of changing the charge state is by increasing the excess carrier concentration (the injection level). This can occur due to the accompanying ionization produced by the

WAYS TO ALTER DEFECT CHARGE STATES

- MATERIAL TYPE AND RESISTIVITY
- IONIZATION BY BOMBARDING PARTICLES
- OPTICAL EXCITATION
- ELECTRICAL INJECTION

Figure 20. Several ways to alter the charge state of defects.

bombarding particles themselves. The injection level of the irradiated material can also be varied by optical excitation and by electrical injection of carriers.

The injection level present during and shortly after defect formation is important in determining the annealing rate in irradiated silicon. This process is referred to as ionization-enhanced (or injection-stimulated) annealing. Changing the mobility of primary defects, such as the vacancy, by charge-state alteration is just one of the mechanisms thought to be responsible for injection-stimulated recovery in irradiated materials and devices. Figure 21 lists several of these mechanisms. Another model, proposed by Bourgoin and Corbett,[11] is referred to as an alternating saddle point mechanism. In this description, illustrated schematically in Figure 21, a defect in a certain charge state (① in the figure) has a maximum potential energy in configuration A and a minimum potential energy in configuration B. When that defect is in a second charge state (② in the figure), it is at a potential maximum in configuration B and at a minimum in configuration A. Thus, the two charge states of the defect are viewed as having opposing stability. By repeatedly changing the charge state between ① and ②, the defect will reconfigure from A to B, from B to A, etc., and thereby migrate athermally through the lattice.

IONIZATION-ENHANCED ANNEALING

- CHARGE STATE EFFECT
- BOURGOIN MECHANISM

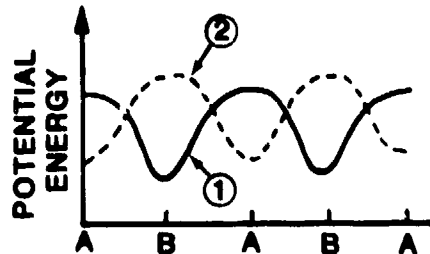

- RECOMBINATION ENHANCEMENT
- OTHER MODELS

Figure 21. Several mechanisms thought to be responsible for ionization-enhanced annealing.

Recombination-enhanced annealing[12] is a process in which the energy given off during nonradiative recombination of electron-hole pairs activates defect reordering. A conversion of electronic energy into vibrational energy is thought to take place through electron-phonon coupling at defect sites. Other models of ionization-enhanced annealing are also described in the literature.[13] The dominant mechanism responsible for this process evidently depends on the type of material being studied (e.g., Si vs. GaAs) and the experimental conditions.

Once defect migration and rearrangement has occurred, a relatively stable defect configuration will be reached for materials and devices irradiated at a given temperature. The electrical properties of these defects also exhibit an "injection-level dependence" which is different in nature from the ionization-enhanced phenomena just described. In particular, minority-carrier lifetime in irradiated silicon is dependent on the excess carrier density present during measurement. Again, this effect is not associated with annealing since defect rearrangement is assumed to have already taken place. Rather, the injection-level dependence of carrier lifetime is

attributable to the recombination properties of radiation-induced defect levels. (The effects to be described also generally apply for non-radiation-induced defects.)

Figure 22 illustrates the dependence of lifetime on excess carrier density for gamma-irradiated silicon measured at four temperatures. The behavior exhibited is typical of that for radiation-induced defects. There is a plateau region at low injection levels. As the injection level is increased, lifetime also increases. At high excess densities, a peak is reached and lifetime then decreases. Such behavior can be accounted for on the basis of recombination through two independent levels in the bandgap, as illustrated in Figure 23. At low injection levels, Level 1 dominates. At high excess densities, recombination through Level 2 becomes important. When the lifetimes τ_1 and τ_2 associated with these two levels are added reciprocally, the solid line in the figure results. The basis for such a description lies in the Hall-Shockley-Read recombination model.[14] In general, the lifetime associated with a single recombination level can either increase or decrease with injection level. At low injection levels, levels relatively deep in the gap typically dominate the recombination process and such levels exhibit an increase in lifetime with excess density. At high injection levels, shallow recombination levels dominate and the recombination rate typically increases with excess density. Qualitatively, the increase in lifetime with excess density observed at low injection levels can be thought of as being due to a "traffic jam" occurring at the dominant recombination level. That is, most centers are occupied by minority carriers and relatively few are available to trap additional minority carriers. Thus, the minority-carrier lifetime increases. At higher excess densities, this "jam" is relieved by recombination through a second level, and lifetime then decreases. The charge state of defect levels can change at high excess densities due to a shift in the quasi-Fermi level, thereby placing specific centers in a more favorable condition for capturing carriers. This charge state change enhances recombination at such centers.

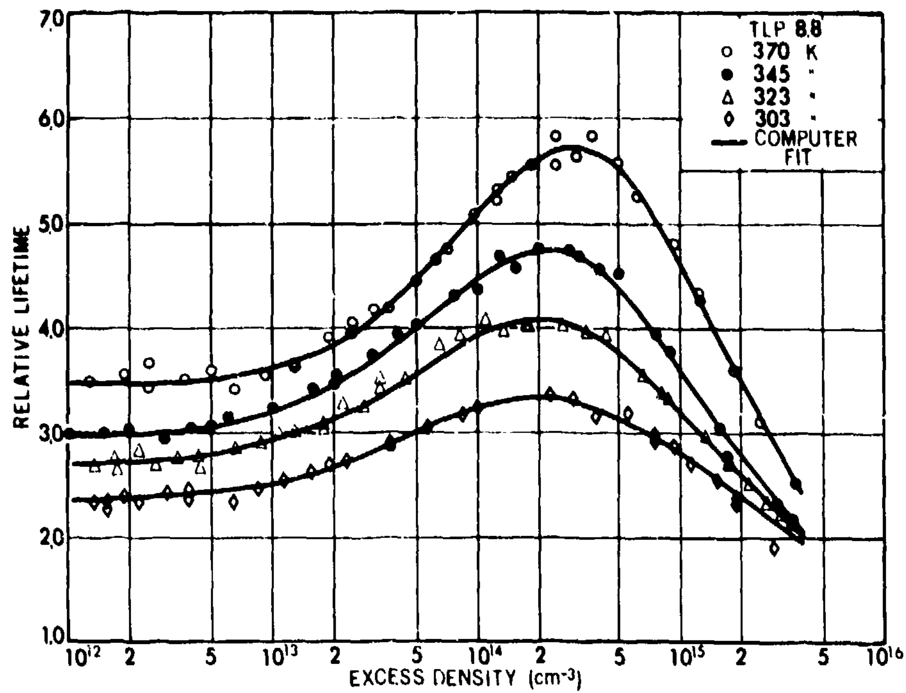

Figure 22. Illustration of the injection-level dependence of minority-carrier lifetime in irradiated silicon.

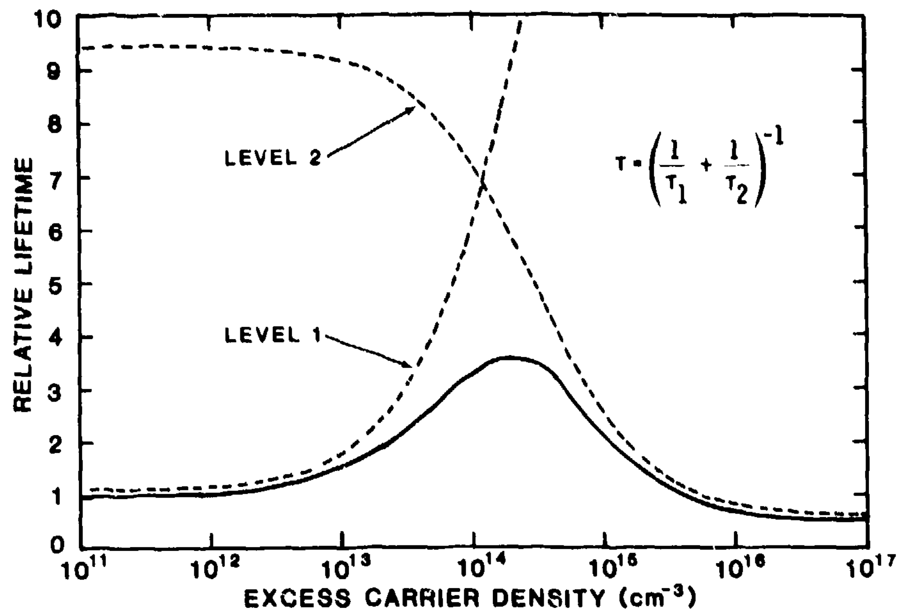

Figure 23. Illustration of the two-level model for describing the observed injection-level dependence of carrier lifetime.

3.3 NEUTRON EFFECTS

A single fast neutron striking a silicon atom can cause a large number (e.g., a few hundred to a few thousand) of displacements to occur in a relatively localized region. The effects of such disordered regions, or defect clusters, have often been described using the Gossick model.[15] In this model (Figure 24), a damaged region of radius R_1 is produced as a result of a single neutron colliding with a target nucleus. (Spherical symmetry is assumed in the Gossick model to simplify the mathematical description. Disordered regions are not thought to be spherical, however, as discussed below.) The interior of the damaged region (radius R_0) is viewed as being compensated intrinsic (electrically neutral). The damaged zone is charged by trapped majority carriers in an outer shell between R_0 and R_1. An undamaged space-charge region (between R_1 and R_2), depleted of majority carriers, surrounds the damaged region. The trapped majority-carrier charge is balanced by the charge associated with ionized impurity atoms in the space-charge region. In the Gossick description, a disordered region presents a potential barrier to majority carriers and a potential well to minority carriers. Thus, defect clusters are viewed as being very efficient regions for minority-carrier recombination.

The effects of neutron bombardment on the electrical properties of silicon have been accounted for reasonably well, at least qualitatively, using the Gossick model, especially in the case of carrier recombination. On the other hand, the actual physical nature of neutron-produced damage in silicon is a subject of current research. It is likely that the damaged zone produced by a single neutron interaction contains a number of subclusters, where defect densities are high, and a larger quantity of relatively isolated defects. The shape of this zone has been viewed by some workers to be ellipsoidal. Other researchers have calculated widely varying shapes. For the present purposes, the important point is that neutron bombardment affects the electrical properties of silicon in unique ways. The major changes that occur are now discussed.

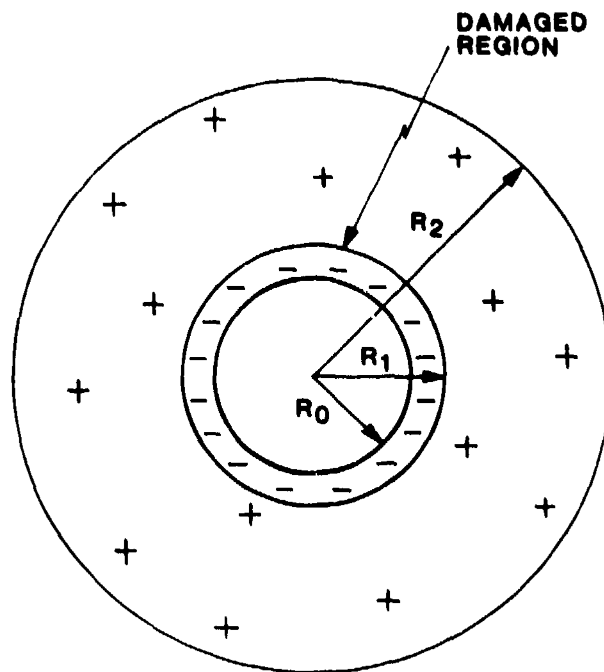

Figure 24. Illustration of the Gossick model for defect clusters in neutron-irradiated n-type silicon.[15]

Neutron bombardment produces the following changes in the electrical properties of bulk silicon (Figure 25): 1) minority-carrier recombination lifetime (τ_r) decreases; 2) majority-carrier concentration (n) decreases (carrier removal); 3) carrier mobility (μ) decreases. In general, these changes are dependent on neutron energy and on time following a neutron burst. (In most of the experiments performed which illustrate these dependences, carrier lifetime (or a device property related to lifetime) has been monitored.) Figure 26 illustrates the relative sensitivity of lifetime, carrier concentration, and mobility to neutron bombardment. Depicted is the case of 2 ohm-cm n-type silicon irradiated with fission neutrons. (The subscript "o" denotes pre-irradiation values.) It is seen that lifetime is much more sensitive to irradiation than the other properties, particularly when the pre-irradiation lifetime is relatively long. Carrier removal becomes important in this example above 10^{13} n/cm^2, whereas mobility changes are unimportant until 10^{14} n/cm^2 is reached.

NEUTRON-INDUCED CHANGES IN THE ELECTRICAL PROPERTIES OF SILICON

- CARRIER LIFETIME DECREASES
- CARRIER CONCENTRATION DECREASES
  (CARRIER REMOVAL)
- CARRIER MOBILITY DECREASES

Figure 25. Effects of neutron bombardment on the electrical properties of bulk silicon.

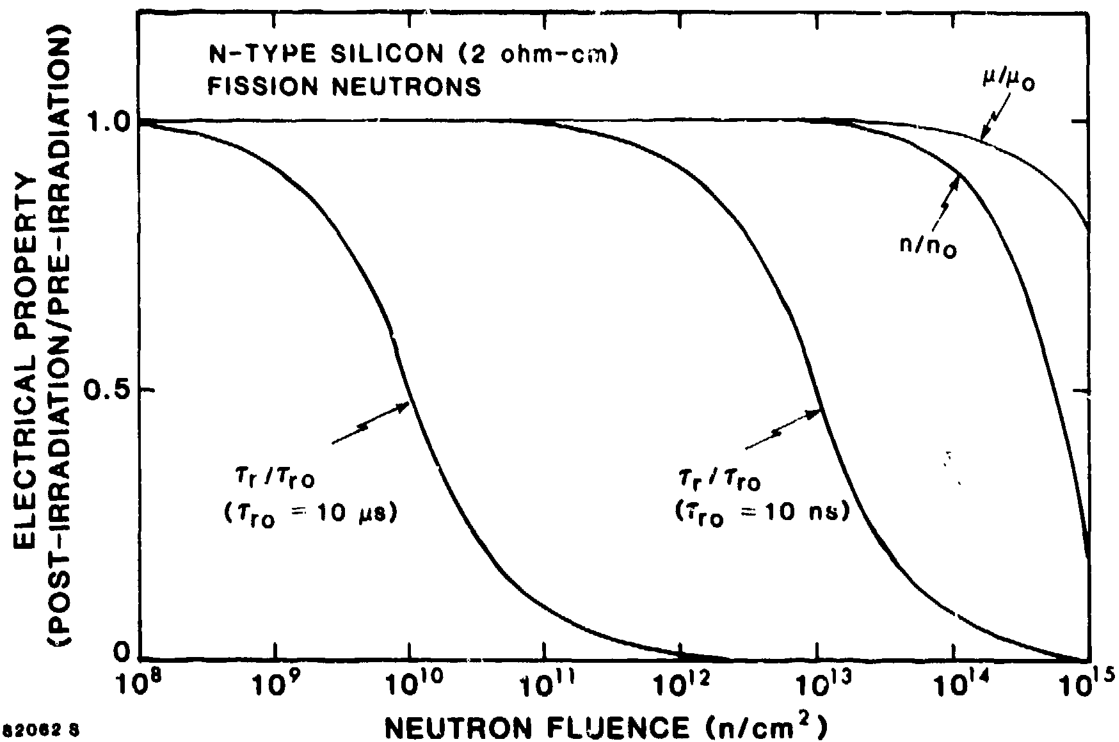

Figure 26. Illustration of the relative sensitivity of lifetime, carrier concentration, and mobility to neutron bombardment. Two values of pre-irradiation lifetime are considered.

Figure 27 illustrates the neutron energy dependence of displacement damage in silicon calculated by Holmes.[16] This dependence was determined by multiplying the energy deposited into displacement damage by the total neutron cross section at each neutron energy. The calculated 14-MeV/fission damage ratio, in terms of lifetime degradation, is 2.5. Experimentally determined values for this ratio range from 2 to 3.

It is important to distinguish between the time-dependent displacement effects occurring after a neutron burst and the permanent effects of such bombardment. Figure 28 illustrates the events following a burst for bulk silicon and silicon devices at room temperature. The change in lifetime (or transistor gain) that occurs is shown. Following an abrupt decrease coincident with the radiation pulse, lifetime then exhibits a recovery due to the recombination (i.e., annihilation) and rearrangement of defects within disordered regions. The effectiveness of these defects in degrading the lifetime decreases with time. The recovery period, referred to as short-term annealing, begins shortly after damage creation and is essentially complete in a time on the order of one minute after the burst.

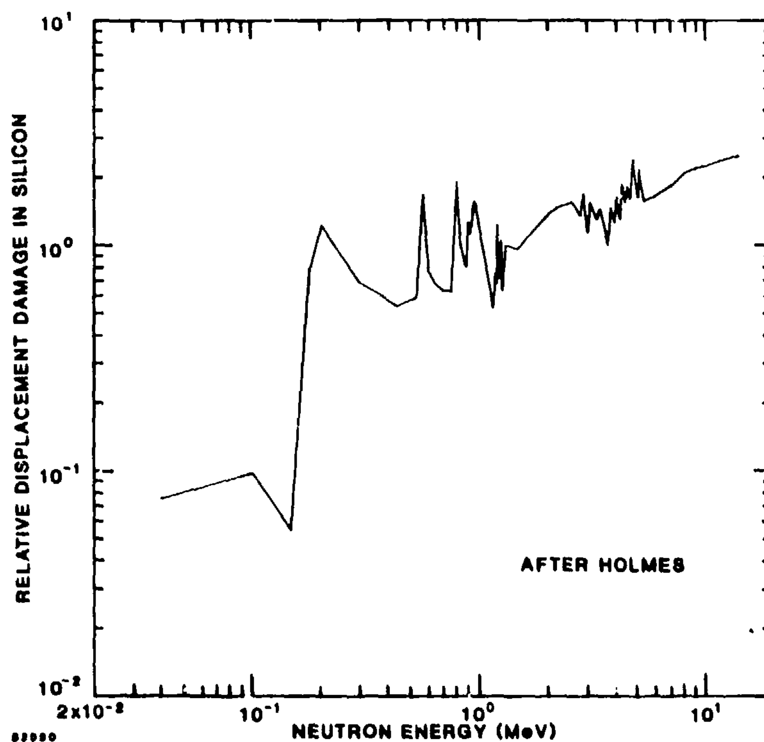

Figure 27. Neutron energy dependence of displacement damage in silicon.[16]

ROOM TEMPERATURE ANNEALING

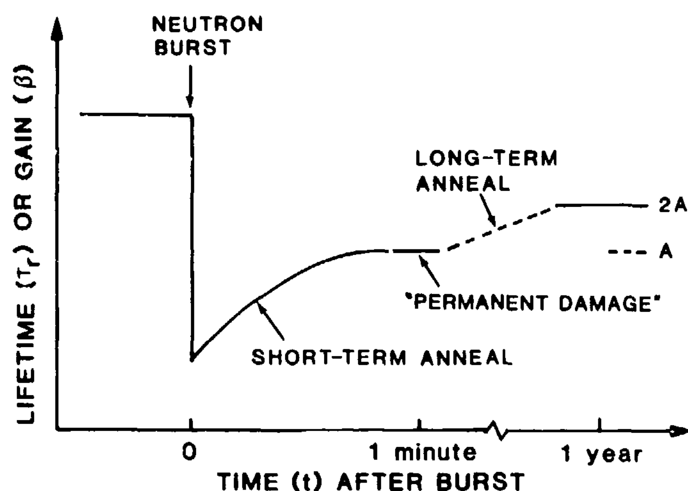

$$\text{SHORT-TERM ANNEALING FACTOR} = AF(t) = \frac{\frac{1}{\tau_r(t)} - \frac{1}{\tau_{ro}}}{\frac{1}{\tau_r(\infty)} - \frac{1}{\tau_{ro}}}$$

FOR TRANSISTORS, SUBSTITUTE β FOR τ_r

Figure 28. Illustration of the short-term and long-term recovery processes that occur in neutron-irradiated silicon.

The damage remaining at that time is called "permanent damage". However, a relatively slow annealing process, or long-term anneal, will continue after the short-term anneal is completed. As much as an additional factor-of-two recovery has been observed over a one-year annealing period at room temperature, as indicated in Figure 28. Also defined in the figure is a short-term annealing factor AF(t), which is commonly employed in the literature as a measure of the recovery that has occurred at a given time following the burst. The annealing factor is the ratio of the amount of radiation-induced damage present at time t to that present at some long time after bombardment (stable damage). Thus, the minimum AF is unity. Note that for transistors the AF definition is the same as for lifetime and is obtained by substituting β (current gain) for τ_r. Examples of short-term annealing phenomena are now presented, followed by examples of permanent damage effects.

Figure 29 presents short-term annealing data for 11 ohm-cm p-type bulk silicon samples irradiated with bursts of both 14-MeV and reactor neutrons.[17] Shown is AF versus time following the burst. For this experiment, minority-carrier lifetime was the monitored quantity. Two important observations are the following. First, the short-term annealing process for neutron bombardment takes place over many decades in time in contrast to the relatively abrupt annealing stage observed for electron-irradiated silicon (Figure 18). This difference is attributable to the various types of defect interactions that may occur in neutron-produced clusters as compared to the less complicated situation that evidently prevails for the case of isolated defect production by electron bombardment. Second, annealing factors at early times are larger in the 14-MeV case than for reactor neutron bombardment. This difference may be due to a slower defect interaction rate in fusion-neutron-produced clusters as a result of a lower defect density therein compared to the fission situation.

Figure 30 shows AF versus time for an irradiated pnp transistor. The neutron energy dependence of short-term annealing is again exhibited. At early times, the 14-MeV AF is ~ 5. Assuming an infinite pre-irradiation gain, this means that the gain at such times will be a factor of ~ 5 less than in the stable-damage situation at long times. This type of consideration needs to be taken into account when designing hardened electronic subsystems.

Gregory and Sander[18] found that the short-term annealing rate is quite sensitive to the injection level present in a device. They also found that the measured AF at a given time correlates quite well with the electron density present in the active region of a device (Figure 31). This may be an injected density or an equilibrium carrier concentration. The injection-level dependence of short-term annealing is an important example of the ionization-enhanced annealing process discussed earlier. Charge state effects appear to play a role in this case.[18]

If carrier lifetime in p-type silicon is monitored at a very low minority-carrier injection level (i.e., electron density), then the correlation shown in Figure 31 suggests that very large AF's will be observed.

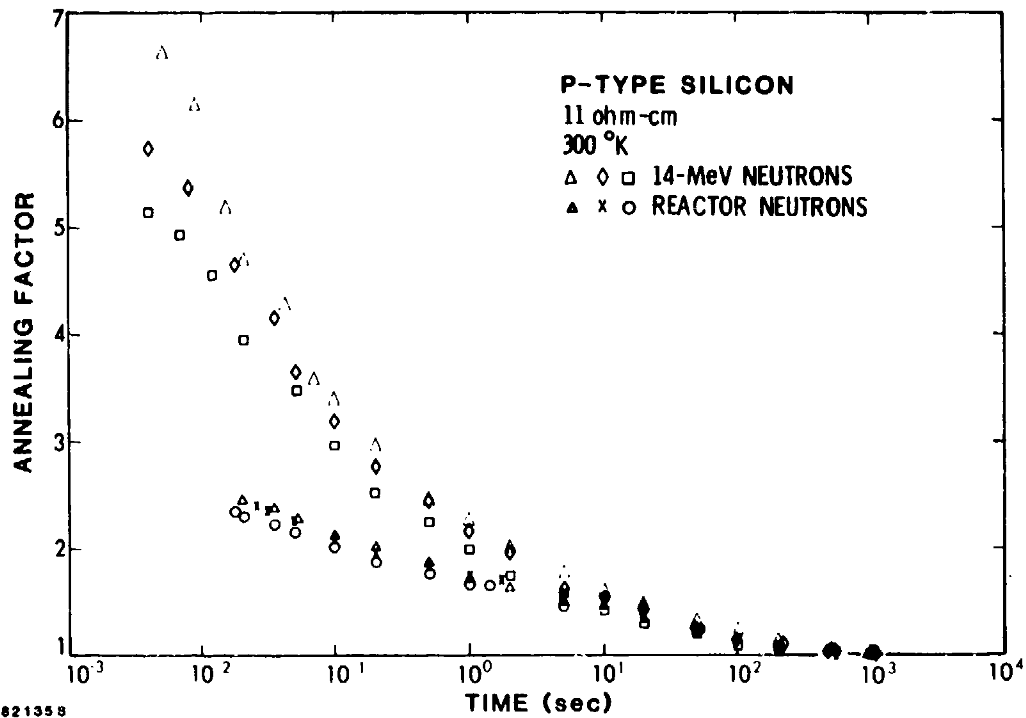

Figure 29. Annealing factor versus time for 11 ohm-cm p-type bulk silicon samples irradiated with bursts of 14-MeV and reactor neutrons.[17]

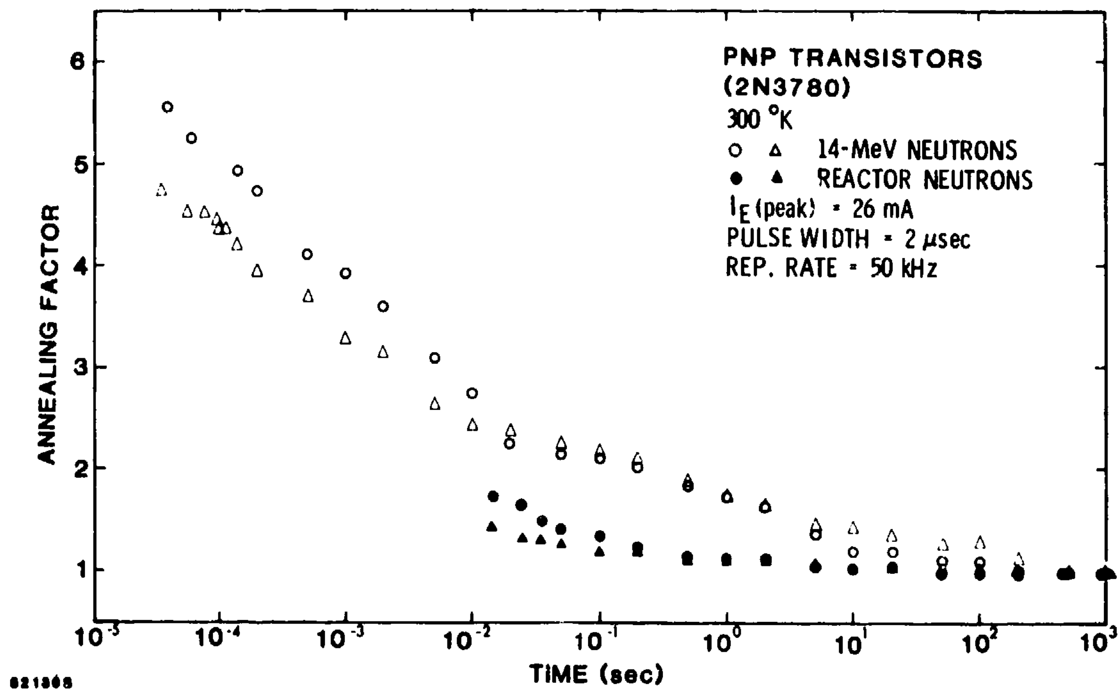

Figure 30. Annealing factor versus time for pnp transistors irradiated with bursts of 14-MeV and reactor neutrons.[17]

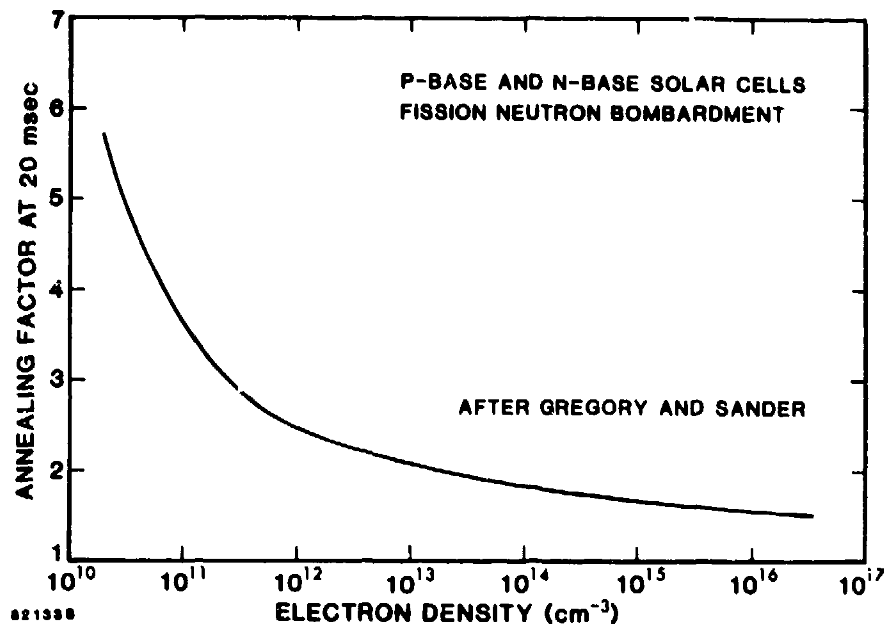

Figure 31. Annealing factor at 20 msec after a fission neutron burst versus electron density for n- and p-base solar cells.[18]

That is the case, as shown in Figure 32 where an AF of 25 occurs at early times.[17] Annealing factors as high as 50 have been observed in other low-injection-level experiments. Figure 33 illustrates the dependence of short-term annealing rate in irradiated npn transistors on the time at which electron injection from emitter to base is initiated.[17] Several microseconds before the neutron burst, the emitter-base bias was reduced to zero. That junction was switched to forward bias after different delay times τ_D, as shown in the figure. After the delay, each 2-μsec pulse of emitter current causes observable recovery to occur.

Sander and Gregory[19] devised a short-term annealing nomograph which aids in the determination of the appropriate AF for a given situation (Figure 34). It was developed for reactor neutron irradiations and assumes, for the case of transistors, that recombination in the emitter-base space charge region dominates gain degradation. This assumption holds for high-frequency transistors. The electron density (which determines the annealing rate) is the same for npn and pnp devices at the center of that region for a given

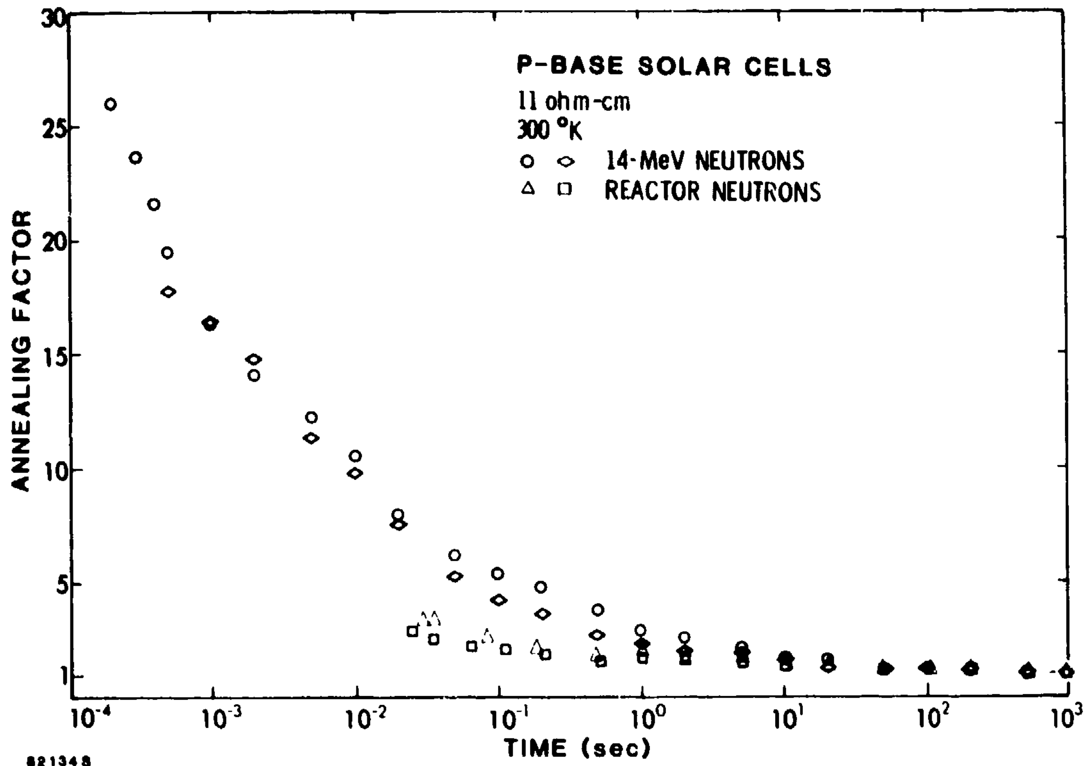

Figure 32. Annealing factor versus time for p-base solar cells irradiated with bursts of 14-MeV and reactor neutrons.[17]

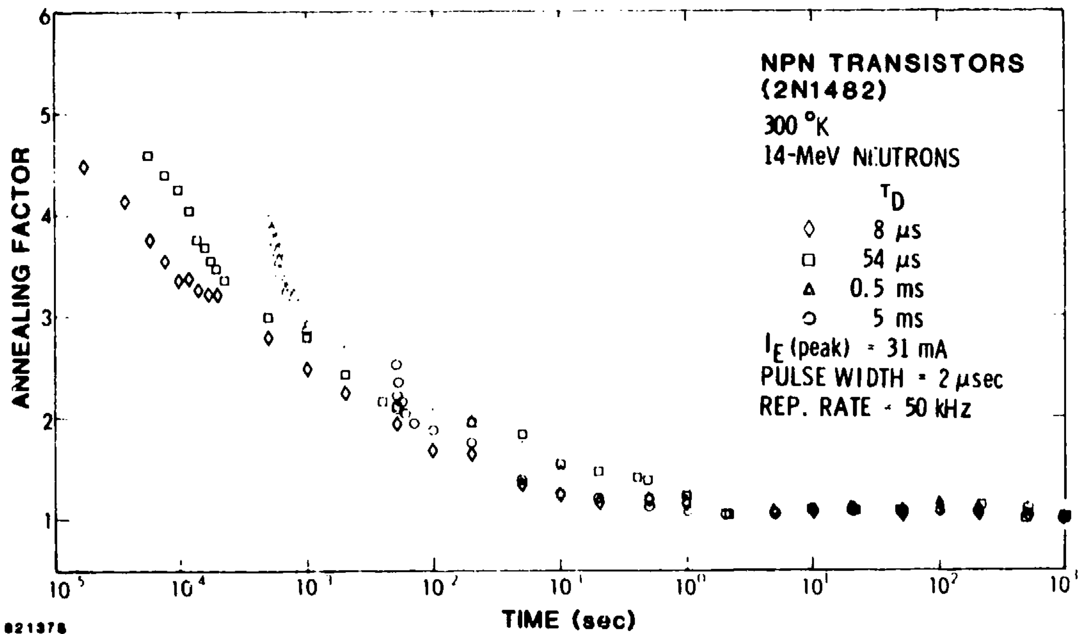

Figure 33. Annealing factor versus time for npn transistors irradiated with a burst of 14-MeV neutrons.[17] The time after the burst at which emitter current was turned on (τ_D) was varied.

SHORT-TERM ANNEALING NOMOGRAPH

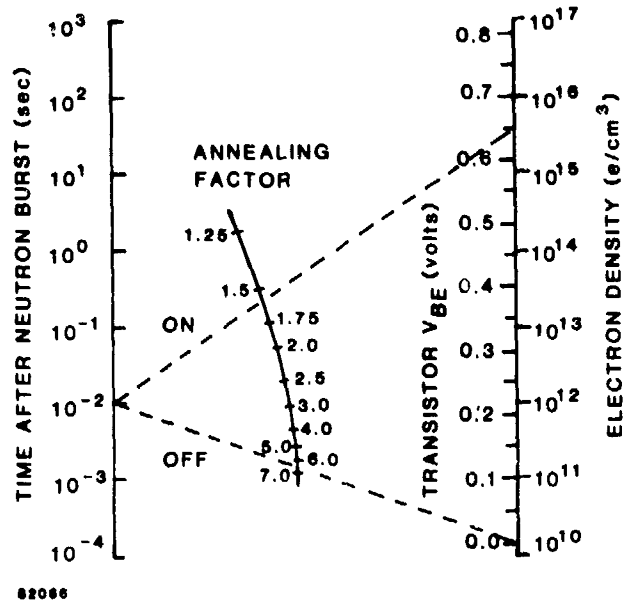

(After Sander and Gregory)

Figure 34. Short-term annealing nomograph for fission-neutron-irradiated silicon devices.[19]

base-emitter bias (V_{BE}). In general, to use the nomograph one must employ the electron density in that region of a device which controls the post-irradiation behavior. A transistor example is illustrated in Figure 34. The AF 10 msec after the burst is $\sim$1.6 for a device that is on (V_{BE} = 0.65 V) during irradiation and during the recovery period. For an off device (V_{BE} = 0 during irradiation and annealing), an AF of $\sim$6.5 is indicated at that same time. Once a device that is off during bombardment is turned on, recovery occurs rapidly, as illustrated in Figure 33.

The permanent damage remaining after short-term annealing has been studied extensively for neutron-irradiated silicon.[20] The rate of stable damage introduction is often expressed in terms of a minority-carrier recombination lifetime damage coefficient K_r (Figure 35):

$$\frac{1}{\tau_r} = \frac{1}{\tau_{ro}} + \frac{\phi}{K_r} \qquad (1)$$

STABLE DAMAGE IN NEUTRON-IRRADIATED SILICON

DEPENDS ON:

- MATERIAL TYPE
- RESISTIVITY
- INJECTION LEVEL
- TEMPERATURE

RECOMBINATION LIFETIME DAMAGE COEFFICIENT (K_r):

$$\frac{1}{\tau_r} = \frac{1}{\tau_{ro}} + \frac{\phi}{K_r}$$

Figure 35. Dependencies for stable damage in neutron-irradiated silicon. Recombination lifetime damage coefficient is also defined.

In this equation, τ_{ro} and τ_r are the pre- and post-irradiation values of lifetime and ϕ is the neutron fluence. (A definition of damage coefficient which is the reciprocal of that given here is also used in the literature.) The value of K_r depends on material type, resistivity, injection level, and temperature. Examples of the room-temperature behavior of K_r (after a one-year anneal) are shown in Figures 36-38.[21] Figures 36 and 37 illustrate the dependence of neutron damage coefficient on resistivity for n- and p-type material, respectively. Data are illustrated for reactor and 14-MeV neutron bombardment. The values of K_r shown were obtained at low injection levels. The increase in K_r with increasing resistivity (i.e., less damage at high resistivities for a given neutron fluence) can be interpreted in terms of the Gossick model as the result of less of a potential well for minority carriers. With a diminished well, defect clusters are less effective in their role as a sink, and recombination region, for such carriers. The diminished well potential results because of a reduced Fermi level difference between the compensated intrinsic interior of the cluster and the neutral bulk.

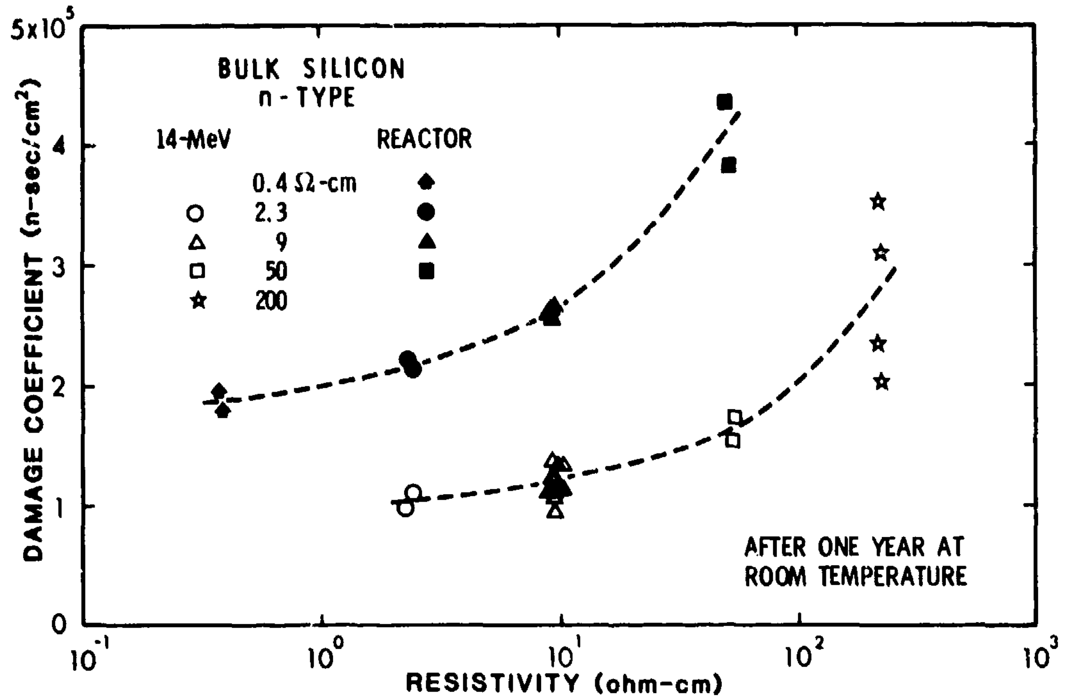

Figure 36. Illustration of the resistivity dependence of the low-injection-level value of K_r for neutron-irradiated n-type bulk silicon.[21]

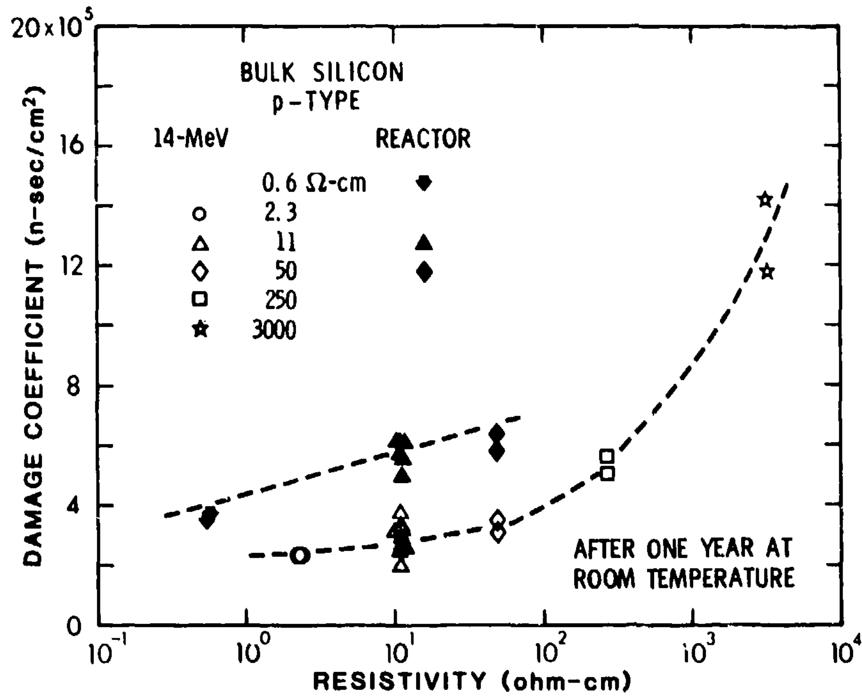

Figure 37. Illustration of the resistivity dependence of the low-injection-level value of K_r for neutron-irradiated p-type bulk silicon.[21]

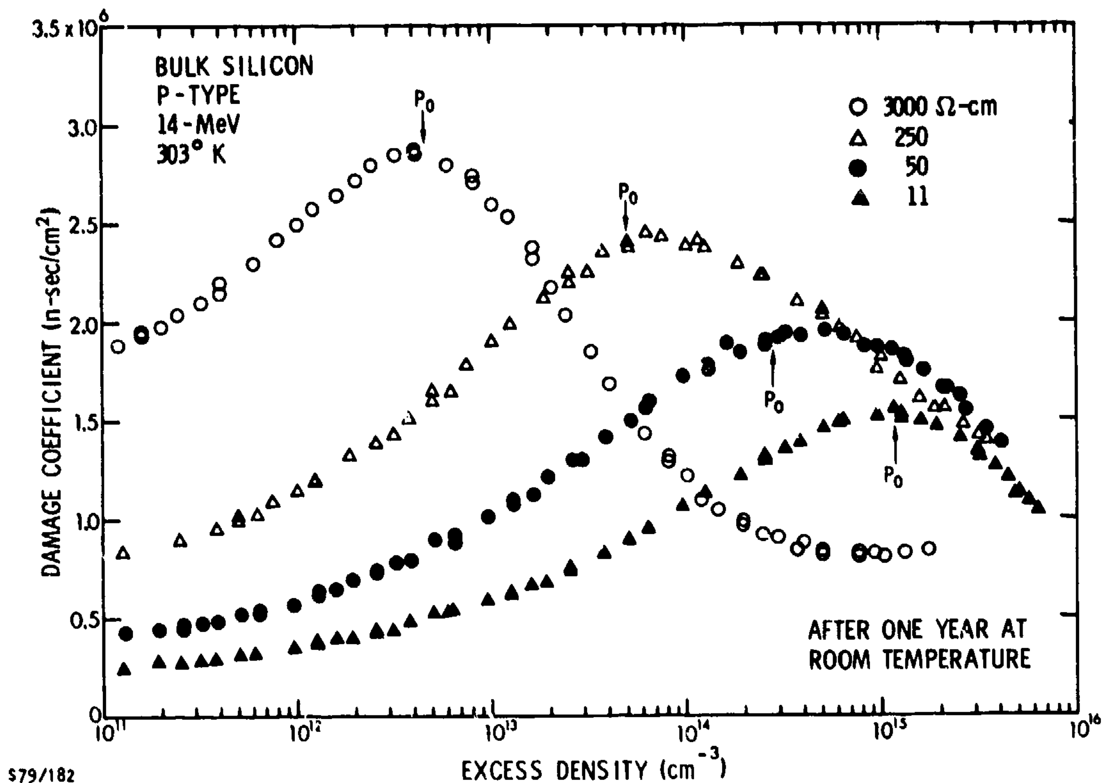

Figure 38. Illustration of the injection-level dependence of recombination lifetime damage coefficient for 14-MeV neutron-irradiated bulk p-type silicon.[21]

The injection-level dependence of K_r is illustrated in Figure 38 for the case of 14-MeV neutron-irradiated bulk p-type silicon samples of several resistivities. These data are qualitatively similar to those described earlier for gamma-irradiated silicon (Figure 22).

3.4 DAMAGE COEFFICIENTS AND DAMAGE CORRELATIONS

The previous section presented example recombination lifetime damage coefficient data for neutron-irradiated silicon. Additional damage coefficients are given in this section. Example comparisons of the effectiveness of different particles in producing damage are also presented. Figure 39 lists the various parameters on which damage coefficients depend, in general. It is beyond the scope of this tutorial to treat this subject in detail because of these numerous functional dependencies. Rather, examples will be given. Damage coefficient values presented apply for the situation that exists after short-term annealing (but not long-term annealing) has been

DAMAGE COEFFICIENT DEPENDENCIES

- PARTICLE TYPE
- PARTICLE ENERGY
- MATERIAL TYPE
- RESISTIVITY
- IMPURITY SPECIES AND CONCENTRATION
- INJECTION LEVEL
- TEMPERATURE
- TIME AFTER IRRADIATION

Figure 39. Parameters that damage coefficients depend on in silicon.

completed. (For a more detailed discussion of damage coefficients and damage correlations, see Refs. 22 and 23.)

Neutron damage coefficients and neutron-induced carrier removal rate are defined in Figure 40. Example values for these quantities are also given. In general, neutron damage coefficients are only weakly dependent on the dopant element used (e.g., P vs. As) and the concentration of other impurities present (e.g., oxygen), but do depend on material type and resistivity. An exception to this is that the values listed for generation lifetime damage coefficient evidently are applicable to both n- and p-type silicon of various resistivities.[24]

In contrast to the situation for neutron bombardment, damage coefficients for particles which produce isolated defects (photons and electrons) are strongly dependent on the impurity element present and its concentration. For example, lifetime damage coefficients for Co^{60} gamma-irradiated silicon depend on oxygen concentration. Again, the variety of functional dependencies that damage coefficients exhibit is too broad to consider in detail here.

NEUTRON DAMAGE COEFFICIENTS FOR SILICON

- RECOMBINATION LIFETIME: $\tau_r^{-1} = \tau_{ro}^{-1} + \phi / K_r$

  FOR N-TYPE, LOW RESISTIVITY, AND LOW INJECTION :

  $K_r \cong 10^5$ n-sec/cm^2 (Reactor Neutrons)

  $K_r \cong 4 \times 10^4$ n-sec/cm^2 (14-MeV Neutrons)

- GENERATION LIFETIME: $\tau_g^{-1} = \tau_{go}^{-1} + \phi / K_g$

  FOR N-TYPE AND P-TYPE:

  $K_g \cong 7 \times 10^6$ n-sec/cm^2 (Reactor Neutrons)

  $K_g \cong 3 \times 10^6$ n-sec/cm^2 (14-MeV Neutrons)

- CARRIER REMOVAL: $n(\text{post}) = n(\text{pre}) - (\Delta n / \Delta \phi)\phi$

  FOR N-TYPE, $N_d = 10^{15}$ cm^{-3}, REACTOR NEUTRONS:

  $\Delta n / \Delta \phi \cong 6$ n^{-1}-cm^{-1}

- MOBILITY : $\mu^{-1} = \mu_0^{-1} + K_\mu \phi$

  FOR 2 ohm-cm, N-TYPE AND P-TYPE, REACTOR NEUTRONS:

  $K_\mu \cong 3 \times 10^{-19}$ V-sec/n

Figure 40. Damage coefficients and carrier removal rate for neutron-irradiated silicon.

Figure 41 illustrates the particle energy dependence of carrier lifetime degradation in electron- and proton-bombarded n-type silicon. Also shown for comparison are relative degradation values for 1-MeV and 14-MeV neutrons and for Co^{60} gamma-ray irradiation. The curves and values shown in the figure are only approximate, but do allow semi-quantitative comparisons to be made of the effectiveness of the various particles. As an example, for a given fluence of particles with energy near 1 MeV, protons are nearly two orders of magnitude more effective than neutrons; neutrons are more damaging than electrons by about the same factor, and electrons are more than an order of magnitude more effective than gamma rays.

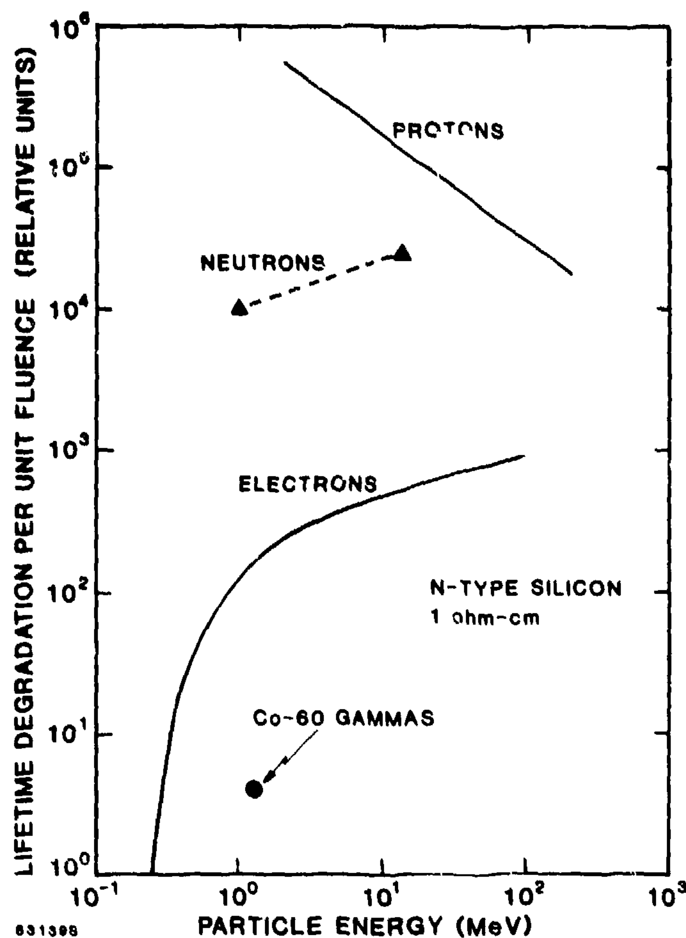

Figure 41. Comparison of the effectiveness of various particles in degrading carrier lifetime in silicon.

Figure 42 shows damage correlations for three types of particles incident on 1 ohm-cm n-type silicon: 1-MeV neutrons, 20-MeV protons, and 3-MeV electrons.[22] The data shown are applicable for high injection conditions (injection ratio = 0.1). The effectiveness of the three particle types in degrading lifetime is compared, and the values shown are consistent with the information in Figure 41. As an example, a given 20-MeV proton fluence is ~300 times more effective than the same 3-MeV electron fluence.

DAMAGE CORRELATIONS

- 1 ohm-cm, N-TYPE SILICON
- INJECTION RATIO: 0.1
- COMPARE 1-MeV NEUTRONS, 20-MeV PROTONS, AND 3-MeV ELECTRONS
- LIFETIME DEGRADATION PER UNIT FLUENCE:

1-MeV NEUTRONS / 3-MeV ELECTRONS:	15 to 50
20-MeV PROTONS / 3-MeV ELECTRONS:	~300
20-MeV PROTONS / 1-MeV NEUTRONS:	5 to 25

AFTER VAN LINT et al.

Figure 42. Example damage correlations for electron-, proton-, and neutron-irradiated silicon.[22]

3.5 RADIATION EFFECTS ON BIPOLAR TRANSISTORS

Ionization and displacement damage alter the electrical properties of bipolar transistors. The important changes are: gain degradation, leakage current increase, and the generation of photocurrents. The first two effects are due to displacement damage (except that one component of gain degradation is ionization-induced, as discussed below) and the last phenomenon is produced by ionization.

The basic effect of ionizing radiation is the generation of electron-hole pairs. Figure 43 gives the average energies required to generate one electron-hole pair in silicon and in silicon dioxide. These values apply for ionizing particle energies considerably greater than the silicon and silicon dioxide bandgaps, respectively. Also given in the figure are the concentrations of electron-hole pairs generated when a dose of 1 rad(Si) is deposited in Si and SiO_2.

ELECTRON-HOLE PAIR GENERATION ENERGIES

- SILICON: 3.6 eV
  - 1 rad(Si) generates 4×10^{13} pairs/cm^3 in Si

- SILICON DIOXIDE: ~18 eV
  - 1 rad(Si) generates $\sim 8 \times 10^{12}$ pairs/cm^3 in Si

Figure 43. Electron-hole pair generation energies for silicon and silicon dioxide.

Figure 44 shows a schematic illustration of a bipolar transistor. Also listed are regions of the device which can contribute to gain degradation. Gain degrades due to the introduction, via displacements, of recombination centers throughout the device and due to the effects of ionizing radiation on the surface. Radiation-induced recombination centers in the neutral emitter, the emitter-base space charge region, the neutral base, and the neutral collector can cause the base current to increase, thus causing the gain to decrease. In practice, lifetime reduction in the neutral collector is unimportant and neutral-base recombination can be substantially reduced by using a narrow base region. (By doing so, the base transit time for carriers can be made much less than the carrier lifetime in that region.) Recombination in the neutral emitter and in the emitter-base space charge region is important for gain degradation.

For bipolar integrated circuit technologies, such as ECL, TTL, and I^2L, radiation-induced recombination in the intrinsic base region is typically unimportant because this region is so narrow. However, the much larger extrinsic base region can contribute to gain degradation, as illustrated in Figure 45 for an I^2L cell. In addition, use of a heavily-doped shallow emitter in ECL and TTL circuits substantially reduces radiation-induced recombination in the neutral emitter. In general, the region (or regions) of a bipolar transistor in an integrated circuit which dominates the radiation-induced gain degradation process depends on device and circuit structures and geometries.

BIPOLAR TRANSISTOR

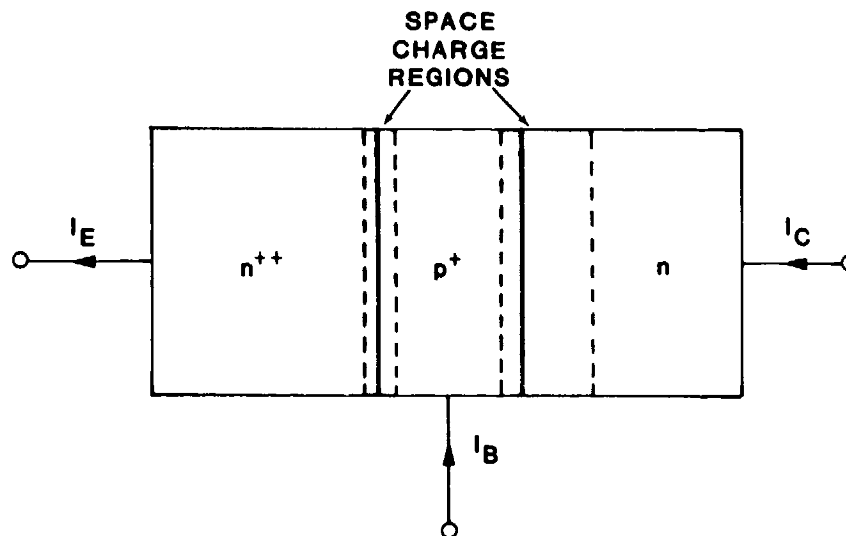

- GAIN DEGRADES DUE TO ENHANCED RECOMBINATION:

Displacement Damage	• Neutral Emitter • Emitter-Base Space Charge Region • Neutral Base • Neutral Collector
Ionization	• Surface

- LEAKAGE CURRENT INCREASES DUE TO GENERATION CENTER INTRODUCTION

Figure 44. Schematic illustration of a bipolar transistor.

Surface recombination can also play an important role in degrading the gain in irradiated transistors. One mechanism for this effect is the change in surface potential produced by the charging up of surface oxide passivation layers by ionizing radiation. Another mechanism is the production of electronic states at the Si-SiO_2 interface. (The charge buildup process and interface state creation are discussed in more detail in Section 4.0.) Alteration of the surface potential can cause the surface recombination velocity to increase, thereby decreasing the gain. Creation of interface states also enhances surface recombination and causes gain degradation.

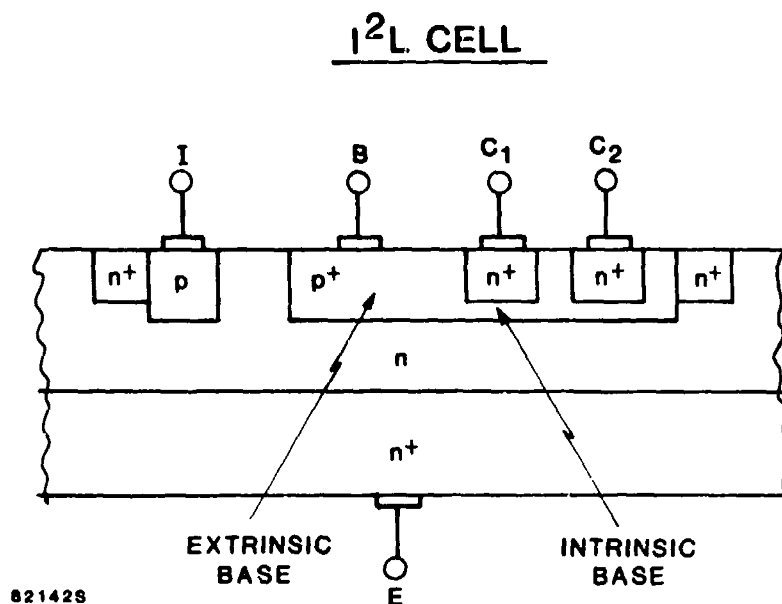

Figure 45. Schematic diagram of an I^2L cell in a bipolar integrated circuit.

An example of neutron-induced current gain degradation in a bipolar transistor is shown in Figure 46.[25] For this example, irradiation to a fluence of 5.6×10^{13} n/cm^2 (1-MeV equivalent) reduced the gain by about one order of magnitude. The temperature dependence of gain is also shown, as are model calculations.

Displacement damage also gives rise to generation centers, and such centers can play an important role in the reverse-biased base-collector junction. The reverse leakage current at that junction will increase due to the thermal generation of electron-hole pairs at radiation-induced centers, and the subsequent sweep-out of these carriers by the high field present. Leakage current can also increase due to generation centers produced at the surface by ionizing radiation.

Figure 47 lists additional radiation-induced effects in bipolar transistors and integrated circuits. Penetrating ionizing radiation, such as Co^{60} gamma rays, will generate electron-hole pairs relatively uniformly throughout a discrete bipolar transistor or an integrated circuit. This pair generation process will give rise to a transient or a steady-state

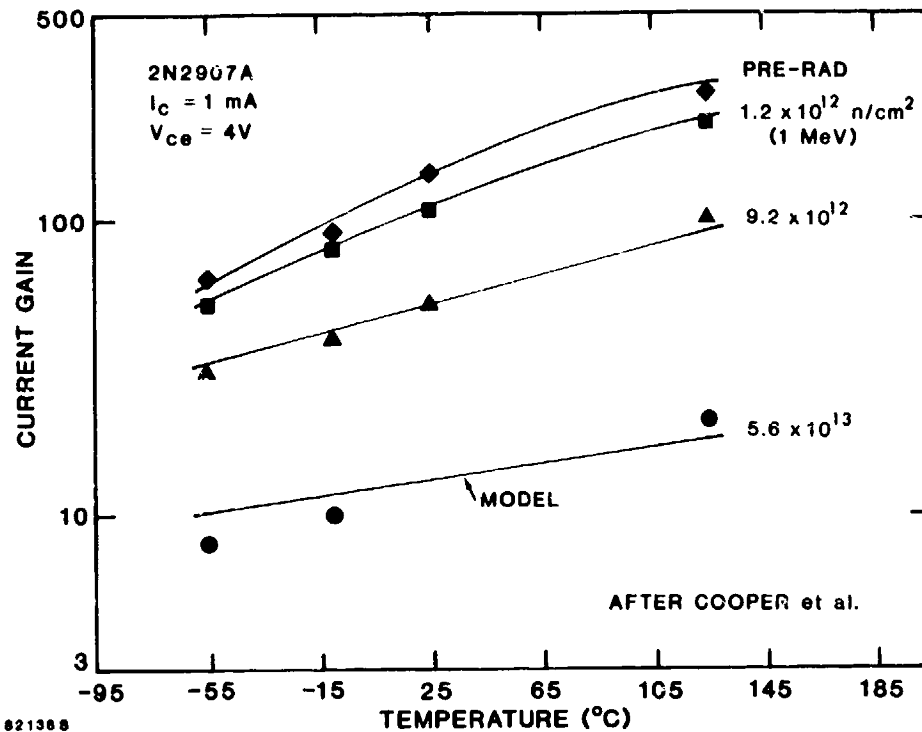

Figure 46. Example of neutron-induced current gain degradation in a bipolar transistor.[25] Shown is gain versus temperature before irradiation and after bombardment to three neutron fluences.

ADDITIONAL EFFECTS IN BIPOLAR DEVICES

- PHOTOCURRENTS
  - TRANSIENT UPSET
  - LATCHUP
- CURRENT HOGGING
- CARRIER REMOVAL EFFECTS
  - DECREASED PUNCHTHROUGH VOLTAGE
  - INCREASED COLLECTOR RESISTANCE

Figure 47. Additional radiation-induced effects in bipolar transistors and integrated circuits.

photocurrent, depending on whether the ionizing radiation is delivered in a pulse or continuously. This photocurrent arises from two sources: 1) carrier pairs generated within the space-charge region of a reverse-biased pn junction are separated by the high field present and are swept out (prompt photocurrent); 2) minority carriers generated within a diffusion length of a reverse-biased pn junction diffuse to that junction where they are swept across (delayed photocurrent). The former mechanism is nearly the same as that for thermally generated carriers. The only difference is that in the thermal case generation occurs through centers near midgap, whereas the generation of carriers by ionizing radiation occurs across the silicon bandgap.

Transient photocurrents created by an ionizing pulse can cause the temporary failure (transient upset) of an integrated circuit. The primary photocurrent arises from device junction regions, and is the sum of the prompt and delayed components described above. When that current is injected into a base region it can forward bias the emitter-base junction, thereby giving rise to a secondary photocurrent which is larger and longer in duration. These currents produce transient errors in both digital and linear circuits. Photocurrents can also cause SCR (silicon-controlled rectifier) action to occur in an integrated circuit (either bipolar or MOS) that contains a parasitic pnpn path. Triggering this parasitic SCR with a pulse of ionizing radiation gives rise to a low-resistance path between two regions in an integrated circuit (usually between the power supply and ground). A high current can flow, and a circuit "latchup" condition results if the low-resistance path remains after the burst. Latchup can cause permanent failure of an integrated circuit to occur.

If the gain of one bipolar transistor in a chain of transistors contained in an integrated circuit degrades more than the gains of neighboring devices, that transistor will require more base current. If the amount of current available is fixed, then a condition of "current hogging" by the degraded device will occur.

Radiation-induced carrier removal can alter the properties of bipolar transistors. The width of the reverse-biased base-collector junction depletion region will increase. This effect gives rise to a decreased punch-through voltage, assuming that the basewidth is reduced due to carrier removal in the base. In addition, carrier removal in the neutral collector will increase the collector resistance.

4.0 IONIZING RADIATION EFFECTS IN SiO_2 FILMS AND SILICON MOS DEVICES

4.1 INTRODUCTION

Ionizing radiation produces effects in SiO_2 films on silicon that alter the electrical properties of MOS devices (Figure 48): buildup of positive charge in the oxide layer, production of electronic states at the Si-SiO_2 interface, and creation of electron traps in the oxide. These effects cause the following changes to occur in devices: threshold voltage shifts and channel mobility degradation. In MOS integrated circuits, photocurrents are produced and transient upset and latchup can also occur. (These topics were addressed in Section 3.0 and are not considered further here.)

This section discusses the important effects of ionizing radiation on MOS devices. A description of the positive charge buildup process is given, followed by discussions of interface state effects and electron trap production. The relation of these phenomena to transient and permanent changes in threshold voltage is then described, including behavior at cryogenic temperatures. Degradation of channel mobility is briefly considered. Ionizing radiation effects on silicon-on-sapphire (SOS) devices are also discussed.

4.2 POSITIVE CHARGE BUILDUP, INTERFACE STATE PRODUCTION, AND ELECTRON TRAP CREATION

Figure 49 shows a schematic illustration of an MOS transistor. There are two types of oxide layers present -- the gate oxide and the field oxide -- and ionizing radiation effects are important in both regions. The mechanisms underlying these effects are the same in both cases, so for simplicity we focus on gate oxide phenomena. It is important to note, however, that the radiation response of MOS structures is quite sensitive to the processing procedures used during device and circuit fabrication. For example, gate oxide processing procedures may differ from those used to prepare the field oxide in the same integrated circuit. This can result in a differing sensitivity to ionizing radiation between the two cases.

IONIZING RADIATION EFFECTS IN SILICON MOS DEVICES

- POSITIVE CHARGE BUILDUP
- INTERFACE STATE PRODUCTION
- ELECTRON TRAP PRODUCTION

THE ABOVE EFFECTS LEAD TO THRESHOLD VOLTAGE SHIFTS AND CHANNEL MOBILITY DEGRADATION

ADDITIONAL EFFECTS:

- PHOTOCURRENTS
  - TRANSIENT UPSET
  - LATCHUP

Figure 48. Effects of ionizing radiation in silicon MOS devices.

MOS TRANSISTOR

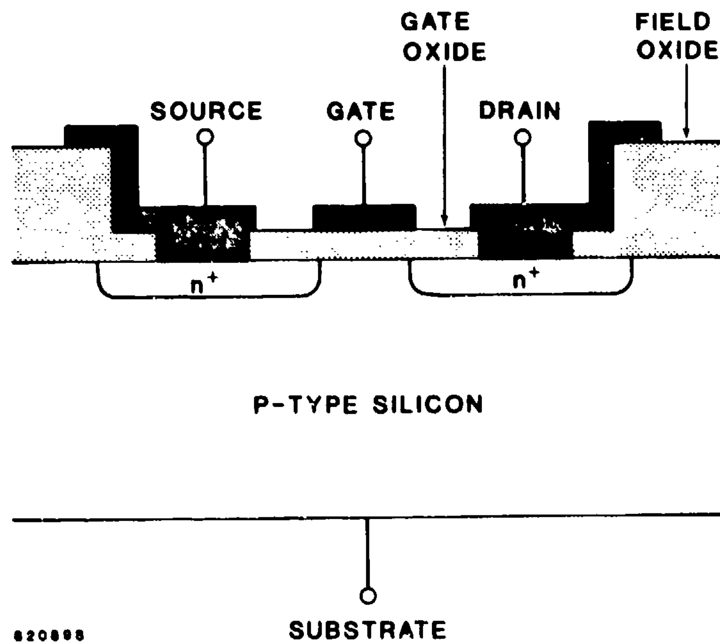

Figure 49. Schematic illustration of an MOS transistor.

Figure 50 shows the energy band diagram for the metal-silicon dioxide-silicon system present in an MOS transistor. In (a), the zero bias condition is illustrated. The SiO_2 bandgap is 8.8 eV, as compared to 1.12 eV for silicon. The slight band bending shown is due to the metal-silicon work function difference. For this example, the surface is already in weak accumulation even for zero bias, and the applied voltage at the metal gate required to make the silicon energy bands "flat" (flatband voltage) is slightly negative. The effect of applying a positive bias to the metal electrode is shown in Figure 50(b). The silicon is now strongly accumulated. Also illustrated is the basic effect of incident ionizing radiation. Shown is the generation of an electron-hole pair by an incident particle. Once generated, the pair may be separated due to the field in the oxide. The electron transports relatively rapidly to the metal and the hole moves relatively slowly toward the silicon. The hole may be trapped near the SiO_2-Si interface in pre-existing sites. This trapping process is referred to as positive charge buildup. Ionizing radiation also creates new states at the interface, as shown in the figure. An important point to note is that charge exchange between the silicon and the interface states occurs in response to Fermi level changes, whereas no such charge communication takes place with the hole traps.

Figure 51 presents a simplified depiction of the charge buildup process in an MOS capacitor on n-type silicon. In (a), the situation prior to irradiation is shown ($t = 0^-$). The corresponding capacitance-versus-voltage (C-V) curve is shown in Figure 52. The flatband voltage pre-irradiation is slightly negative, as was the case in the example of Figure 50. At $t = 0$, an ionizing burst occurs which generates electron-hole pairs throughout the oxide layer (Figure 51(b)). Immediately after the burst ($t = 0^+$), two processes begin to occur simultaneously: recombination and electron transport. Some of the electron-hole pairs will recombine, leaving the situation shown in Figure 51(c). At room temperature, the electron mobility in SiO_2 is ~ 20 cm^2/V-sec whereas the hole mobility is $\sim 2 \times 10^{-5}$ cm^2/V-sec. Thus, electrons that escape initial recombination will transport to the metal electrode in picoseconds, leaving behind the relatively immobile hole population (51(d)). This positive charge causes the C-V curve to shift in a negative direction, as illustrated in Figure 52 for $t = 0^+$. Holes then

ENERGY BAND DIAGRAM FOR THE METAL-SiO_2-SILICON SYSTEM

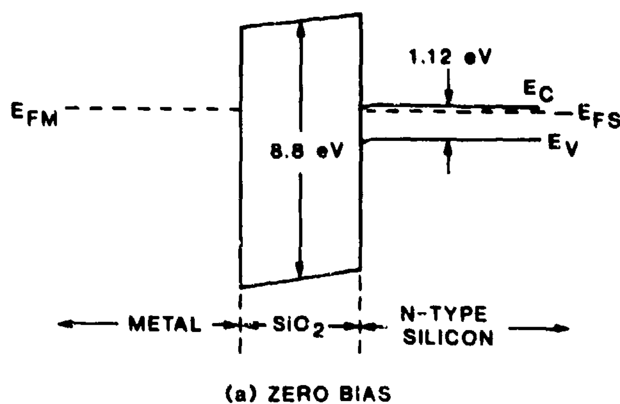

(a) ZERO BIAS

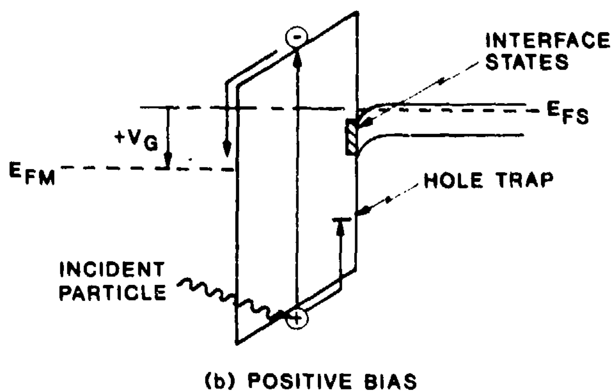

(b) POSITIVE BIAS

821418

Figure 50. Energy band diagram for the metal-SiO_2-silicon system: a) zero bias; b) positive bias plus ionizing radiation.

begin a relatively slow transport toward the SiO_2-Si interface. When holes reach that interface, a portion of them are trapped at centers very near the interface and the remainder pass into the silicon. An intermediate situation during hole transport is illustrated in Figure 51(e); the corresponding C-V curve (Figure 52) has shifted in a positive direction because there is less positive charge present in the oxide. Figure 51(f) shows the stable situation after hole transport has been completed. The final C-V curve is shown in Figure 52 ($t = t_2$); a permanent shift in flatband voltage has occurred as a result of positive charge buildup.

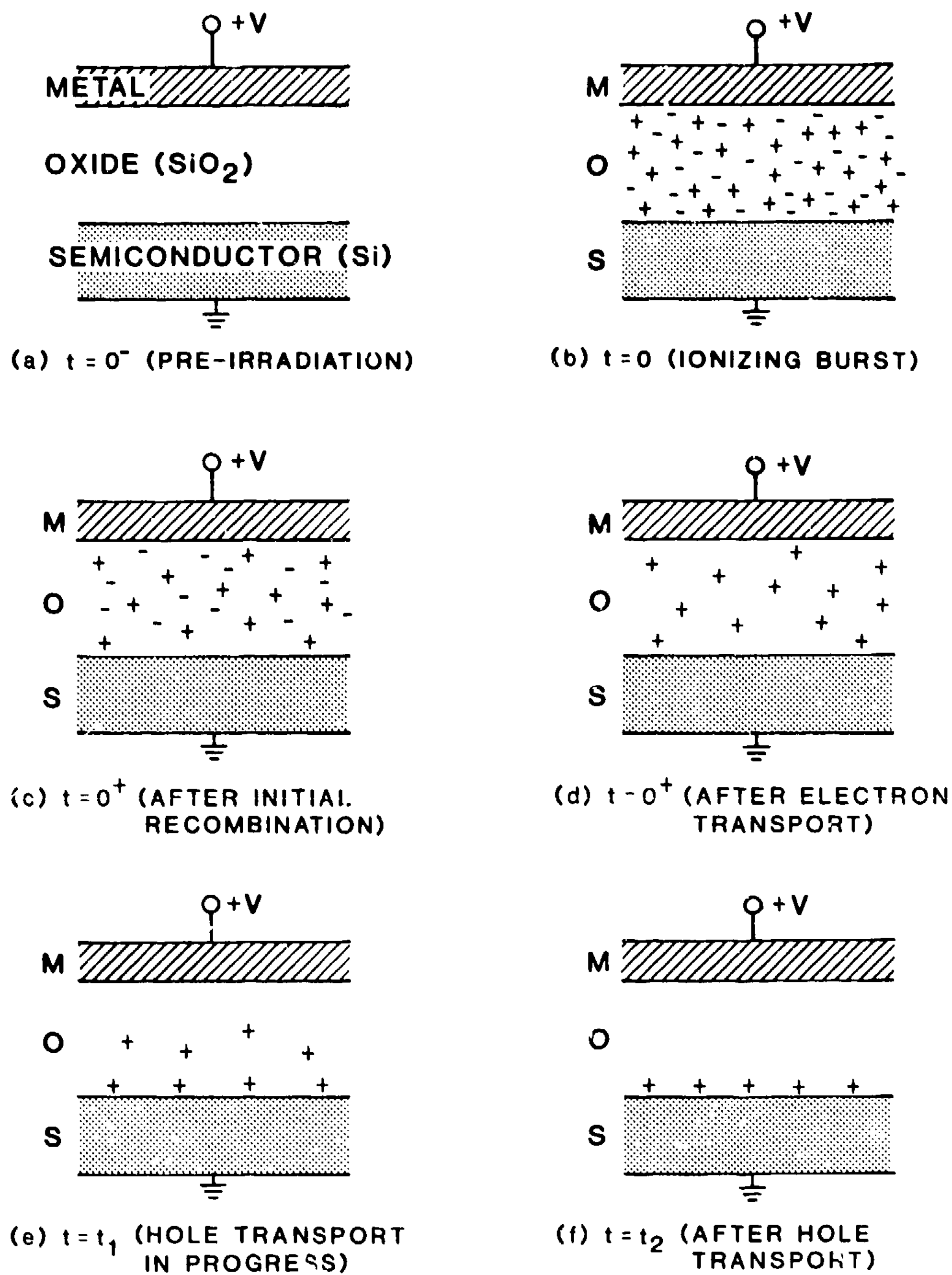

Figure 51. Illustration of recombination, transport, and trapping of carriers in SiO_2 films.

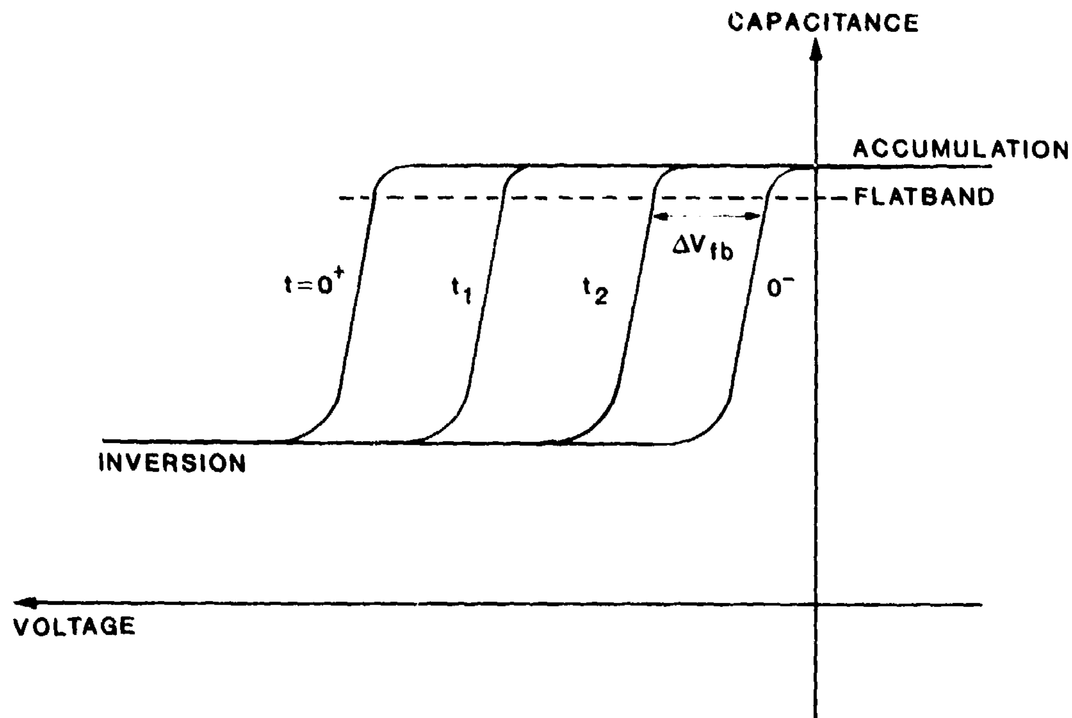

Figure 52. Capacitance-voltage curves corresponding to the conditions illustrated in Figure 51.

In the above discussion, electron trapping in the oxide was neglected because it is negligible compared to hole trapping for the situation described. Electron trapping is considered below in conjunction with electron trap production by ionizing radiation.

The percentage of the holes generated in the oxide by ionizing radiation that eventually are trapped near the SiO_2-Si interface can range from ~1% for hardened oxides to 20-30% or higher for unhardened oxides. The processing procedures used to prepare gate oxides have a significant effect on the radiation hardness of MOS transistors.[26] Another factor to be taken into account is that fraction of the electron-hole pairs generated in the oxide which escape initial recombination. As the oxide field is increased, the fractional yield of pairs increases, as illustrated in Figure 53 for several types and energies of particles incident on SiO_2 films.[27] For example, at a field of 2 x 10^6 V/cm for the 12-MeV electron case, nearly all the generated pairs escape recombination, thereby maximizing the number of holes available to be trapped near the

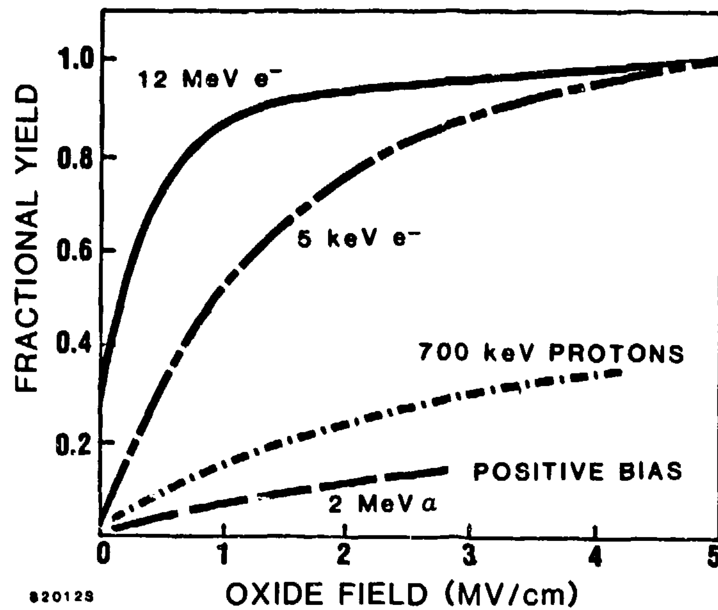

Figure 53. Yield versus field curves for various particles incident on SiO_2 films.[27]

interface. The dependence of yield on particle type and energy is due to differences in the energy loss per unit path length and to details of the recombination process.[27]

At low temperatures, holes are essentially immobile in SiO_2 films except at high fields. Thus, positive charge buildup is considerably larger in this situation. Figure 54 illustrates this effect for MOS capacitors irradiated to 10^5 rads(Si) at both 77°K and room temperature.[28] Flatband voltage shift is plotted versus the voltage applied during bombardment. The room-temperature shifts are relatively small at all applied voltages, whereas flatband shifts at 77°K are quite large due to the "frozen-in" hole population. As the applied voltage is increased from the origin, the flatband shift increases due to the dependence of yield (collected electrons in this case) on field (Figure 53). The decrease in flatband shift evident at high applied voltages is due to a field-activated transport of holes out of the oxide.

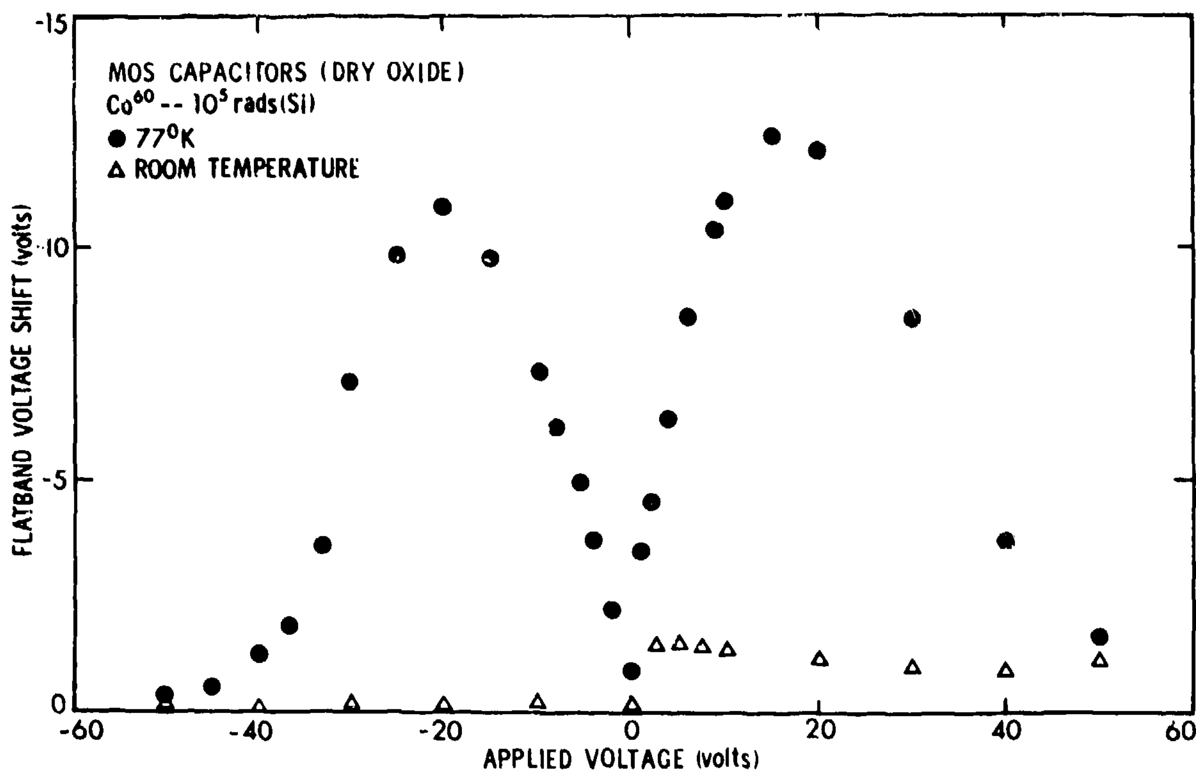

Figure 54. Flatband voltage shift versus voltage applied during irradiation for MOS capacitors irradiated at both 77°K and room temperature.[28]

Ionizing radiation also creates electronic states at the SiO_2-Si interface. Figure 55 gives information concerning radiation-induced interface states. (For a recent description of this process and a proposed model, see Ref. 29.) As noted above, interface states communicate with the silicon and undergo charge exchange in response to changes in the applied gate bias (i.e., to Fermi level changes). The presence of interface states will cause the post-irradiation C-V curve to be stretched out along the voltage axis, as opposed to the idealized parallel shift depicted in Figure 52. This stretch-out occurs because less silicon band bending is achieved at a given gate bias when interface states are present, which in turn is attributable to the required change in interface charge that accompanies a bias change.[30] Interface states are often observed to be negatively charged and thus can affect the threshold voltage in MOS transistors, as described below. The buildup

RADIATION–INDUCED INTERFACE STATES

- CHARGE EXCHANGE WITH SILICON
- CAUSE STRETCHOUT OF C-V CURVES
- CAN AFFECT THRESHOLD VOLTAGE
- TWO-STAGE BUILDUP PROCESS
- FORMATION DEPENDS ON:
  - TIME AFTER IRRADIATION
  - APPLIED FIELD
  - TEMPERATURE
  - IONIZING DOSE
- MECHANISMS NOT COMPLETELY UNDERSTOOD
  - HOLE TRANSPORT IMPORTANT
  - POSITIVE ION RELEASE AND TRANSPORT TO INTERFACE MAY BE IMPORTANT

Figure 55. Information concerning radiation-induced interface states at the SiO_2-Si interface.

of interface states following irradiation occurs in two stages, and their formation depends on time, applied field, temperature, and ionizing dose. The mechanisms of the formation process are not completely understood at present. Hole transport is an important part of the process. One proposed description is the liberation of positive ions by holes as they move through the oxide, followed by the transport of these ions to the interface where a subsequent interaction creates interface states.[29]

Ionizing radiation can cause the creation of neutral electron traps in SiO_2 films[31] (Figure 56). This occurs in practice as a result of radiation received during integrated circuit processing procedures. Examples include electron-beam lithography (~25-keV electrons) and electron-beam deposition of aluminum. (The latter procedure gives rise to X-rays as keV

RADIATION-INDUCED ELECTRON TRAPS

- INTRODUCED BY PROCESSING PROCEDURES
- ELECTRICALLY NEUTRAL
- FORMATION MECHANISM NOT WELL UNDERSTOOD
- UNOBSERVABLE BY C-V UNLESS CHARGED
- CHARGE BY ELECTRON INJECTION
- ENHANCE HOT-ELECTRON INSTABILITIES

Figure 56. Information concerning radiation-induced electron traps in SiO_2 films.

electrons impinge on an aluminum target.) The mechanism responsible for neutral electron trap formation is not well understood at present.

Since they are electrically neutral, the presence of these radiation-induced traps cannot be detected by C-V techniques unless they are first charged by electrons. Use of an ionizing radiation environment, where electron-hole pairs are created, is not an effective way to accomplish such charging because hole trapping usually dominates over electron trapping. Thus, the shift in a C-V curve would only indicate the presence of net positive charge in the oxide. By electrically injecting electrons at the contacts, the neutral traps can be charged and then observed in C-V measurements.[31] This leads us to an important practical problem produced by radiation-induced neutral electron traps: enhancement of hot-electron instabilities. For MOS transistors with VLSI dimensions, hot electron emission from the silicon substrate into the SiO_2 layer can occur, and a portion of these electrons are trapped.[32] This trapped charge causes undesirable effects such as threshold voltage shifts and transconductance degradation.

4.3 THRESHOLD VOLTAGE SHIFTS AND CHANNEL MOBILITY DEGRADATION

The behavior of MOS transistors in an ionizing radiation environment can be accounted for using the same framework as employed above to describe effects in MOS capacitors. Figure 57 illustrates radiation-induced threshold voltage shifts for radiation-tolerant, enhancement-mode n- and p-channel MOS transistors.* In the p-channel case, positive charge buildup in the gate oxide causes a negative shift in threshold voltage (V_t); i.e., a larger gate voltage is now required to turn the device on after irradiation to relatively high doses. For the n-channel transistor, positive charge buildup also causes a negative shift in V_t, but this shift makes it easier to turn the device on. At high doses, two effects can occur, as shown in the figure. A turn-around in the V_t curve is often observed due to the formation of negatively charged interface states which compensate for a portion of the built-up positive charge. The dose at which this effect occurs is processing dependent. The dashed line in Figure 57 illustrates that the shift in V_t may be large enough to cause an enhancement-mode device to convert to depletion mode (i.e., to be turned on with zero gate bias applied). Thus, it is desirable in this case to have the compensating effect of negatively charged interface states.

Positive charge buildup in the p-channel case is less severe than for n-channel devices because the applied gate bias is negative. Thus, holes generated in the oxide move toward the gate electrode and are less effective in shifting V_t. In addition, if the interface state creation model discussed above is correct, significantly less creation of such states should occur. Experimental data support this position, as illustrated in Figure 57 where no turn-around in the p-channel curve is observed at high doses. Further, if interface states introduced in the p-channel case are of the same type as in n-channel devices (i.e., acceptors, which are negative when occupied and neutral when unoccupied), then they should be much less effective. The reason for this is that the Fermi level at turn-on for p-channel transistors is below nearly all interface states in the bandgap and thus they would be neutral.

Transient changes in threshold voltage following an ionizing burst are illustrated in Figure 58.[33] The threshold voltage shift decreases with increasing time, and a dependence on processing procedures is evident. This

*Threshold voltage shifts in transistors are due to the same mechanisms as flatband voltage shifts in capacitors.

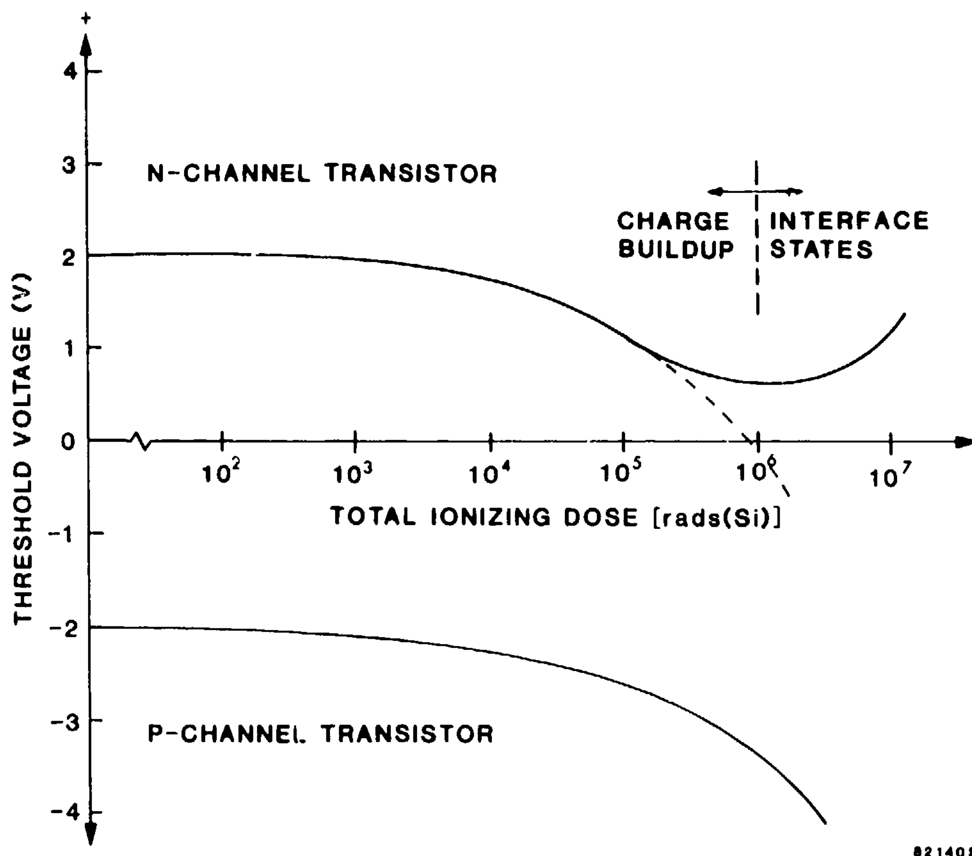

Figure 57. Illustration of the effect of positive charge buildup and interface state production on the threshold voltage in irradiated n- and p-channel MOS transistors.

transient behavior of V_t can be understood qualitatively on the basis of time-dependent hole transport through the oxide, as depicted in Figure 51. It should also be noted that transient and permanent changes in threshold voltage can be much larger for transistors irradiated at cryogenic temperatures, which is consistent with the MOS capacitor data of Figure 54 and the accompanying description.

The channel mobility in irradiated MOS devices degrades due to the presence of both trapped oxide charge near the SiO_2-Si interface and interface states. Additional scattering results for carriers being transported along the channel. Channel mobility degradation is only important at relatively high ionizing doses. Figure 59 shows the variation of field-effect mobility (a quantity related to, but less than, channel mobility) with

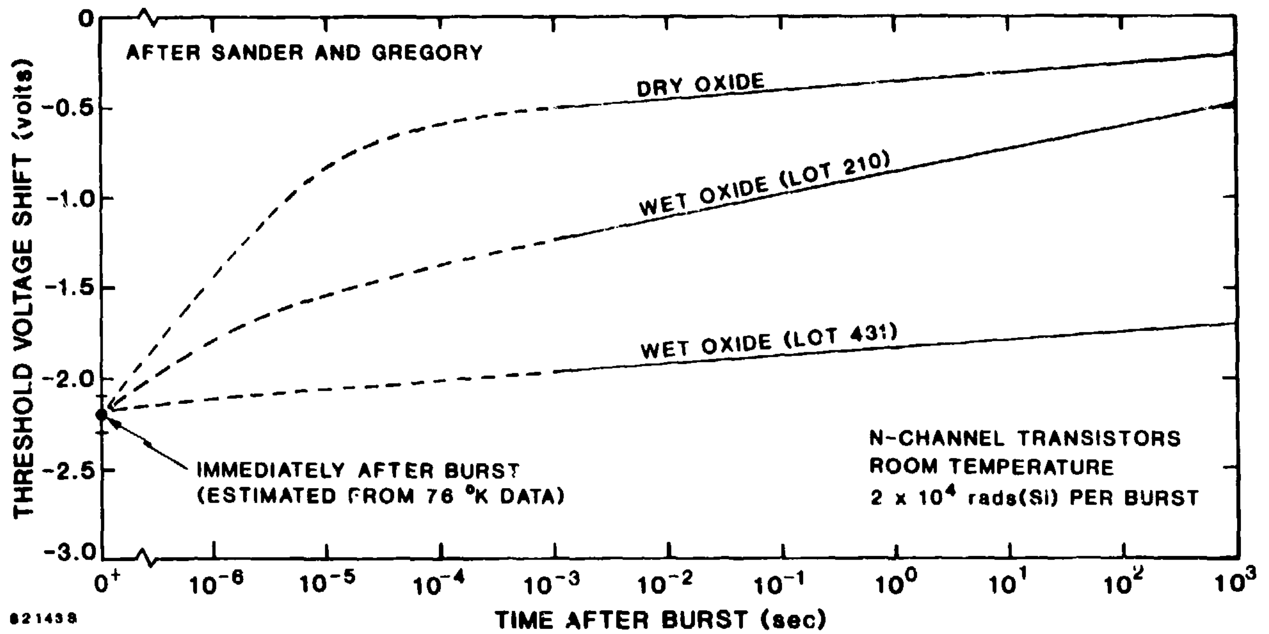

Figure 58. Illustration of transient changes in threshold voltage following an ionizing burst.[33]

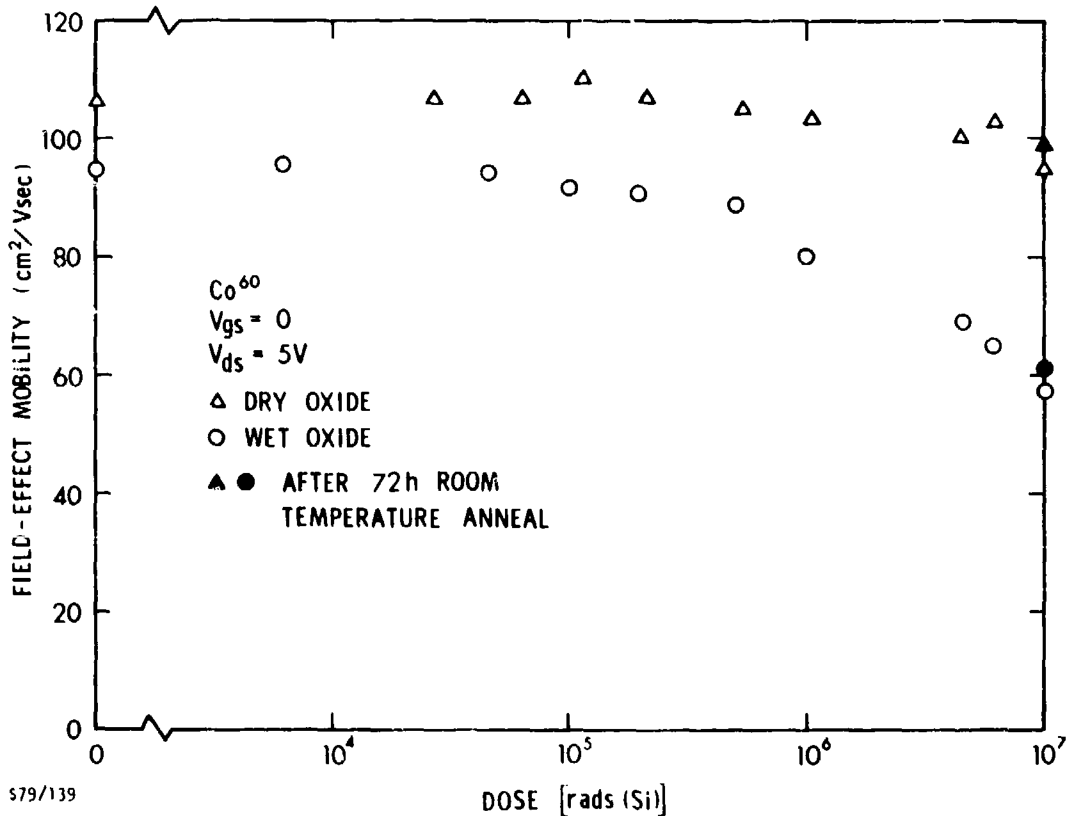

Figure 59. Illustration of channel mobility degradation in irradiated MOS transistors.

ionizing dose for n-channel MOS transistors fabricated with both dry-grown and wet-grown hardened gate oxides. After 10^7 rads(Si), the mobility degradation in the dry case is rather small compared to the change for wet-oxide devices. This indicates that the dominant channel-mobility degradation mechanism is interface state creation since the introduction rate of such states has been observed to be higher in wet-oxide devices.[34]

4.4 SILICON-ON-SAPPHIRE DEVICES

Figure 60 illustrates an n-channel silicon-on-sapphire (SOS) MOS transistor. Such devices are an example of the general category of silicon-on-insulator (SOI) devices. SOS transistors have several potential advantages over their MOS-on-bulk-silicon counterparts from a radiation effects viewpoint: reduced transient photoresponse; elimination of latchup; reduced susceptibility to soft errors. SOS devices are susceptible to the same ionizing radiation effects described above for bulk transistors, which are associated with the gate oxide. In addition, ionizing radiation gives rise to a back-channel leakage current in n-channel transistors that is unique to SOS (or, in general, to SOI) technology.

Referring to Figure 60, when a voltage is applied between drain and source a fringing field will exist in the sapphire. When electron-hole pairs are generated in the sapphire by ionizing radiation, that field will serve to separate these pairs. By analogy with the previously described situation for SiO_2 films, electrons may be quickly swept out, leaving a portion of the generated holes trapped near the sapphire-silicon interface. That trapped charge would then induce a conducting channel in the silicon (referred to as a back channel). A dc leakage current would then flow between source and drain independent of the gate bias, which only controls the front channel adjacent to the SiO_2 layer.

Figure 61 illustrates the increase in back-channel leakage current that occurs when n-channel SOS transistors are irradiated.[35] A difference is observed between devices with a dry-grown and a wet-grown gate oxide, again illustrating the effect of processing procedures on MOS device hardness.

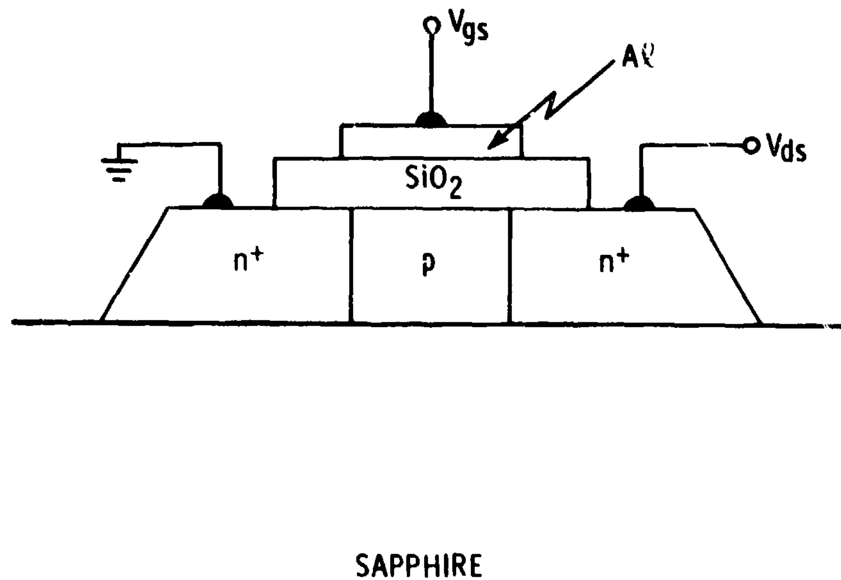

Figure 60. Schematic illustration of an n-channel silicon-on-sapphire MOS transistor.

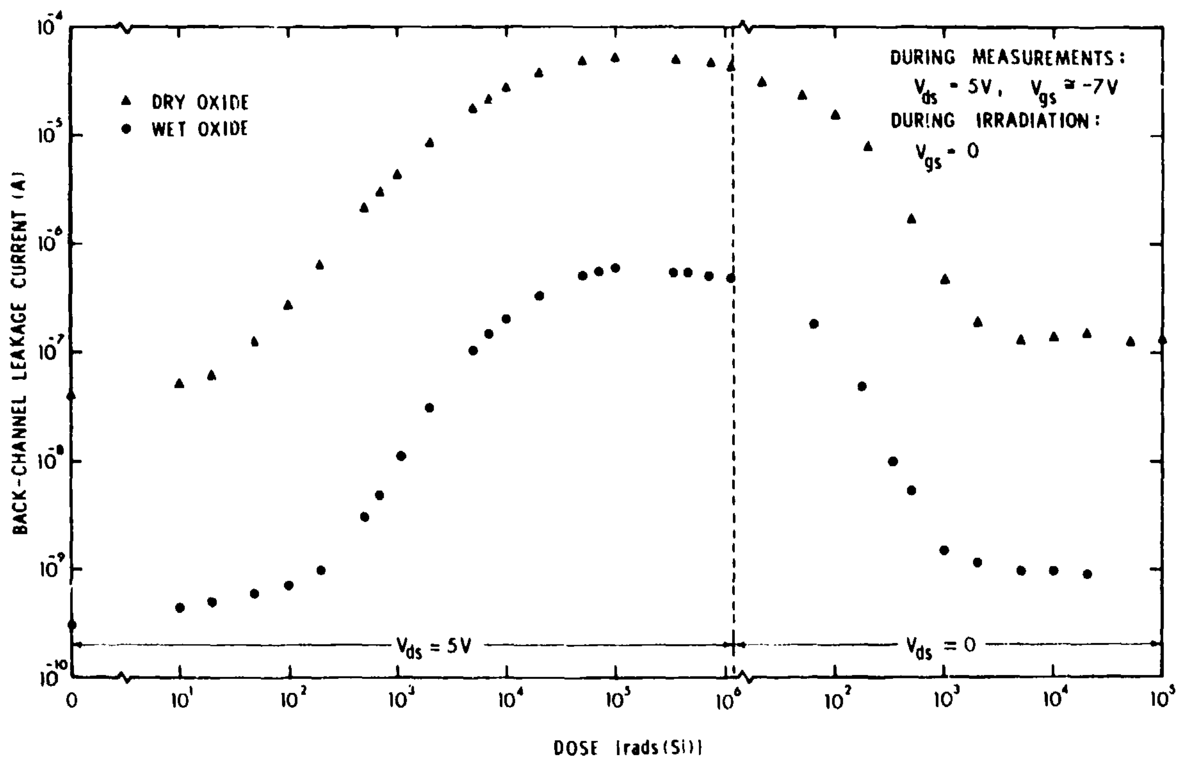

Figure 61. Illustration of radiation-induced changes in back-channel leakage current for silicon-on-sapphire MOS transistors.[35] (Values of V_{ds} applied during irradiation are shown near the bottom of the figure.)

A saturation in leakage current occurs at 10^5 rads(Si). These experimental observations are qualitatively consistent with the model described above. It is interesting to note that the back-channel leakage current can be reduced from its maximum to near the pre-irradiation value by simply reducing V_{ds} to zero and continuing to irradiate. This effect is illustrated in the right-hand portion of Figure 61. (Note the change in dose scale.) The mechanism for this recovery may be radiation-induced injection of electrons from the silicon into the sapphire where they recombine with trapped holes.[35]

5.0 SINGLE EVENT PHENOMENA

As integrated circuit geometries decrease, the possibility arises that new types of radiation vulnerabilities will be uncovered. An important example of this is the area referred to as single event phenomena. A single event error is a radiation-induced change in one cell of an integrated circuit due to one particle striking that cell. Single event phenomena can be separated into soft errors, or transient upsets, and hard errors, or permanent failure of a cell (Figure 62).

Soft errors are due to the ionization produced by a single particle as it passes through an integrated circuit. Such errors were first observed in 1975,[36] and have been the subject of intensive study since that time.[37-41] Soft errors can arise due to alpha particles emitted by the decay of trace radioactive elements, such as uranium and thorium, present in integrated circuit packaging materials.[38] These elements may also be present in materials actually used in circuit processing, such as the metallization.[41] Soft errors can also be produced by cosmic rays[36,37] (listed in Figure 4) and by neutrons.[39] For particles other than alphas incident on a circuit, the primary mechanism which results in soft errors appears to be the production of alpha particles through nuclear reactions. Alphas then lose most of their energy into ionization and create a densely ionized track. The charge in this track gives rise to upsets.

An ionized track produced by a 5-MeV alpha particle incident on a dynamic RAM cell is illustrated in Figure 63. The particle range is about 25 μm and the initial spread of the track is on the order of 1000 Å. Charge in the track will transport to the RAM-cell storage node by drift and by diffusion. The track conductivity is initially high compared to the silicon substrate, so the track will control the field line distribution. Experimental and analytical results[40] indicate that a large longitudinal field will be established along the track which rapidly sweeps carriers to the storage node (10^{-10}-10^{-9} sec). This process is referred to as field funneling. Once the track conductivity diminishes, field funneling stops and diffusion of the remaining charge takes place. Soft upsets in MOS dynamic RAMs are sensitive to the total amount of charge collected at a storage node

SINGLE EVENT PHENOMENA

- SOFT ERRORS (TRANSIENT UPSET)
  - MATERIALS
  - COSMIC RAYS
  - NEUTRONS
- HARD ERRORS (PERMANENT DAMAGE)
  - IONIZATION
  - DISPLACEMENT DAMAGE

Figure 62. Types of single event phenomena.

SOFT ERROR MECHANISMS (DYNAMIC RAM EXAMPLE)

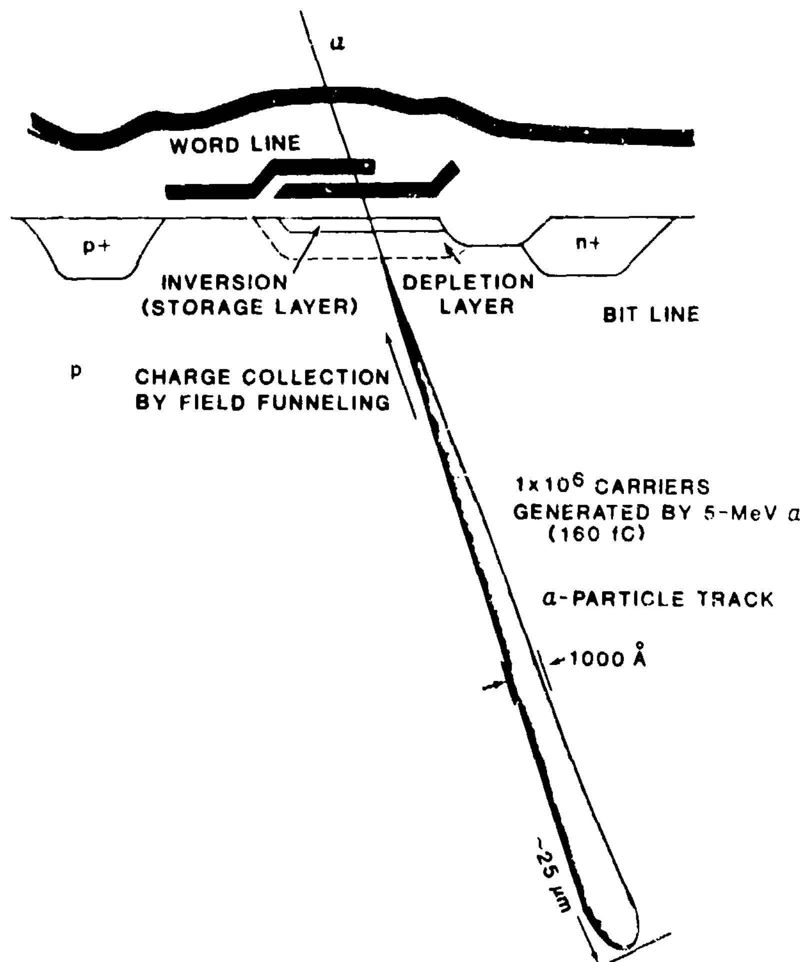

Figure 63. Illustration of the ionized track produced by a 5-MeV alpha particle incident on a dynamic RAM cell.

relative to the critical charge necessary to differentiate between two logic states. On the other hand, soft errors in bipolar technologies and in MOS static memories occur as a result of a current transient of sufficient magnitude. Thus, one category of circuits is charge sensitive and the other is current sensitive with regard to their soft-error susceptibility.

The possibility of single-particle-induced hard errors has recently been under investigation. Two potential causes of the permanent failure of a VLSI cell are (Figure 62): 1) ionization-induced charge buildup in an MOS transistor; 2) a dense region of displacement damage with dimensions comparable to those of an MOS or bipolar VLSI cell. Oldham and McGarrity[27] recently explored the possibility that a single alpha particle, or other highly ionizing heavy charged particles, passing through an SiO_2 gate oxide would cause a significant threshold voltage shift in an MOS/VLSI transistor. Figure 64 shows their calculated threshold shifts as a function of gate oxide thickness for several sizes of the gate electrode (assumed square here for simplicity). A 2-MeV alpha particle is assumed to be incident on the gate oxide at a 45° angle, and the fractional yield of generated pairs is assumed to be 10%. (See Figure 53.) They conclude that threshold voltage shifts induced by single ionizing particles will most likely be unimportant until device geometries are reduced to less than 0.5 μm.

The possibility that a neutron-induced defect cluster could give rise to a hard error is being explored. Figure 65 shows a calculated average defect cluster, or disordered region, produced in silicon by a single incident 14-MeV neutron.[42] (The depiction of this disordered region is based on the Gossick model, which is illustrated in Figure 24.) The dimensions of this calculated cluster are comparable to VLSI geometries, particularly for the case of a bipolar cell, as illustrated in Figure 66. The intrinsic basewidth in present-day devices is ~0.1-0.2 μm, which is considerably less than the cluster dimensions. If the situation illustrated in Figure 66 occurred, one would expect the gain of the vertical npn transistor to degrade substantially due to the large number of recombination centers present in the cluster. However, neutron-induced hard errors have not yet been observed, and there are differing opinions at present regarding the structure of damaged regions produced by neutrons. These issues are a subject of current research.

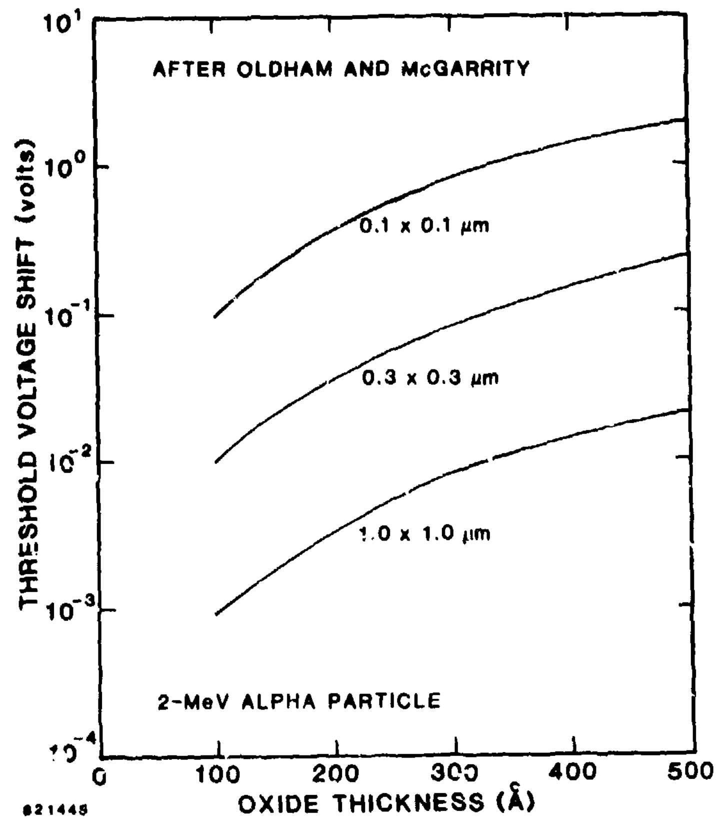

Figure 64. Calculated threshold voltage shift as a function of gate oxide thickness for a single 2-MeV alpha particle incident on MOS transistors of various sizes.[27]

CALCULATED AVERAGE DISORDERED REGION PRODUCED IN SILICON BY AN INCIDENT 14-MeV NEUTRON

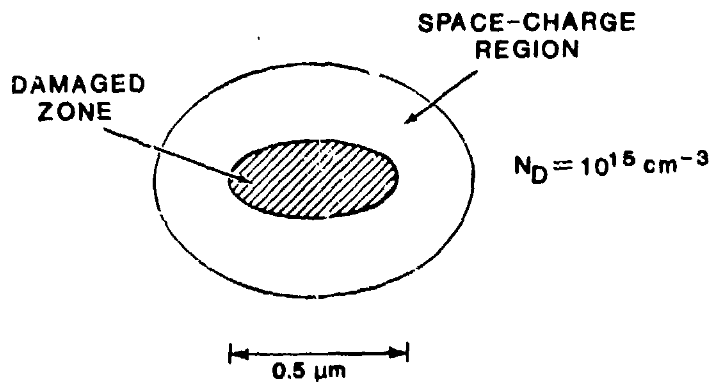

Figure 65. Calculated dimensions for an average disordered region produced in silicon by an incident 14-MeV neutron.[42]

I^2L CELL CONTAINING A DISORDERED REGION

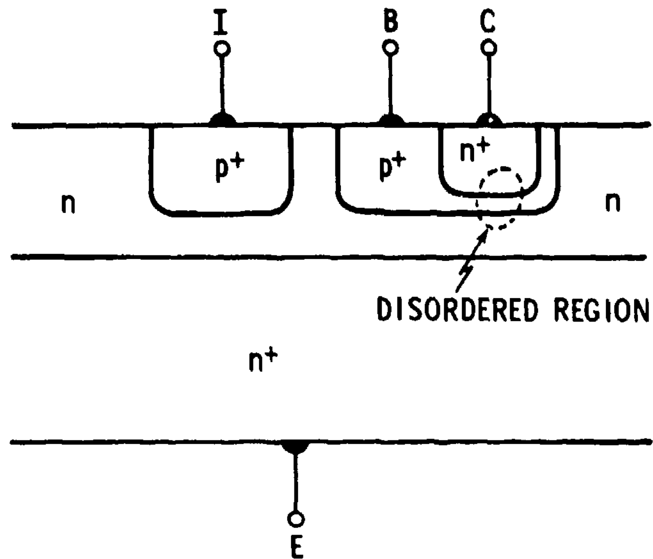

Figure 66. Illustration of a neutron-produced disordered region in an I^2L cell.

6.0 ADDITIONAL TOPICS

This section presents several additional topics, including a tabulation of device failure mechanisms, a brief discussion of radiation effects on GaAs devices, consideration of radiation-induced changes in the optical properties of materials, and an example of a hardness assurance technique.

6.1 DEVICE FAILURE MECHANISMS

Gregory and Gwyn[43] identified the important radiation-induced failure mechanisms for various types of semiconductor devices (Figure 67). Both primary (P) and secondary (S) failure modes are given. The information shown is for permanent damage. Transient upsets due to photocurrents or to single events can also cause temporary failure of devices and circuits, as discussed in previous sections.

6.2 GALLIUM ARSENIDE DEVICES

Gallium arsenide integrated circuits are under development at present. There is less information available concerning radiation effects on GaAs material and devices than for the silicon case. (For a review, see Ref. 44.) Figure 68 lists a portion of the findings that have been made. Because carrier lifetimes are very short in GaAs, radiation-induced lifetime degradation is relatively unimportant compared to silicon except for some GaAs optoelectronic devices. Information concerning carrier removal and mobility degradation for fission neutron irradiation is given in the figure. GaAs field-effect transistors are relatively insensitive to total ionizing dose effects. In a transient ionizing radiation environment, a relatively long-term (tens of seconds) response has been observed for FETs and attributed to electron trapping in the GaAs substrate.[45] Radiation levels that state-of-the-art devices and circuits will survive are also shown in Figure 68.[44]

6.3 OPTICAL PROPERTIES

Radiation effects on the electrical properties of SiO_2 films, bulk silicon, and silicon devices and integrated circuits have been the focus of this tutorial. Radiation-induced changes in the optical properties of

Device Type	Failure Mechanisms			
	Lifetime Degradation	Carrier Removal and Trapping	Mobility Degradation	Oxide Charge and Surface Effects
Semiconductor Resistors		P	S	
Diodes (Breakdown voltage, depletion capacitance)	S	P		
Diodes (leakage, forward current, photocurrent)	P	S		S
Microwa[illegible] Sources (IMPATT, TRAPATT, BARITT)	S	P		
Junction Field Effect Devices	S	P		
MIS Field Effect Devices and Capacitors				P
Microwave Bulk Oscillators (Gunn, LSA)		P	S	
Bipolar Transistors	P	S		S
Switching Devices (SCR, UJT)	P	S		
Optoelectronic Devices (LED, junction laser)	P			
	P - Primary; S - Secondary			

AFTER GREGORY AND GWYN

Figure 67. Failure mechanisms for semiconductor devices.[43]

materials also occur, and Figure 69 lists specific properties that can be altered. These changes can be produced as a result of either ionizing radiation or displacement damage. (See Ref. 23 for a discussion of the optical effects of ionization and displacement and for literature references.)

RADIATION EFFECTS ON GaAs MATERIAL AND DEVICES

- LIFETIME DEGRADATION UNIMPORTANT
- DAMAGE COEFFICIENTS

  FISSION NEUTRONS, $n = 10^{17}\ cm^{-3}$:

  $\frac{\Delta n}{\Delta \phi} \cong 7\ n^{-1} cm^{-1}$

  $K_{\mu} \cong 10^{-20}$ V-sec/n

- DEVICES AND CIRCUITS
  - INSENSITIVE TO TOTAL IONIZING DOSE
  - LONG-TERM TRANSIENT RESPONSE OBSERVED
  - STATE-OF-THE-ART HARDNESS LEVELS:
    - $10^{15}\ n/cm^2$
    - 10^7 rad(GaAs)
    - 5×10^9 to 1×10^{10} rad(GaAs)/s

Figure 68. Radiation effects on GaAs material and devices.

RADIATION-INDUCED CHANGES IN OPTICAL PROPERTIES

- ABSORPTION
- PHOTOCONDUCTIVITY
- LUMINESCENCE
- REFLECTIVITY
- REFRACTIVE INDEX

Figure 69. Optical properties of materials that are altered by radiation.

6.4 HARDNESS ASSURANCE EXAMPLE

As suggested at the beginning of this tutorial (Figure 1), a detailed understanding of the basic mechanisms of radiation effects can lead to the development of hardness assurance procedures. These procedures are required to assure that devices and integrated circuits will withstand exposure to specific levels of radiation. A brief example is presented here which illustrates how basic insight can lead to such developments.

Boesch and McGarrity[46] developed an electrical technique which can be used to simulate ionizing radiation effects on MOS devices. Figure 70 illustrates their approach, which is referred to as the F4I (Field-Induced Injection and Impact Ionization) technique. The basic effect of ionizing radiation on an MOS structure is illustrated in the upper part of Figure 70, as discussed earlier. In the lower part of the figure, application of a high field to the gate oxide is shown. This field is applied in pulses, and results in electron injection into the oxide through Fowler-Nordheim tunneling. Some of these injected carriers create electron-hole pairs through impact ionization. These created carriers then behave similarly to those generated by ionizing radiation (upper part of Figure 70); i.e., positive charge buildup occurs.

Figure 71 compares the C-V curves obtained by: (a) Co^{60} irradiation, and (b) the F4I technique. These sets of curves are qualitatively similar. Boesch and McGarrity were then able to obtain a good quantitative correlation of the C-V shifts for the two cases. The technique they developed may prove to be valuable as a wafer-level screening approach for determining radiation tolerance without the need for performing irradiations.

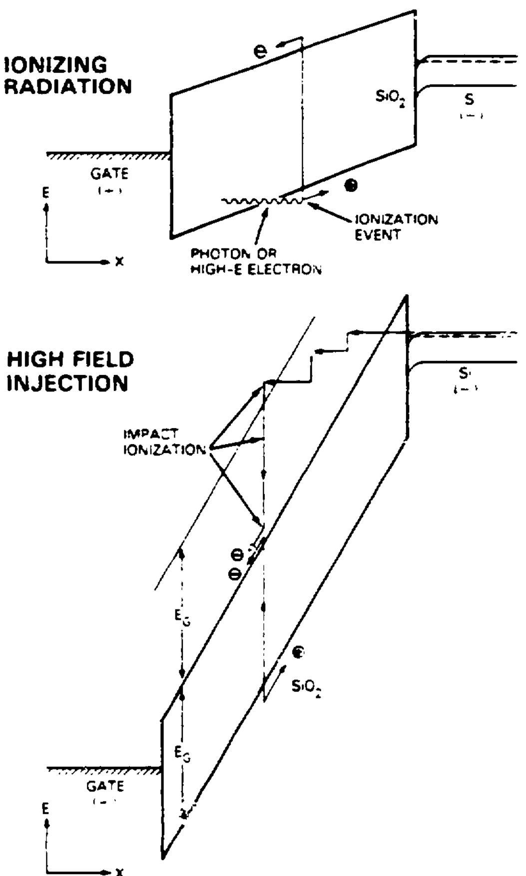

Figure 70. Comparison of the charge buildup process in an MOS structure produced by ionizing radiation and by the F4I technique.[46]

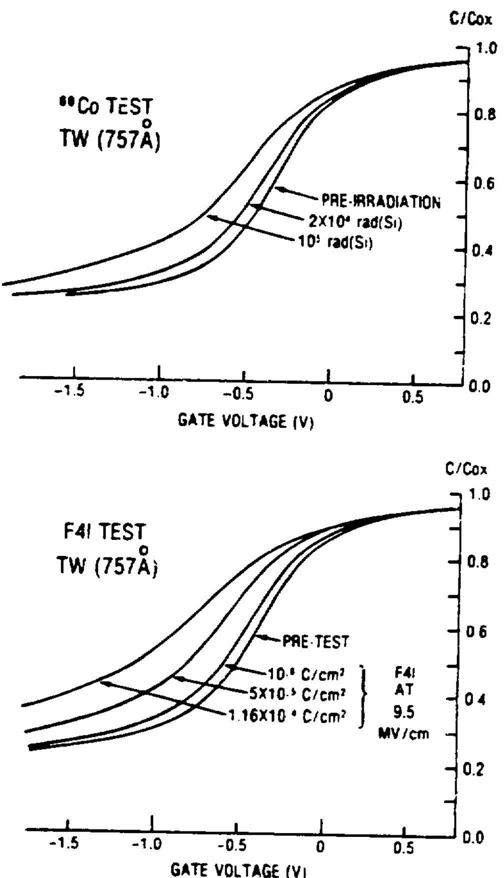

Figure 71. Comparison of C-V curves obtained after Co^{60} irradiation and after the F4I test.[46]

7.0 REFERENCES AND BIBLIOGRAPHY

7.1 REFERENCES

1. M.J. Berger and S.M. Seltzer, NASA-SP Publication 3036 (1966).

2. J.F. Janni, AFWL-TR-65-150 (1966).

3. J.W. Corbett, Electron Radiation Damage in Semiconductors and Metals (Academic Press, New York, 1966).

4. D.I. Garber and R.R. Kinsey, "Neutron Cross Sections: Vol. II, Curves," BNL 325, Third Edition, Jan. 1976.

5. J. Lindhard, M. Scharff, and H.E. Schiott, Mat. Fys. Medd. Dan. Vid. Selsk. 33, No. 14, pp. 1-42 (1963).

6. For a description of the Lindhard model, see J.W. Mayer, L. Eriksson, and J.A. Davies, Ion Implantation in Semiconductors (Academic Press, New York, 1970).

7. A.S. Grove, Physics and Technology of Semiconductor Devices (Wiley, New York, 1967).

8. J.R. Srour, R.A. Hartmann, and S. Othmer, IEEE Trans. Nucl. Sci. 27, 1402 (1980).

9. J.R. Srour, IEEE Trans. Nucl. Sci. 17, 118 (Dec. 1970); see also IEEE Trans. Nucl. Sci. 19, 897 (Feb. 1972).

10. G.D. Watkins, J. Phys. Soc. Japan 18, Suppl. II, 22 (1962); see also Radiation Damage in Semiconductors (Academic Press, New York, 1964), pp. 97-113.

11. J.C. Bourgoin and J.W. Corbett, Phys. Lett. 38A, 135 (1972).

12. D.V. Lang and L.C. Kimerling, Phys. Rev. Lett. 33, 489 (1974).

13. For a review, see M.I. Klinger and T.V. Mashovets, Crystal Lattice Defects 9, 113 (1981).

14. For a description, see J.S. Blakemore, Semiconductor Statistics (Pergamon Press, New York, 1962).

15. B.R. Gossick, J. Appl. Phys. 30, 1214 (1959).

16. R.R. Holmes, Bell Telephone Laboratories Report to Advance Ballistic Missile Defence Agency, Oct. 1, 1970.

17. J.R. Srour and O.L. Curtis, Jr., IEEE Trans. Nucl. Sci. 19, 362 (Dec. 1972); see also Radiation Damage and Defects in Semiconductors, J.E. Whitehouse, Ed., Conference Series No. 16 (The Institute of Physics, London, 1973), pp. 87-95.

18. B.L. Gregory and H.H. Sander, Proc. IEEE 58, 1328 (1970).

19. H.H. Sander and B.L. Gregory, IEEE Trans. Nucl. Sci. 18, 250 (Dec. 1971).

20. For example, see B.L. Gregory, IEEE Trans. Nucl. Sci. 16, 53 (Dec. 1969).

21. J.R. Srour, IEEE Trans. Nucl. Sci. 20, 190 (Dec. 1973).

22. V.A.J. van Lint, G. Gigas, and J. Barengoltz, IEEE Trans. Nucl. Sci. 22, 2663 (1975).

23. V.A.J. van Lint, T.M. Flanagan, R.E. Leadon, J.A. Naber, and V.C. Rogers, Mechanisms of Radiation Effects in Electronic Materials, Vol. I (Wiley, New York, 1980).

24. J.R. Srour, S.C. Chen, S. Othmer, and R.A. Hartmann, IEEE Trans. Nucl. Sci. 26, 4784 (1979).

25. M.S. Cooper, J.P. Retzler, and G.C. Messenger, IEEE Trans. Nucl. Sci. 26, 4758 (1979).

26. G.F. Derbenwick and B.L. Gregory, IEEE Trans. Nucl. Sci. 22, 2151 (1975).

27. T.R. Oldham and J.M. McGarrity, IEEE Trans. Nucl. Sci. 28, 3975 (1981).

28. J.R. Srour and K.Y. Chiu, IEEE Trans. Nucl. Sci. 24, 2140 (1977).

29. F.B. McLean, IEEE Trans. Nucl. Sci. 27, 1651 (1980).

30. E.H. Nicollian and J.R. Brews, MOS (Metal Oxide Semiconductor) Physics and Technology (Wiley, New York, 1982), p. 321.

31. J.M. Aitken, D.R. Young, and K. Pan, J. Appl. Phys. 49, 3386 (1978).

32. For a review, see T.H. Ning, et al., IEEE Trans. Electron Devices 26, 346 (1979).

33. H.H. Sander and B.L. Gregory, IEEE Trans. Nucl. Sci. 22, 2157 (1975).

34. P.S. Winokur and H.E. Boesch, IEEE Trans. Nucl. Sci. 27, 1647 (1980).

35. J.R. Srour, S. Othmer, and S.C. Chen, IEEE Trans. Nucl. Sci. 24, 2119 (1977).

36. D. Binder, E.C. Smith, and A.B. Holman, IEEE Trans. Nucl. Sci. 22, 2675 (1975).

37. J.C. Pickel and J.T. Blandford, Jr., IEEE Trans. Nucl. Sci. 25, 1166 (1978).

38. T.C. May and M.H. Woods, IEEE Trans. Electron Devices 26, 3 (1979).

39. C.S. Guenzer, E.A. Wolicki, and R.G. Allas, IEEE Trans. Nucl. Sci. 26, 5048 (1979).

40. C.M. Hsieh, P.C. Murley, and R.R. O'Brien, IEEE Electron Device Letters 2, 103 (1981).

41. G.A. Sai-Halasz, M.R. Wordeman, and R.H. Dennard, IEEE Trans. Electron Devices 29, 725 (1982).

42. J.R. Srour, S. Othmer, A. Bahraman, and R.A. Hartmann, IEEE Trans. Nucl. Sci. 28, 3968 (1981).

43. B.L. Gregory and C.W. Gwyn, Proc. IEEE 62, 1264 (1974).

44. R. Zuleeg and K. Lehovec, IEEE Trans. Nucl. Sci. 27, 1343 (1980).

45. M. Simons and E.E. King, IEEE Trans. Nucl. Sci. 26, 5080 (1979).

46. H.E. Boesch and J.M. McGarrity, IEEE Trans. Nucl. Sci. 26, 4814 (1979).

7.2 BIBLIOGRAPHY

R.D. Evans, The Atomic Nucleus (McGraw-Hill, New York, 1955).

E. Segre, Nuclei and Particles (W.A. Benjamin, New York, 1965).

December issues of the IEEE Transactions on Nuclear Science (1966-1982).

A.S. Grove, Physics and Technology of Semiconductor Devices (Wiley, New York, 1967).

B.L. Gregory and C.W. Gwyn, "Radiation Effects on Semiconductor Devices," Proc. IEEE 62, 1264 (1974).

V.A.J. van Lint, T.M. Flanagan, R.E. Leadon, J.A. Naber, and V.C. Rogers, Mechanisms of Radiation Effects in Electronic Materials, Volume 1 (Wiley-Interscience, New York, 1980).

S.M. Sze, Physics of Semiconductor Devices, Second Edition (Wiley-Interscience, New York, 1981).

E.H. Nicollian and J.R. Brews, MOS (Metal Oxide Semiconductor) Physics and Technology (Wiley, New York, 1982).

DISTRIBUTION LIST

DEPARTMENT OF DEFENSE

Armed Forces Radiobiology Rsch Institute
ATTN: J. Hsieh

Assistant to the Secretary of Defense
Atomic Energy
ATTN: Executive Assistant
ATTN: Military Applications

Command & Control Technical Ctr
ATTN: C-310
ATTN: C-330

Defense Advanced Rsch Proj Agency
ATTN: R. Reynolds
ATTN: S. Roosild
ATTN: J. Fraser

Defense Communications Engr Ctr
ATTN: Code R410
ATTN: Code R720, C. Stansberry

Defense Electronic Supply Ctr
ATTN: DEFC-ESA

Defense Intelligence Agency
ATTN: DT-1B
ATTN: DB-4C, Rsch, Phys Vuln Br

Defense Logistics Agency
ATTN: DLA-QEL, J. Slattery
ATTN: DLA-SE
ATTN: DLA-SEE, F. Harris

Defense Nuclear Agency
3 cy ATTN: RAEV, TREE
4 cy ATTN: TITL

Defense Tech Info Ctr
12 cy ATTN: DD

Field Command Defense Nuclear Agency
Det 1
Lawrence Livermore Lab
ATTN: FC-1

Field Command
Defense Nuclear Agency
ATTN: FCTT, W. Summa
ATTN: FCPF, R. Blackburn
ATTN: FCTXE
ATTN: FCPR
ATTN: FCTT

Joint Chiefs of Staff
ATTN: C3S Evaluation Office, HD00

National Communications System
ATTN: NCS-TS
ATTN: NCS-TS, D. Bodson

Under Secretary of Defense for Rsch & Engrg
ATTN: Strat & Space Sys (OS), C. Knowles
ATTN: Strategic & Space Sys (OS)
ATTN: Strat & Theater Nuc Forces, B. Stephan

DEPARTMENT OF DEFENSE (Continued)

National Security Agency
ATTN: T. Neal
ATTN: K. Schaffer
ATTN: R. Light
ATTN: R-52, O. Van Gunten
ATTN: T. Livingston
ATTN: P. Deboy
ATTN: T. Brown

DEPARTMENT OF THE ARMY

Aberdeen Proving Ground
ATTN: S. Harrison

Applied Sciences Div
ATTN: R. Williams

BMD Advanced Technology Ctr
ATTN: ATC-T
ATTN: ATC-O, F. Hoke

BMD Systems Command
ATTN: BMDSC-HW
ATTN: BMDSC-AV, J. Harper
ATTN: BMDSC-HW, R. Dekalb
ATTN: BMDSC-AU, R. Webb

Deputy Chief of Staff for Rsch Dev & Acq
ATTN: G. Ogden

Fort Huachuca
ATTN: Tech Ref Div

Harry Diamond Labs
ATTN: R. Reams
ATTN: DELHD-NW-RC, E. Boesch
ATTN: DELHD-NW-R, C. Self
ATTN: C. Fazi
ATTN: DELHD-NW-RH
ATTN: DELHD-NW-EA, J. Miletta
ATTN: DELHD-NW-RA, W. Vault
ATTN: T. Conway
ATTN: DELHD-NW-P
ATTN: DELHD-NW, J. Bombardt
ATTN: T. Griffin
ATTN: DELHD-NW-R, B. Dobriansky
ATTN: DELHD-NW-RC, J. McGarrity
ATTN: P. Winokur
ATTN: DELHD-NW-R, H. Eisen
ATTN: DELHD-NW-R, T. Oldham
ATTN: DELHD-NW-P, T. Flory
ATTN: J. Vallin
ATTN: DELHD-NW-RA
ATTN: T. Taylor
ATTN: L. Harper
ATTN: DELHD-NW-EC, Chief Lab 21000
ATTN: DELHD-NW-R, F. Mclean

US Army Armament Rsch Dev & Cmd
ATTN: DRDAR-LCN-F
ATTN: DRDAR-TSS, Tech Div
ATTN: DRDAR-LCA-PD
ATTN: DRDAR-TSI-E, A. Grinoch

PRECEDING PAGE BLANK-NOT FILMED

DEPARTMENT OF THE ARMY (Continued)

US Army Armor & Engr Board
ATTN: ATZK-AE-AR, J. Dennis

US Army Ballistic Rsch Labs
ATTN: DRDAR-BLB, W. VanAntwerp
ATTN: DRDAR-BLT
ATTN: DRDAR-BLV, D. Rigotti

US Army Chemical School
ATTN: ATZN-CM-CS

US Army Communications R&D Cmd
ATTN: DELET-IR, E. Hunter
ATTN: DRSEL-NL-RO, R. Brown
ATTN: DRSEL-CT-HDK, A. Cohen

US Army Communications Sys Agency
ATTN: CCM-RD-T, S. Krevsky

US Army Engr Div, Huntsville
ATTN: HNDED-ED, J. Harper

US Army Intell & Sec Cmd
ATTN: IARDA-OS, R. Burkhardt

US Army Material & Mechanics Rsch Ctr
ATTN: DRXMR-HH, J. Dignam
ATTN: DRZMR-B, J. Hofmann

US Army Mobility Equip R&D Cmd
ATTN: DRDME-E, J. Bond, Jr

US Army Nuclear & Chemical Agency
ATTN: MONA-WE
ATTN: Library
ATTN: MONA-MS, H. Wells

US Army Rsch Ofc
ATTN: R. Griffith

US Army Signal Warfare Lab, VHFS
ATTN: F. Erwin

US Army Test and Evaluation Comd
ATTN: DRSTE-EL
ATTN: DRSTE-FA

US Army TRADOC Sys Analysis Actvy
ATTN: ATAA-TFC, O. Miller

US Army Training and Doctrine Comd
ATTN: ATCD-Z

US Army White Sands Missile Range
ATTN: STEWS-TE-AN, R. Hays
ATTN: STEWS-TE-AN, A. De La Paz
ATTN: STEWS-TE-N, K. Cummings
ATTN: STEWS-TE-NT, M. Squires
ATTN: STEWS-TE-AN, J. Meason
ATTN: STEWS-TE-AN, T. Arellanes
ATTN: STEWS-TE-AN, R. Dutchover

USA Missile Comd
ATTN: Hawk Project Officer, DRCPM-HAER
ATTN: DRCPM-PE-EA, W. Wagner
ATTN: DRSMI-SF, H. Hendriksen
3 cy ATTN: Doc Sec

DEPARTMENT OF THE ARMY (Continued)

USA Night Vision & Electro-Optics Lab
ATTN: DRSEL-NV-SD, J. Carter
ATTN: DRSEL-NV-SD, A. Parker

XM-1 Tank System
ATTN: DRCPM-GCM-SW

DEPARTMENT OF THE NAVY

Naval Air System Command
ATTN: AIR 310
ATTN: AIR 350F
ATTN: AIR 5324K

Naval Avionics Ctr
ATTN: Code B415, D. Repass

Naval Electronic Systems Command
ATTN: NAVELEX 51024, C. Watkins
ATTN: Code 50451
ATTN: Code 5045.11, C. Suman
ATTN: PME 117-21

Naval Intell Support Ctr
ATTN: NISC, Library

Naval Ocean Systems Ctr
ATTN: Code 4471
ATTN: Code 7309, R. Greenwell

Naval Postgraduate School
ATTN: Library, Code 1424

Naval Sea Systems Command
ATTN: SEA-04531
ATTN: SEA-06J, R. Lane

Naval Surface Weapons Ctr
ATTN: Code F31
ATTN: Code F31, F. Warnock
ATTN: Code F30
ATTN: Code WA-52, R. Smith
ATTN: Code F31, K. Caudle
ATTN: F31, J. Downs

Naval Weapons Ctr
ATTN: Code 343, FKA6A2, Tech Svcs

Naval Weapons Evaluation Facility
ATTN: Code AT-6

Naval Weapons Support Ctr
ATTN: Code 6054, D. Platterter
ATTN: Code 605, J. Ramsey
ATTN: Code 3073, T. Ellis
ATTN: Code 70242, J. Munarin

Nuclear Weapons Tng Group, Pacific
ATTN: Code 32

Office of the Deputy Asst Secretary of the Navy
ATTN: L. Abella

Office of the Deputy Chief of Naval Ops
ATTN: NOP 985F

DEPARTMENT OF THE NAVY (Continued)

Naval Rsch Lab
ATTN: Code 6635, G. Mueller
ATTN: Code 6814, M. Peckerar
ATTN: Code 6611, E. Petersen
ATTN: Code 6816, E. Richmond
ATTN: Code 6510, H. Rosenstock
ATTN: Code 6813, N. Saks
ATTN: Code 6611, P. Shapiro
ATTN: Code 6612, D. Walker
ATTN: Code 6612, R. Statler
ATTN: Code 4020, J. Adams
ATTN: Code 6603-J, J. McElhinney
ATTN: Code 6816, G. Davis
ATTN: Code 6653, A. Namenson
ATTN: Code 6816, H. Hughes
ATTN: Code 6810, J. Davey
ATTN: Code 6601, E. Wolicki
ATTN: Code 6611, J. Ritter
ATTN: Code 4040, J. Boris
ATTN: Code 6611, A. Campbell
ATTN: Code 6701
ATTN: Code 2627
ATTN: Code 6612, G. McLane
ATTN: Code 6680, D. Nagel
ATTN: Code 6816, D. Patterson
ATTN: Code 6610, R. Marlow
ATTN: Code 6814, D. McCarthy
ATTN: Code 6813, J. Killiany
ATTN: Code 6611, L. August
ATTN: Code 6613, R. Lambert
ATTN: Code 6682, D. Brown
ATTN: Code 6683, C. Dozier
ATTN: Code 6600, J. Schriempf
ATTN: Code 6673, A. Knudson
ATTN: Code 6816, R. Hevey
ATTN: Code 6813, W. Jenkins

Office of Naval Rsch
ATTN: Code 220, D. Lewis
ATTN: Code 414, L. Cooper
ATTN: Code 427

Strategic Systems Project Ofc
ATTN: NSP-2301, M. Meserole
ATTN: NSP-2701, J. Fitsenberger
ATTN: NSP-2430, J. Stillwell
ATTN: NSP-27331, P. Spector
ATTN: NSP-27334, B. Hahn

DEPARTMENT OF THE AIR FORCE

Aeronautical Systems Div
ATTN: ASD/ENESS, P. Marth
ATTN: ASD/ENACC, R. Fish
ATTN: ASD/YH-EX, J. Sunkes
ATTN: ASD/ENTV, L. Robert

Air Force Geophysics Lab
ATTN: PHG, M/S 30, E. Mullen
ATTN: SULL
ATTN: SULL, S-29
ATTN: PLIG, R. Filz

Air Force Institute of Technology
ATTN: ENP, J. Bidgeman

Air Force Technical Applications Ctr
ATTN: TAE

DEPARTMENT OF THE AIR FORCE (Continued)

Headquarters
Air Force Systems Command
ATTN: DLCAM
ATTN: DLW

Air Force Weapons Lab
ATTN: NTYEE, C. Baum
ATTN: NTYC
ATTN: NTYC, J. Ferry
ATTN: NTYCT, J. Mullis
ATTN: NTYC, M. Schneider
ATTN: NTYCT, R. Tallon
ATTN: SUL
ATTN: NTYC, R. Maier

Air Force Wright Aeronautical Lab
ATTN: POE-2, J. Wise
ATTN: POD, P. Stover

Air Force Wright Aeronautical Lab
ATTN: TEA
ATTN: LTE
ATTN: LPO, R. Hickmott
ATTN: TEA, R. Conklin
ATTN: DHE-2
ATTN: DHE

Air Logistics Command
ATTN: MMIFM, S. Mallory
ATTN: MMETH, R. Blackburn
ATTN: MMETH
ATTN: MMEDD
ATTN: OO-ALC/MM
ATTN: MMGRW, G. Fry
ATTN: A. Cossens

Air University Library
ATTN: AUL-LSE

Assistant Chief of Staff
Studies & Analyses
2 cy ATTN: AF/SAMI, Tech Info Div

Ballistic Missile Office
ATTN: ENSN, H. Ward
ATTN: ENBE
ATTN: SYST, L. Bryant
ATTN: ENMG
ATTN: SYDT
ATTN: ENSN, M. Williams
ATTN: ENSN

Headquarters
Electronic Systems Div
ATTN: INDC

Foreign Technology Div
ATTN: PDJV
ATTN: TQTD, B. Ballard

Office of the Secretary of the Air Force
ATTN: Director

Rome Air Development Ctr
ATTN: RDC, R. Magoon
ATTN: RBR, J. Brauer
ATTN: RBRP, C. Lane

DEPARTMENT OF THE AIR FORCE (Continued)

Rome Air Development Ctr
ATTN: ESR, P. Vail
ATTN: ESR/ET, E. Burke, M/S 64
ATTN: ESR, W. Shedd
ATTN: ESE, A. Kahan
ATTN: ESR, J. Bradford, M/S 64
ATTN: ESR, B. Buchanan

Sacramento Air Logistics Ctr
ATTN: MMEAE, R. Dallinger

Space Div
ATTN: AQM
ATTN: AQT, S. Hunter
ATTN: YB
ATTN: YD
ATTN: YE
ATTN: YGJ, R. Davis
ATTN: YG
ATTN: YKA, C. Kelly
ATTN: YKS, P. Stadler
ATTN: YLS, L. Darda
ATTN: YLVM, J. Tilley
ATTN: YLS
ATTN: YL
ATTN: YN
ATTN: YR
ATTN: YV
ATTN: YK

Strategic Air Command
ATTN: XPFS, M. Carra
ATTN: NRI-STINFO, Library

Tactical Air Command
ATTN: XPG

3416th Technical Tng Squadron (ATC)
ATTN: TTV

DEPARTMENT OF ENERGY

Department of Energy
Albuquerque Operations Office
ATTN: WSSB
ATTN: WSSB, R. Shay

OTHER GOVERNMENT AGENCIES

Central Intelligence Agency
ATTN: OSWR/STD/MTB
ATTN: OSWR, T. Marquitz
ATTN: OSWR/NED

Department of Transportation
ATTN: ARD-350

NASA
ATTN: H. Yearwood
ATTN: EG02
ATTN: M. Nowakowski
ATTN: L. Hamiter

NASA
ATTN: J. Murphy

NASA
ATTN: M. Baddour

OTHER GOVERNMENT AGENCIES (Continued)

NASA
ATTN: Code 724.1, M. Jhabvala
ATTN: Code 311.3, D. Cleveland
ATTN: Code 311A, J. Adolphsen
ATTN: Code 654.2, V. Danchenko
ATTN: Code 5301, G. Kramer
ATTN: Code 701, W. Redisch
ATTN: Code 710.2, D. Haykin, Jr
ATTN: Code 310, W. Womack
ATTN: Code 660, J. Trainor
ATTN: Code 601, E. Stassinopoulos
ATTN: Code 695, M. Acuna

NASA
ATTN: G. DeYoung

NASA Headquarters
ATTN: Code DP, B. Bernstein
ATTN: Code D, W. McInnes
ATTN: Code DP, R. Karpen

Department of Commerce
National Bureau of Standards
ATTN: T. Russell
ATTN: C. Wilson
ATTN: R. Scace
ATTN: Code A361, J. French
ATTN: Code A353, S. Chappell
ATTN: Code A327, H. Schafft
ATTN: Code C216, J. Humphreys
ATTN: Code A305, K. Galloway
ATTN: Code A347, J. Mayo-Wells

NATO

NATO School, SHAPE
ATTN: US Documents officer

DEPARTMENT OF ENERGY CONTRACTORS

University of California
Lawrence Livermore National Lab
ATTN: Tech Info Dept Library
ATTN: L-156, J. Yee
ATTN: L-389, R. Ott
ATTN: L-10, H. Kruger
ATTN: W. Orvis
ATTN: L 153, D. Meeker
ATTN: L-156, R. Kalibjian

Los Alamos National Lab
ATTN: D. Lynn
ATTN: C. Spirio
ATTN: J. Freed
ATTN: MS D450, B. McCormick
ATTN: D. Wilde

Sandia National Labs
ATTN: Div 2143, H. Weaver
ATTN: Div 4232, L. Posey
ATTN: Div 2143, H. Sander
ATTN: Div 2144, W. Dawes
ATTN: Org 2100, B. Gregory
ATTN: T. Wrobel
ATTN: Org 2150, J. Hood
ATTN: Org 9336, J. Renken
ATTN: Div 1232, G. Baldwin

DEPARTMENT OF DEFENSE CONTRACTORS

Advanced Research & Applications Corp
ATTN: L. Palkuti
ATTN: R. Armistead
ATTN: T. Magee

Advanced Research & Applications Corp
ATTN: A. Larson

Aerojet Electro-Systems Co
ATTN: P. Lathrop
ATTN: D. Toomb
ATTN: SV/8711/70
ATTN: D. Huffman

Aerospace Corp
ATTN: R. Crolius
ATTN: J. Stoll
ATTN: H. Phillips
ATTN: J. Wiesner
ATTN: J. Reinheimer
ATTN: A. Carlan
ATTN: W. Kolasinkski, MS/259
ATTN: V. Josephson, MS-4-933
ATTN: R. Slaughter
ATTN: D. Fresh
ATTN: I. Garfunkel
ATTN: S. Bower
ATTN: C. Huang
ATTN: W. Crane, A2/1083
ATTN: P. Buchman
ATTN: G. Gilley
ATTN: D. Schmunk
ATTN: B. Blake

Aerospace Industries Assoc of America, Inc
ATTN: S. Siegel

Ampex Corp
ATTN: D. Knutson
ATTN: J. Smith

Analytic Services, Inc
ATTN: P. Szymanski
ATTN: J. O'Sullivan
ATTN: A. Shostak

Applied Systems Engrg Dir
ATTN: J. Retzler, Nuc S/V Mang

AVCO Systems Div
ATTN: W. Broding
ATTN: D. Fann
ATTN: C. Davis
ATTN: D. Shrader

Battelle Memorial Institute
ATTN: R. T[illegible]tcher

BDM Corp
ATTN: S. Meth
ATTN: C. Stickley

BDM Corp
ATTN: R. Antinone
ATTN: Marketing
ATTN: D. Wunsch

Advanced Microdevices, Inc
ATTN: J. Schlageter

DEPARTMENT OF DEFENSE CONTRACTORS (Continued)

Beers Associates, Inc
ATTN: B. Beers
ATTN: S. Ives

Bell Labs
ATTN: R. McPartland
ATTN: D. Yaney

Bendix Corp
ATTN: Doc Con

Bendix Corp
ATTN: M. Frank

Bendix Corp
ATTN: E. Meeder

Boeing Aerospace Co
ATTN: MS-81-36, P. Blakely
ATTN: O. Mulkey
ATTN: [illegible]. Dixon
ATTN: MS-2R-00, A. Johnston
ATTN: MS-2R-00, E. Smith
ATTN: MS-2R-00, I. Arimura
ATTN: MS-81-36, W. Doherty
ATTN: MS-2R-00, C. Rosenberg

Boeing Co
ATTN: 8K-38
ATTN: H. Wicklein
ATTN: R. Caldwell
ATTN: D. Egelkrout

Booz, Allen and Hamilton, Inc
ATTN: R. Chrisner

Burr-Brown Research Corp
ATTN: H. Smith

Burroughs Corp
ATTN: Product Evaluation Lab

California Institute of Technology
ATTN: F. Grunthaner
ATTN: D. Nichols, T-1180
ATTN: R. Covey
ATTN: K. Martin
ATTN: W. Scott
ATTN: A. Shumka
ATTN: W. Price, MS-83-122
ATTN: J. Bryden
ATTN: P. Robinson

Charles Stark Draper Lab, Inc
ATTN: A. Schutz
ATTN: W. Callender
ATTN: D. Gold
ATTN: J. Boyle
ATTN: A. Freeman
ATTN: N. Tibbetts
ATTN: R. Ledger
ATTN: R. Haltmaier
ATTN: Tech Library
ATTN: P. Greiff
ATTN: R. Bedingfield

DEPARTMENT OF DEFENSE CONTRACTORS (Continued)

Cincinnati Electronics Corp
ATTN: L. Hammond
ATTN: C. Stump

Clarkson College of Technology
ATTN: P. McNulty

Computer Sciences Corp
ATTN: A. Schiff

Control Data Corp
ATTN: D. Newberry, BRR 142
ATTN: T. Frey

University of Denver
ATTN: Sec Officer for F. Venditti

Develco, Inc
ATTN: G. Hoffman

Dikewood
ATTN: Tech Library for L. Davis

E-Systems, Inc
ATTN: K. Reis

E-Systems, Inc
ATTN: Div Library

Eaton Corp
ATTN: A. Anthony
ATTN: R. Bryant

Electronic Industries Assoc
ATTN: J. Kinn

Exp & Math Physics Consultants
ATTN: T. Jordan

University of Florida
ATTN: H. Sisler

FMC Corp
ATTN: M. Pollock, Mail Drop 080

Ford Aerospace & Communications Corp
ATTN: H. Linder
ATTN: J. Davison
ATTN: Tech Info Svcs

Ford Aerospace & Communications Corp
ATTN: E. Hahn

Franklin Institute
ATTN: R. Thompson

Garrett Corp
ATTN: H. Weil

General Dynamics Corp
ATTN: R. Fields, MZ 2839
ATTN: O. Wood

General Electric Co
ATTN: L. Hauge
ATTN: B. Flaherty
ATTN: G. Bender
ATTN: J. Reidl

DEPARTMENT OF DEFENSE CONTRACTORS (Continued)

General Electric Co
ATTN: R. Benedict
ATTN: Tech Library
ATTN: J. Palchefsky, Jr
ATTN: Tech Info Ctr for L. Chasen
ATTN: W. Patterson
ATTN: J. Andrews
ATTN: J. Peden
ATTN: R. Casey
ATTN: D. Tasca

General Electric Co
ATTN: G. Gati, MD-E184

General Electric Co
ATTN: C. Hewison
ATTN: J. Gibson
ATTN: D. Cole

General Electric Co
ATTN: D. Pepin

General Research Corp
ATTN: E. Steele
ATTN: R. Hill
ATTN: Tech Info Office
ATTN: A. Hunt

George Washington University
ATTN: A. Friedman

Georgia Institute of Technology
ATTN: Res & Sec Coord for H. Denny

Goodyear Aerospace Corp
ATTN: Security Control Station

Grumman Aerospace Corp
ATTN: J. Rogers

GTE Microcircuits
ATTN: F. Krch

Harris Corp
ATTN: W. Abare
ATTN: C. Davis
ATTN: E. Yost

Harris Corp
ATTN: Mgr Linear Engrg
ATTN: J. Cornell
ATTN: C. Anderson
ATTN: J. Schroeder
ATTN: B. Gingerich, MS-51-120
ATTN: D. Williams, MS-51-75
ATTN: T. Sanders, MS-51-121
ATTN: Mngr Bipolar Digital Eng

Hazeltine Corp
ATTN: C Meinen
ATTN: J. Okrent

Honeywell, Inc
ATTN: R. Gumm
ATTN: F. Hampton
ATTN: D. Nielsen, MN 14-3015
ATTN: J. Moylan

DEPARTMENT OF DEFENSE CONTRACTORS (Continued)

Honeywell, Inc
ATTN: J. Zawacki
ATTN: R. Reinecke
ATTN: C. Cerulli
ATTN: J. Schafer
ATTN: H. Noble
ATTN: MS 725-5

Honeywell, Inc
ATTN: Tech Library

Honeywell, Inc
ATTN: L. Lavoie

Honeywell, Inc
ATTN: D. Herold, MS-MN 17-2334
ATTN: D. Lamb, MS-MN 17-2334
ATTN: R. Belt, MS-MN 17-2334

Hughes Aircraft Co
ATTN: K. Walker
ATTN: D. Binder
ATTN: R. McGowan
ATTN: CTDC, 6/E110

Hughes Aircraft Co
ATTN: E. Smith, MS V347
ATTN: E. Kubo
ATTN: W. Scott, S32/C332
ATTN: D. Shumake
ATTN: A. Narevsky, S32/C332

Hughes Aircraft Co
ATTN: R. Henderson

Hughes Aircraft Co
ATTN: MS-A2408, J. Hall
ATTN: P. Coppen

IBM Corp
ATTN: Mono Memory Systems
ATTN: Electromagnetic Compatability
ATTN: H. Mathers
ATTN: T. Martin

IBM Corp
ATTN: J. Ziegler

IBM Corp
ATTN: MS 110-036, F. Tietze
ATTN: A Edenfeld
ATTN: L. Rockett, MS 110-020
ATTN: W. Doughten
ATTN: O. Spencer
ATTN: N. Haddad
ATTN: S. Saretto
ATTN: H. Kotecha
ATTN: W. Henley

IIT Research Institute
ATTN: I. Mindel
ATTN: R. Sutowski

Illinois Computer Research Inc
ATTN: E. Davidson

Institute for Defense Analyses
ATTN: Tech Info Services

DEPARTMENT OF DEFENSE CONTRACTORS (Continued)

Intel Corp
ATTN: T. May

International Tel & Telegraph Corp
ATTN: Dept 608
ATTN: A. Richardson

IRT Corp
ATTN: N. Rudie
ATTN: M. Rose
ATTN: J. Harrity
ATTN: MDC
ATTN: R. Judge
ATTN: R. Mertz
ATTN: Systems Effects Div
ATTN: Physics Div

JAYCOR
ATTN: L. Scott
ATTN: R. Stahl
ATTN: R. Berger
ATTN: M. Treadaway
ATTN: T. Flanagan
ATTN: J. Azarewicz

JAYCOR
ATTN: E. Alcaraz
ATTN: R. Sullivan

JAYCOR
ATTN: R. Poll

Johns Hopkins University
ATTN: R. Maurer
ATTN: P. Partridge

Johns Hopkins University
ATTN: G. Masson, Dept of Elec Engr

Kaman Sciences Corp
ATTN: Dir Science & Technology Div
ATTN: C. Baker
ATTN: W. Rich
ATTN: N. Beauchamp
ATTN: J. Erskine

Kaman Tempo
ATTN: W. McNamara
ATTN: DASIAC
ATTN: R. Rutherford

Kaman Tempo
ATTN: DASIAC
ATTN: W. Alfonte

Kinon, John M.
ATTN: J. Kinon

Litton Systems, Inc
ATTN: F. Motter
ATTN: G. Maddox
ATTN: J. Retzler

Lockheed Missiles & Space Co, Inc
ATTN: F. Junga, S2/54-202
ATTN: J. Smith
ATTN: Reports Library
ATTN: J. Crowley

DEPARTMENT OF DEFENSE CONTRACTORS (Continued)

Lockheed Missiles & Space Co, Inc
ATTN: K. Greenough
ATTN: B. Kimura
ATTN: L. Rossi
ATTN: S. Taimuty, Dept 81-74/154
ATTN: D. Wolfhard
ATTN: J. Cayot, Dept 81-63
ATTN: J. Lee
ATTN: Dr G. Lum, Dept 81-63
ATTN: P. Bene
ATTN: E. Hessee
ATTN: A. Borofsky, Dept 66-60, B/577N

M.I.T. Lincoln Lab
ATTN: P. McKenzie

Magnavox Advanced Products & Sys Co
ATTN: W. Hagemeier

Magnavox Govt & Indus Electronics Co
ATTN: W. Richeson

Martin Marietta Denver Aerospace
ATTN: M. Shumaker Denver Aerospace
ATTN: Goodwin
ATTN: D-6074, G. Freyer
ATTN: E. Carter
ATTN: P. Kase
ATTN: Research Library
ATTN: MS-D6074, M. Polzella

University of Maryland
ATTN: H. Lin

McDonnell Douglas Corp
ATTN: M. Stitch, Dept E003
ATTN: Library
ATTN: R. Kloster, Dept E451
ATTN: T. Ender, 33/6/618
ATTN: D. Dohm
ATTN: A. Munie

McDonnell Douglas Corp
ATTN: P. Bretch
ATTN: D. Fitzgerald
ATTN: M. Onoda
ATTN: P. Albrecht
ATTN: M. Ralsten
ATTN: J. Holmgrem
ATTN: J. Imai
ATTN: R. Lothringer

McDonnell Douglas Corp
ATTN: Tech Library

Martin Marietta Corp
ATTN: R. Gaynor
ATTN: MP-163, W. Bruce
ATTN: P. Fender
ATTN: S. Bennett
ATTN: H. Cates
ATTN: W. Janocko
ATTN: W. Brockett
ATTN: TIC/MP-30
ATTN: R. Yokomoto
ATTN: J. Ward
ATTN: J. Tanke
ATTN: MP-163, N. Redmond

DEPARTMENT OF DEFENSE CONTRACTORS (Continued)

Messenger, George C.
ATTN: G. Messenger

Mission Research Corp
ATTN: C. Longmire
ATTN: M. Van Blaricum

Mission Research Corp
ATTN: R. Turfler
ATTN: R. Pease
ATTN: D. Mereweather
ATTN: D. Alexander

Mission Research Corp
ATTN: B. Passenheim
ATTN: J. Raymond

Mission Research Corp
ATTN: J. Lubell
ATTN: R. Curry
ATTN: W. Ware

Mitre Corp
ATTN: M. Fitzgerald

Mostek
ATTN: MS 640, M. Campbell

Motorola, Inc
ATTN: A. Christensen

Motorola, Inc
ATTN: L. Clark
ATTN: C. Lund
ATTN: O. Edwards

National Academy of Sciences
ATTN: National Materials Advisory Board

National Semiconductor Corp
ATTN: A. London
ATTN: F. Jones
ATTN: J. Martin

University of New Mexico
ATTN: H. Southward

New Technology, Inc
ATTN: D. Divis

Norden Systems, Inc
ATTN: D. Longo
ATTN: Tech Library

Northrop Corp
ATTN: P. Eisenberg
ATTN: A. Kalma
ATTN: Z. Shanfield
ATTN: A. Bahraman
ATTN: S. Othmer
4 cy ATTN: J. Srour

Pacific-Sierra Research Corp
ATTN: H. Brode, Chairman SAGE

Palisades Inst for Rsch Services, Inc
ATTN: Secretary

DEPARTMENT OF DEFENSE CONTRACTORS (Continued)

Physics International Co
ATTN: Div 6000
ATTN: J. Shea
ATTN: J. Huntington

Power Conversion Technology, Inc
ATTN: V. Fargo

R&D Associates
ATTN: W. Karzas
ATTN: C. Rogers
ATTN: P. Haas

Rand Corp
ATTN: C. Crain
ATTN: P. Davis

Raytheon Co
ATTN: G. Joshi
ATTN: T. Wein
ATTN: J. Ciccio

Raytheon Co
ATTN: H. Flescher
ATTN: A. Van Doren

Rand Corp
ATTN: B. Bennett

Northrop Corp
ATTN: L. Apodaca
ATTN: P. Besser
ATTN: D. Strobel
ATTN: P. Eisenberg
ATTN: T. Jackson
ATTN: P. Gardner
ATTN: S. Stewart
ATTN: E. King, C3323/WC

RCA Corp
ATTN: V. Mancino

RCA Corp
ATTN: L. Minich
ATTN: D. O'Connor
ATTN: Office N103
ATTN: G. Hughes
ATTN: R. Smeltzer
ATTN: L. Napoli

RCA Corp
ATTN: R. Killion

RCA Corp
ATTN: W. Allen
ATTN: L. Debacker
ATTN: E. Schmitt

RCA Corp
ATTN: E. Van Keuren
ATTN: J. Saultz
ATTN: W. Heagerty
ATTN: R. Magyarics

Rensselear Polytechnic Institute
ATTN: R. Gutmann
ATTN: R. Ryan

DEPARTMENT OF DEFENSE CONTRACTORS (Continued)

Research Triangle Institute
ATTN: M. Simons

Rockwell International Corp
ATTN: J. Bell
ATTN: GA50 TIC/L, G. Green
ATTN: A. Rovell
ATTN: V. Strahan
ATTN: L. Blandford
ATTN: C. Kleiner
ATTN: K. Hull
ATTN: J. Pickel, Code 031-BB01
ATTN: V. De Martino
ATTN: R. Pancholy
ATTN. V. Michel

Rockwell International Corp
ATTN: D. Stevens
ATTN: TIC D/41-092, AJ01

Rockwell International Corp
ATTN: A. Langenfeld
ATTN: TIC 106-216

Rockwell International Corp
ATTN: TIC BA08
ATTN: T. Yates

Sanders Associates, Inc
ATTN: L. Brodeur
ATTN: M. Aitel

Science Applications, Inc
ATTN: V. Verbinski
ATTN: J. Spratt
ATTN: V. Orphan
ATTN: R. Fitzwilson
ATTN: J. Beyster
ATTN: J. Naber
ATTN: D. Strobel
ATTN: D. Millward
ATTN: D. Long
ATTN: L. Scott

Science Applications, Inc
ATTN: C. Cheek
ATTN: J. Swirczynski

Science Applications, Inc
ATTN: W. Chadsey
ATTN: J. Wallace

Science Applications Inc
ATTN: D. Stribling

Scientific Research Assoc, Inc
ATTN: H. Grubin

Signetics Corp
ATTN: J. Lambert

Singer Co
ATTN: Tech Info Ctr
ATTN: J. Laduca
ATTN: R. Spiegel
ATTN: J. Brinkman

DEPARTMENT OF DEFENSE CONTRACTORS (Continued)

Sperry Corp
ATTN: Engrg Lab

Sperry Corp
ATTN: J. Inda

Sperry Rand Corp
ATTN: R. Viola
ATTN: C. Craig
ATTN: F. Scaravaglione
ATTN: Maraffino

SRI International
ATTN: A. Whitson

SRI International
ATTN: A. Padgett

Sundstrand Corp
ATTN: Research Dept

GTE Communications Products Corp
ATTN: L. Pauplis
ATTN: C. Thornhill
ATTN: L. Blaisdell
ATTN: W. Dunnet

GTE Communications Products Corp
ATTN: H. Ullman
ATTN: P. Fredrickson
ATTN: H & V Group
ATTN: C. Ramsbottom

GTE Communications Products Corp
ATTN: J. Waldron

Sperry Flight Systems
ATTN: D. Schow

Teledyne Brown Engrg
ATTN: J. McSwain
ATTN: D. Guice
ATTN: T. Henderson

Texas Instruments, Inc
ATTN: R. McGrath
ATTN: R. Stehlin
ATTN: T. Cheek, MS 3143
ATTN: E. Jeffrey, MS 961
ATTN: F. Poblenz, MS 3143
ATTN: D. Manus
ATTN: R. Carroll, MS 3143

DEPARTMENT OF DEFENSE CONTRACTORS (Continued)

Teledyne Systems Co
ATTN: R. Suhrke

TRW Electronics & Defense Sector
ATTN: A. Witteles, MS R1/2144
ATTN: D. Clement
ATTN: J. Bell
ATTN: W. Willis
ATTN: H. Hollaway
ATTN: Vulnerability & Hardness Lab
ATTN: P. Gardner
ATTN: W. Rowan
ATTN: P. Guilfoyle
ATTN: H. Hennecke
ATTN: P. Reid, MS R6/2541
ATTN: H. Volmerange, R1/1126
ATTN: Tech Info Ctr
ATTN: R. Kingsland
ATTN: M. Ash
ATTN: F. Friedt
2 cy ATTN: R. Plebuch
2 cy ATTN: O. Adams

TRW Electronics & Defense Sector
ATTN: J. Gorman
ATTN: F. Fay
ATTN: C. Blasnek
ATTN: R. Kitter

Vought Corp
ATTN: Library
ATTN: Tech Info Ctr
ATTN: R. Tomme

Westinghouse Electric Corp
ATTN: MS 330, D. Grimes
ATTN: N. Bluzer
ATTN: E. Vitek, MS 3200
ATTN: L. McPherson
ATTN: H. Kalapaca, MS 3330
ATTN: J. Cricchi
ATTN: MS 3330

Westinghouse Electric Corp
ATTN: S. Wood